ROLE OF METAVINCULIN IN ACTIN REORGANIZATION AND FORCE TRANSMISSION

Hyunna Theresa Lee

A dissertation submitted to the faculty at the University of North Carolina at Chapel Hill in partial fulfillment of the requirements for the degree of Doctor of Philosophy in the Department of Biochemistry and Biophysics in the School of Medicine.

Chapel Hill
2019

Approved by:

Sharon Campbell

Keith Burridge

Nikolay Dokholyan

Qi Zhang

Joan Taylor

Stephanie Gupton

ABSTRACT

Hyunna Theresa Lee: Role of metavinculin in actin reorganization and force transmission
(Under the directions of Sharon L. Campbell and Keith Burridge)

Vinculin is an essential cytoskeletal protein that acts as a scaffold to link transmembrane receptors to actin filaments, thereby playing a crucial role in cell adhesion, motility, and force transmission between cells. While vinculin is ubiquitously expressed, metavinculin, a larger isoform of vinculin, is selectively expressed in smooth and cardiac muscle cells. Metavinculin contains an additional exon that encodes a 68-residue insert. Point mutations in the 68-residue insert have been associated with altered actin organization and heart disease, notably dilated cardiomyopathy (DCM) and hypertrophic cardiomyopathy (HCM). As metavinculin expression is higher in muscle cells that require greater force transmission, we postulate that metavinculin plays an important role in force generation and transmission through its interaction with the actin cytoskeleton. Results from cryo- and negative-stain electron microscopy (EM), in conjunction with actin co-sedimentation experiments, indicate that the tail domain of vinculin (Vt) and metavinculin (MVt) possess similar F-actin binding interactions yet are distinct in their ability to remodel actin filaments. Whereas actin binding of Vt promotes actin filament bundling *in vitro*, the MVt domain does not. Intriguingly, addition of MVt to Vt interferes with Vt-induced actin filament bundling. In contrast, cardiomyopathy-associated MVt mutants do not antagonize Vt-induced actin bundling. Based on these findings, we hypothesize that metavinculin plays a role in negatively regulating vinculin-mediated actin bundling in contractile tissues. Hence, we next examined the roles of vinculin and metavinculin within cells. To investigate functional

differences between metavinculin and vinculin in cells, we additionally stably expressed either vinculin or metavinculin in *vinculin*-null mouse embryonic fibroblasts. While both metavinculin and vinculin were observed at focal adhesions (FA), metavinculin-expressing cells had larger but fewer FAs per cell compared to vinculin-expressing cells. Metavinculin-expressing cells migrated faster and exhibited greater persistence compared to vinculin-expressing cells, even though vinculin-containing FAs assembled and disassembled faster. Magnetic tweezer measurements on vinculin-expressing cells show a typical cell stiffening phenotype in response to externally applied force; however, this was absent in *vinculin*-null and metavinculin-expressing cells. Our findings that metavinculin expression leads to larger but fewer number of FAs per cell, in conjunction with the inability of metavinculin to bundle F-actin *in vitro* and rescue cell stiffening response, are consistent with our previous findings of actin bundling deficient vinculin variants, suggesting that deficient actin-bundling may account for some of the differences between vinculin and metavinculin.

To my parents, my sister, and my close friends. I could not be where I am today without your unconditional love and support. To my advisors, Sharon Campbell and Keith Burridge. Thank you both for your trust and confidence in me as your student. Your support and mentoring cannot be expressed into words.

ACKNOWLEDGMENTS

This section is, in some ways, the most difficult section of the dissertation to write. I have received support and encouragement from numerous individuals throughout my journey, and I cannot express into words the gratitude I feel towards them. Without their intellectual inspiration, mental and scientific support, and encouragement to go after my curiosities, I would not be where I am today.

I would like to start by acknowledging and thanking my mentors, Drs. Sharon Campbell and Keith Burridge, who have pushed me to be a better and critical scientist. First, I would like to thank Dr. Sharon Campbell for always allowing me to go after my scientific interests and supporting me in my experimental endeavors. Without her encouragement, I would not have been able to explore the cell biology/cytoskeleton field and discover a whole new field of interest. I immensely appreciate her trust and dedication in my training. Just as importantly, I would additionally like to thank Dr. Keith Burridge, who have always encouraged me to go after my curiosities as I pursued this project. He was always a source of motivation for me due to his positive outlook towards scientific results. However, he never sacrificed the quality of data he expected, which has trained me to be a better scientist. Perhaps I learned the most important life lessons from both of my mentors. From Sharon, I learned to enjoy the challenges that come my way, and from Keith, I learned that the only thing we have to fear is fear itself.

In addition to my mentors, I would also like to acknowledge my lab mates from both Burridge and Campbell laboratories. They have supported me tremendously as I struggled with experiment after experiment, and their mental and scientific support will definitely be missed.

The amazing people in these labs have carried me through the darkest of times and also celebrated all the happy moments alongside me as if they were my family. It is with them that I celebrated every little personal and scientific growth. I will dearly miss the outside lunches and coffee runs in the morning.

Next, I would like to thank my committee members. I would first like to thank Dr. Stephanie Gupton for her numerous experimental mentorship and career discussions. I love these discussions with Dr. Gupton as she seems to always know the answer to my questions. Reaching out to ask about focal adhesion experiments was probably one of the best things I did while I was here. I would also like to thank Dr. Joan Taylor. She has provided me with tremendous support, especially toward the beginning of my thesis project. When I was having problems with expressing metavinculin in cells, it was because of her scientific advice that I was able to continuously look for solutions. For this, I will always be grateful. Subsequently, I would like to thank Dr. Qi Zhang, who has been one of the best mentors in my program. Dr. Zhang's commitment to teaching and mentoring students is inspirational. Finally, I'd like to thank Dr. Nikolay Dokholyan, as discussions with his group about the vinculin project always provided me with a more interesting perspective.

I would like to thank my department, the Department of Biochemistry and Biophysics as well, in part for their financial support for my training (Biophysics training grant) but also because of the support they show to the well-being of their graduate students. Their assistance and support keeps the department and experiments running. I would like to especially thank Lisa Phillippie for her foundational role. Additionally, I would like to thank National Heart and Lung Institute (NHLBI) for their funding of my F31 predoctoral training grant.

I also want to acknowledge my close friends, as hanging out with them made my life so much more fun. Your unconditional love and encouragement have brought me where I am today. You have been my inspiration.

Lastly, I would like to thank my parents and my sister. Without their encouragement and confidence, I would not have been able to finish. My family have been nothing but patient and supportive as I pursued my thesis, and at times, reminded me that it was okay to go slow. It was through them that I learned that it is most important to hold the values that are key to me, and never compare myself with others. My parents have always stressed the importance of education and encouraged me to test my limits. They have also instilled the value of hard work and persistence as I grew up, which is one of reasons that I am where I am today. Their dedication to my personal and professional growth keeps me motivated to become better.

I am truly blessed to be in a place where I receive so much love and support. I cannot express into words my gratitude and love for you all.

PREFACE

Parts of this work were done in collaboration with other talented scientists. Chapter 2 represents work that was done in collaboration with the labs of Dr. Greg Alushin, Dr. Nikolay Dokholyan, and Dr. Jack Griffith. My contribution focused on the protein purification for vinculin and metavinculin samples, site-directed mutagenesis for generating the necessary constructs, and performing actin co-sedimentation assays to determine actin binding and bundling levels. Figures 4-7 were generated by the Alushin lab. I contributed to the Figures generated in 8, 11, and 12 with Dr. Muzaddid Sarker from the Campbell lab while Figures 9 was generated by Dr. Sarker in collaboration with the Griffith lab. Figures 10 and 13 were generated by the Alushin lab, and Figure 14 was generated by the Dokholyan lab based on their discrete molecular dynamics (DMD) models. This work resulted in two publications that I co-authored. The papers were published previous to writing this thesis with the following citations:

> Kim LY, Thompson PM, Lee HT, Pershad M, Campbell SL, Alushin GM. The Structural Basis of Actin Organization by Vinculin and Metavinculin. J Mol Biol. 2016;428(1):10-25. PMCID: 4738167.
>
> Sarker M, Lee HT, Mei L, Krokhotin A, de Los Reyes SE, Yen L, et al. Cardiomyopathy Mutations in Metavinculin Disrupt Regulation of Vinculin-Induced F-Actin Assemblies. J Mol Biol. 2019;431(8):1604-18.

Permission to include the articles in a PhD dissertation was retained from Elsevier (publisher of JMB) as explained at https://www.elsevier.com/about/policies/copyright.

Chapter 3 represents work currently in revision that was done primarily by myself. However, I have collaborated with many talented scientists from UNC to generate these data,

including Dr. Stephanie Gupton and Dr. Richard Superfine. I am the lead author on the paper, but Fabio Urbina from the Gupton lab has helped me to generate Figure 23. Additionally, all the 3DFM-related data in Figures 25 and 26 could not have been generated without the help of Dr. Timothy O'Brien in the Superfine lab. Finally, Minh Hyunh from the Campbell/Der lab has provided me with the constructs that were necessary for the generation of stable cell lines. This paper is currently in revision:

> Lee, H.T**.**, Sharek, L., O'Brien, E.T., Fabio L. Urbina, Gupton, S.L., Superfine, R., Burridge, K., and Campbell, S.L. (2019) Vinculin and Metavinculin Exhibit Distinct Effects on Focal Adhesion Properties, Cell migration, and Mechanotransduction. *PLoS One, **in revision***.

TABLE OF CONTENTS

LIST OF TABLES

LIST OF FIGURES

LIST OF ABBREVIATIONS

3DFM	Three-dimensional force microscopy
ΔC5	Vinculin C-terminal hairpin deletion (lacks residues 1061-1066)
AJ	Adherens junction
AF	Aggregation factor
ARP 2/3	Actin-related protein 2/3
BME	β-mercaptoethanol
BSA	Bovine serum albumin
CM	Cardiomyopathy
cryo-EM	cryo-electron microscopy
DCM	Dilated cardiomyopathy
DMD	Discrete molecular dynamics
DMEM	Dulbecco Modified Eagle Medium
DMSO	Dimethylsulfoxide
DTT	Dithiothreitol
ECM	Extracellular matrix
EM	Electron microscopy
FA	Focal adhesion
FACS	Fluorescent activated cell sorting
F-actin	Filamentous actin
FAK	Focal adhesion kinase
FBS	Fetal Bovine serum

FN	Fibronectin
FRNK	Focal adhesion kinase-related nonkinase
G-actin	Monomeric actin
IPTG	β-D-1-thiogalactopyranoside
HCM	Hypertrophic cardiomyopathy
IRM	Interference reflection microscopy
Kd	Dissociation constant
KO	Knock-out
LB	Lysogeny broth
MEF	Mouse embryonic fibroblast
μm/nm	Micrometer/nanometer
MVt	Metavinculin tail domain
NMR	Nuclear magnetic resonance
PBS	Phosphate buffered saline
PCR	Polymerase chain reaction
PDB	Protein data bank
PI3K	Phophoinositide 3-kinase
PIP2	Phosphatidylinositol 4,5-bisphosphate
PIPKIγ	Phosphatidylinositol phosphate kinase type 1 gamma
ROI	Region of interest
RT	Real-time
RTCA	Real-time cell analyzer

SDS	Sodium dodecyl sulfate
TEV	Tobacco etch virus
VASP	Vasodilator-stimulated phosphoprotein
Vh	Vinculin head domain
Vt	Vinculin tail domain
WT	Wild-type

CHAPTER 1 - INTRODUCTION

Focal adhesion architecture and signaling

When many cells migrate in culture dishes, structures called focal adhesions (FAs) assemble and disassemble, allowing cells to regulate points of adhesion and force. Cell adhesion and mechanotransduction regulation contributes to normal physiological control of cell motility, morphology, and survival. FAs are macromolecular structures that consist of ~150 different proteins that form adhesion plaques between cell membrane and the extra cellular matrix (ECM). FAs physically link actin cytoskeleton inside the cell to the outside environment, and they can be largely divided into three layers: integrin signalling layer, force transduction layer, and actin regulatory layer (1) (Fig. 1).

Historically, FAs were initially observed by Abercrombie *et al.* in 1971, who used electron microscopy (EM) to examine lamelliopodia in cultured migrating fibroblasts lamelliopodia in cultured migrating fibroblasts (2). Though not yet termed FAs, the discovery of these adhesion plaques ultimately grew into a field that significantly impacted our understanding of mechanotransduction and signaling. Following the study by Abercrombie *et al.*, Izzard and Lochner utilized interference reflection microscopy (IRM) and detected FAs, though the intent of the study was to determine the distance between the underside of chick heart fibroblasts and the glass coverslip where they are attached. The vocabulary for FAs varied as this term hadn't been coined yet (3). Combining both EM and IRM, Heath and Dunn showed that the plaques observed by Abercrombie *et al.* and Izzard and Lochner were the same, and first defined this structures as

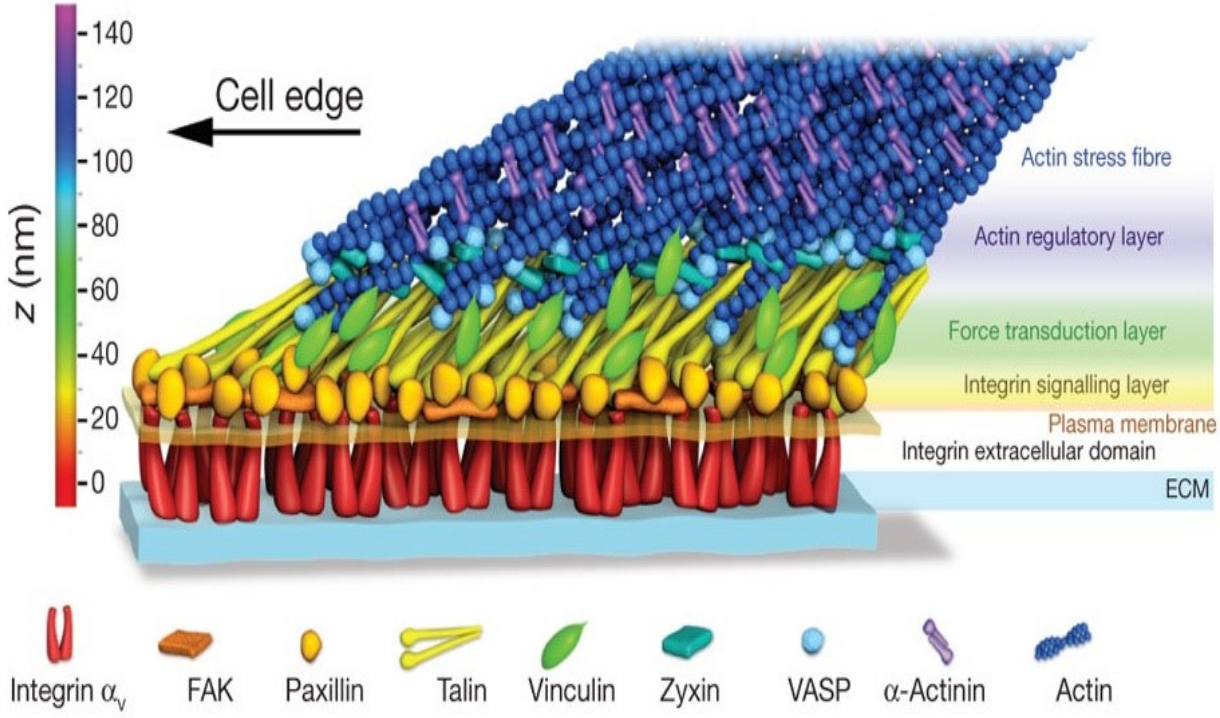

Figure 1. Nanoscale architecture of focal adhesions.

Originally published by Kanchanawong, P. *et al.* Nature. 2010 Nov 25;468(7323):580-4.

"focal adhesions" (4). Couchman and Rees subsequently used this term upon studying cardiac fibroblasts migrating out of heart explants (5). Interestingly, these authors observed that during the initial phase of rapid cells migration, the fibroblasts barely showed any FAs but as these cells slowed down, FAs developed. It is important to note that FAs are not necessary for cell migration as many cells have been shown to migrate without them. While integrin-mediated adhesion to the ECM still forms in cells that do not develop FAs, these adhesions do not form stable clusters of integrins. Nobes and Hall introduced the term "focal complex" to refer to smaller, more transient adhesions than FAs (6). In general, the term nascent adhesions has been widely adopted in the field to describe the initial small adhesions, which eventually develop into focal complexes and ultimately into FAs as the adhesion matures and stabilizes. Burridge provides an excellent review on a historical perspective of the focal adhesion field (7).

With the development of immunofluorescence microscopy in the mid-1970s and the discovery of vinculin by Geiger in 1979 (8), there was a breakthrough in the field of focal adhesion and cytoskeleton research. A number of FA components have been discovered since that time. Notably, several key components have been identified at FA, including integrin, talin, vinculin, and α-actinin, which will be discussed in more detail below. These FA components reside distinctly throughout the three layers that comprise the FA structure.

With the exception of integrin transmembrane receptors and syndecan-4, the vast majority of proteins that comprise FAs consist of cytoplasmic proteins. The integrin signalling layer is apposed to the cell membrane and contains integrin cytoplasmic tails, focal adhesion kinase (FAK), and paxillin (1). As mentioned above, integrins play a key role in FAs as a transmembrane receptor that connects the extracellular matrix (ECM) via their extracellular domain to the cell's cytoskeleton via their cytoplasmic tails. They are the main receptor proteins

that cells use to both bind and respond to the ECM ligands, including collagen, fibronectin, and laminin. An integrin molecule consists of two non-covalently associated transmembrane subunits called α and β determines its affinity for specific ECM ligands. Integrins exist in 3 states: closed (inactive), bent, and open (active) conformations (9). Activation of integrins occur through either "outside-in" or "inside-out" signaling, where both the environmental cues and the intracellular signals regulate how FAs function (10, 11). Outside-in signaling initiates as the integrin extracellular domain binds to ECM ligand, driving a conformational change that exposes their cytoplasmic tails, which recruits specific proteins that form and mature FAs. In the context of FAs, integrins have been found to bind to other FA components such as talin (12) and α-actinin (13), providing a physical link between plasma membrane and FA. Force has been speculated to play a role in integrin activation as well, although it is still being determined. Some studies suggest that external mechanical loading is necessary for integrin activation (14). Inside-out signaling is also hypothesized to occur through actomyosin-driven force generation and regulated at the integrin signaling layer since by altering the activation state of integrins, intracellular signals can modulate the bindng affinity between integrins and ECM ligands (15). Furthermore, integrin signaling layer may be important for regulating feedback between inside-out and outside-in signaling as well. In this layer, integrin activation has been shown to autophosphorylate FAK, which has been linked to mechanosensing, cell shape control, and focal adhesion dynamics (16-18). Then FAK, in turn, can regulate intracellular signals involving GTPase RhoA, which plays important roles in functions such as actomyosin contractility and FA formation (19, 20). FAK has additionally been implicated in the regulation of cell adhesion and migration. Notably, FAK-deficient cells spread more slowly on ECM proteins, exhibit an increased number of FAs, and migrate poorly in response to chemotactic and haptotactic signals

(21-24). C-terminal domain of FAK is also a site of many protein-protein interactions, and overexpression of focal adhesion kinase-related nonkinase (FRNK), an autonamously expressed C-terminus of FAK, has been shown to inhibit the rate of cell spreading and migration rates in response to chemotactic and haptotactic cues (24-26). Therefore, the integrin signaling layer of FA is important for both responding to external forces and the generation of intracellular forces.

With respect to the cell membrane surface, the force transduction layer lies on top of the integrin signaling layer, and it consists various scaffolding and signaling proteins. Of note, talin and vinculin (though vinculin has been found in all FA layers) have been shown to play important roles in mechanotransduction (1, 27). Talin can bind both integrins and filamentous actin (F-actin) and reinforce this connection to F-actin by further recruiting vinculin (12, 28, 29). Application of force on talin has been shown to expose the cryptic vinculin-binding sites (VBS) by unfurling talin, which then recruits vinculin to talin (30). This force is thought to occur as myosin-generated forces are transmitted across FAs or from forces resulting from actin retrograde flow that are transmitted across FAs to create traction to drive the cell forward (actin retrograde flow will be discussed below). Under applied load, the affinities for vinculin on VBS of talin increase after a certain threshold, supporting the idea of "molecular clutch" at these sites of mechanotransduction (30). Vinculin also similarly increases its affinity to specific ligands past a certain threshold of applied load/force (31, 32), additionally supporting the idea of "molecular clutch" at FAs. Molecular clutch model demonstrates that force transmission is regulated by a dynamic clutch mechanism, where force transduction only occurs once talin (or vinculin) unfurls above a stiffness threshold (27, 33-35). Below this threshold, integrins unbind and release force before talins can unfold. Above this threshold, talin unfolds and binds to vinculin, which then further drives the FA maturation through vinculin's function as a scaffolding protein. Whether

talin and/or vinculin can overcome this stiffness threshold depends on the stiffness of the cell's environment, as the cell's ability to sense mechanical cues and transduce force into biochemical signals depends on the rigidity of the environment that the cell is in. Coupled with the molecular clutch model is the role of actin retrograde flow in cells. Actin retrograde flow refers to actin that flows back toward the body of the cell as the cell migrates, resulting from the actin polymerization against the cell membrane at the leading edge (36). It has been proposed that FAs at the cell's leading edge act as "clutches" for the flowing actin that impede actin's retrograde movement. By clutching onto the retrograde flow of actin, FAs can transduce the force from this actin flow to the ECM, creating the traction needed to push the cell forward (36). Hence, the speed of actin retrograde flow should be inversely related to the traction force at FAs: the more FAs clutch onto the flowing actin to create more traction against ECM, the slower the actin retrograde flow should be. Talin and vinculin act as molecular clutches that bind to F-actin at the force transduction layer of FAs, playing important roles for how FAs transmit force into intracellular biochemical signals and vice versa.

Finally, the actin regulatory layer is the uppermost FA layer (with respect to the cell membrane surface) containing zyxin, vasodilator-stimulated phosphoprotein (VASP), and α-actinin (1). Actin regulatory layer engages in actin assembly, actin disassembly, and stress fiber reinforcement. Increased stress fiber formation is one of the ways that cells respond to tension or mechanical stress, and the proteins VASP and zyxin play critical roles for this function (37). When stress fibers experience strain, VASP and zyxin relocate from the actin regulatory layer of FAs to sites of tension along stress fibers, which results in stress fiber reinforcement (37, 38). With the help of VASP protein, zyxin enhances actin polymerization at these sites (37, 38). Furthermore, α-actinin has also been found to localize along stress fibers with a periodic pattern

and was found to be concentrated at FAs in non-muscle cells (39). α-actinin is a protein that can bundle actin in an anti-parallel manner and lines the stress fibers as it bundles the actin filaments there. Aside from binding to actin, α-actinin can also associate with a number of cytoskeletal and signaling molecules, including the cytoplasmic tail of integrin (13), which renders it an important structural and regulatory protein in cytoskeletal organization (40). Through the proteins that comprise the actin regulatory layer at FAs, this layer plays a significant role in transmitting signals to actin cytoskeleton from force transduction and integrin signaling layers. On the other hand, the actin regulatory layer can also participate in inside-out signaling by transmitting intracellular cues to force transduction and integrin signaling layers.

All three layers of FAs work together to link extracellular ECM to the intracellular actin cytoskeleton, where each layer plays a distinct role in sensing and responding to environmental cues or intracellular signals. Various force-sensitive mechanisms are at play in FAs and therefore, further studies of how FA phenotypes relate to force will clarify the underlying mechanisms. Collins *et al.* provides an excellent overview of FA layers (41).

The cell adhesion protein vinculin

Vinculin is an essential, ubiquitously expressed cytoskeletal protein that acts as a scaffold to link actin cytoskeleton to transmembrane receptors at FAs (vinculin binds to F-actin and talin, which binds to integrin transmembrane receptor) and at adherens junctions (AJs) (vinculin binds to F-actin and α-catenin, which binds to cadherin transmembrane receptor). Vinculin was initially discovered in chicken gizzards in 1979 (42), and since then much about this protein has been studied at both the structural and cellular level. At the sites of adhesion, vinculin's role as a physical link between actin and transmembrane receptor plays a crucial part in cell adhesion, motility, and force transmission. Without vinculin, mouse embryos do not survive past E10, and they exhibit defects in cardiac and neural tube development (43). Furthermore, lack of vinculin in mouse embryonic fibroblasts (MEFs) leads to rounded morphology, increased motility, and resistance to apoptosis and anoikis (43-45). Vinculin regulates these processes by binding to multiple biomolecules at specific times and at specific domains, thereby playing a key role in signaling at adhesion sites and creating physical linkages between proteins.

Vinculin is a 117 kDa protein that functions as a molecular scaffold. It is comprised of a large ~90 kDa head domain (Vh), flexible proline-rich linker, and the tail domain (Vt) (46) (Fig. 2). Vh interacts with talin at FAs, α-catenin at AJs, and α-actinin at both cellular locations (47-49) (Fig. 2). The proline-rich linker that connects Vh to Vt can bind to VASP, vinexin, CAP/ponsin, and Arp2/3 complex (50-53). Vt directly binds to filamentous actin (F-actin) (54), phosphatidylinositol (4,5) biphosphate (PIP_2) (55), and raver 1 (56-58) (Fig. 2). In my dissertation, direct interaction between Vt and F-actin will be discussed in detail. However, other ligands that bind to Vt additionally appear to play important roles for cellular processes. First, PIP_2 is an important signaling lipid for numerous cellular processes, including membrane ruffle

formation (59), exocytosis (60), and phagocytosis (61). In the case of FAs, PIP_2 is generated by phosphatidylinositol phosphate kinase type 1 gamma (PIPKIγ) (62), which is recruited to focal adhesions by talin (63, 64). Talin recruits vinculin, meaning that vinculin colocalizes with and PIP_2, which regulates the interaction of vinculin with talin (28, 47). PIPKIγ regulates FA dynamics (65, 66), is required for FA formation (67), and is thought to be involved in recruitment and activation of vinculin at FAs (66, 68). While much is known about the general role of PIP_2 at FAs, the consequences of the vinculin:PIP_2 interaction are much less understood. Raver 1, an 80 kDa multidomain protein that is widely expressed in different cell lines, is shown to form complexes *in vitro* with not only vinculin but also with α-actinin and metavinculin (57), a vinculin isoform that will be introduced in the next section. Raver1's interaction with vinculin tail domain at FAs is particularly intriguing as raver1 is a RNA-binding protein that plays an important role in mRNA processing regulation through its interaction with the splicing regulator polypyrimidine tract binding protein (PTB) (56, 69-71). Crystal structure of vinculin:raver1 show that raver 1 binds to a RNA sequence found in *vinculin* mRNA, and that this interaction is permissive for vinculin's interaction with F-actin at the tail domain (56). These findings suggest that vinculin acts as a scaffold for the recruitment of raver1 and that *vinculin* mRNA cargo to FAs, which would promote localized synthesis of adhesion complexes (56). Autoinhibitory interactions between Vh and Vt promote the closed inactive state which obscures ligand binding (46) (Fig. 2). Although mechanisms of activation are not fully understood, it is currently believed that the engagement of talin or catenin to Vh in conjunction with binding of additional ligands (47, 72, 73), post-translational modifications (74), and/or force (75-78) promotes activation and exposure of multiple ligand binding sites.

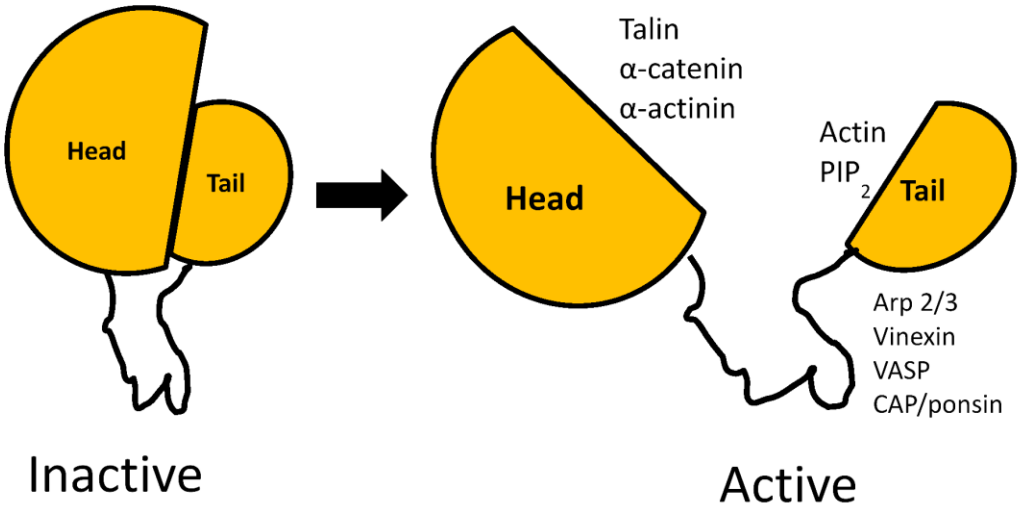

Figure 2. Vinculin is an autoinhibitory scaffolding protein.

Vinculin is a scaffolding protein that typically exists in an autoinhibited, closed (inactive) conformation where the head and the tail domain are in tight interaction. Upon activation, this interaction is released, exposing various ligand binding sites on the head and the tail domain, as well as the flexible proline-rich linker.

Metavinculin is a splice isoform of vinculin expressed in muscle cells

While vinculin is ubuitously expressed in all cell types, vinculin has one alternative splice isoform, termed metavinculin, that is co-expressed with vinculin in diverse muscle tissues and at low levels in platelets (42, 79-81). The metavinculin transcript contains an extra exon (exon 19) compared to the vinculin transcript, and this exon translates into an additional 68-residue insert in the tail domain (82). Metavinculin is expressed at sub-stoichiometric levels relative to vinculin (9-42%), and its expression correlates with the elevated contractile needs of these muscle cells (83, 84). It is currently believed that metavinculin plays a special role in mechanotransduction, as its expression levels positively correlate with the force exerted on cells (84). Metavinculin was initially discovered in chicken gizzards (42). Since then, it has been shown that the expression level of metavinculin in various tissues and cultured cells differ (83-88). Studies by Glukhova *et al.* showed that in adult human tissues, metavinculin was found in cardiac and smooth muscle of aorta and uterus, respectively (85); subsequent studies by Belkin *et al.* showed that metavinculin expression level in these tissues positiviely correlated with muscle contractility (83-85). Since this initial characterization of metavinculin, many groups investigated the (1) association of metavinculin with human cardiomyopathy patients at the tissue level, (2) the effect of disrupting the vinculin gene at the organismal level (mostly using mice), and (3) the characterization of the molecular structure and function of metavinculin.

In 1997, Maeda *et al.* found an association between deficiency of metavinculin expression and human dilated cardiomyopathy (DCM) patients (89). This observation led to several studies looking at the relationship between human cardiomyopathy patients and metavinulin in these patients' tissues (90, 91). Olson *et al.* found that in human DCM patients, point mutations/single amino acid deletions in metavinculin were located at residues within the

68 amino acid insert (A934V, ΔL954, and R975W). Of the three variants, R975W-associated patient showed the most pronounced defect in the organization of intercalated discs (90). Following this study, Vasile *et al.* also found that R975W is additionally associated with both hypertrophic cardiomyopathy (HCM) and DCM in human patients and that the reduced level of both vinculin and metavinculin at the intercalated disc is associated with HCM (91, 92).

Metavinculin and its association with cardiomyopathies was also studied at the organismal level using mice by Zemljic-Harpf et al (93, 94). Zemljic-Harpf *et al.* observed that mice that have heterozygous inactivation of the vinculin gene are predisposed to stress-induced cardiomyopathy (94). These mice not only showed reduced expression levels of both vinculin (58% reduction) and metavinculin (63% reduction), but also abnormal myocardial ultrastructure and increased mortality rate (94). Furthermore, they found that the cardiac-myocyte-specific excision of the vinculin gene in mice led to disruptions in cellular junctions, leading to sudden death of DCM in these mice (93). One limitation of these studies, however, was that disruption of vinculin genes led to the deletion of both vinculin and metavinculin variants. Therefore, these studies were not able to tease apart individual functions due to vinculin or metavinculin.

Finally, metavinculin's structure and function has been characterized at the molecular level, in relation to how these molecular structures may affect the associated cardiomyopathies. The crystal structure of metavinculin was first solved by Rangarajan *et al.* in 2010, and this structure revealed a helix-replacement of the helix 1 (H1) sequence of Vt by helix 1' (H1') sequence of MVt (95). The specific details of the structural difference between vinculin and metavinculin will be discussed in the next section. One interesting observation made by this study was that all DCM and HCM associated mutations in metavinculin (A934V, ΔL954, and R975W) lie within or near the H1' region, implying that H1' plays an important role for

metavinculin function (90). Additionally, Olson *et al.* had found that MVt A934V, ΔL954, and R975W have all led to an actin bundling phenotype in vitro, although MVt does not typically bundle actin filaments (90). Further structural studies will need to be done to elucidate how the structure of MVt contributes to DCM and HCM, as well as to clarify how A934V, ΔL954, and R975W mutations disrupt metavinculin function.

Both DCM and HCM are diseases of the myocardium that diminish blood flow within the heart due to reduced force transmission. Association between metavinculin expression and mutations with diseases of the heart muscle further support the view that metavinculin plays a crucial role in the mechanotransduction properties of the cell. However, the direct cellular consequences of metavinculin need to be further studied.

Differences between vinculin and metavinculin structure and function

Metavinculin and vinculin structurally share the same head domains (95, 96); however, their tail domains differ (Fig. 3). Vinculin tail domain possesses an N-terminal strap followed by a 5-helix bundle and C-terminal hairpin (46), while the metavinculin tail domain contains an additional exon that encodes a 68 amino acid insert (79) (Fig. 3). This extra exon codes for the residues between helices 1 and 2 in the vinculin tail domain and confers unique functions to the metavinculin tail domain (82). Structurally, while metavincuiln tail has a 5-helix bundle fold similar to vinculin tail, the sequence that makes up the helix 1 (H1) and strap of vinculin tail is displaced in the metavinculin tail by homologous sequences, which we term H1', contained within this insert (95) (Fig. 3). Specifically, these new residues replace the vinculin residues 879-915, which translate to the N-terminal strap and the H1 in vinculin tail. The original vinculin tail sequence 879-915, in the context of metavinculin, is no longer observable in the existing crystal structures (95), which indicates that this region is either disorganized or dynamic. The altered tail domain structure in metavinculin increases the affinity for raver 1 (54) and decrease the affinity for PIP_2 (97) compared to vinculin. This difference in raver 1 and PIP_2 affinity with either Vt or MVt is especially interesting as vinculin and metavinculin differ structurally at the tail domain (95). Interestingly, raver 1 binds to not only both vinculin and metavinculin, but also to *vinculin* mRNA (56-58). Additionally, structural studies show that raver 1 can bind to full-length metavinculin but not vinculin, suggesting that raver 1 can bind to inactive conformation of metavinculin and active conformation of vinculin (56-58). Along with the binding data that show that raver 1 forms a ternary structure with MVt and *vinculin* mRNA (58), I speculate that raver 1 plays a critical role for the splicing regulation of *vinculin* mRNA in muscle tissues. As raver 1 has been shown to regulate tropomysin mRNA splicing that occurs specifically in smooth muscle

(69), perhaps raver 1 plays a similar role in regulating exon 19 splicing in the translation of *vinculin* mRNA. Since metavinculin expresses exon 19 in *vinculin* mRNA, perhaps this exon skipping is repressed in muscle cells when metavinculin is translated through the ternary structure that form among MVt: raver1:*vinculin* mRNA. The presence of the insert and the altered tail domain structure in metavinculin may alter other ligand interactions in cells as well.

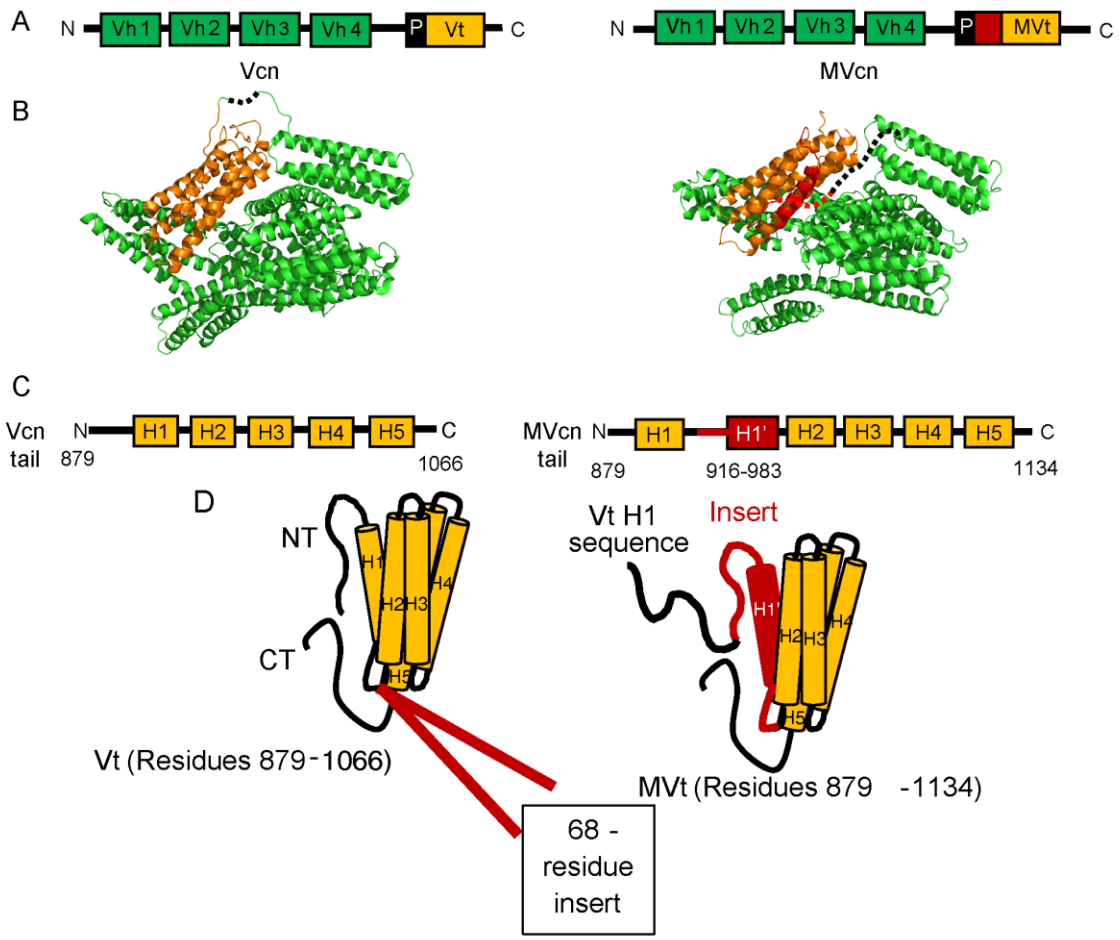

Figure 3. Sequence and structural differences between Vcn and MVcn.

(A) Diagram comparing domain architecture of full-length Vcn and MVcn. (B) Crystal structures of Vcn (PDB: 1TR2) and MVcn (95). Regions that lack electron density are represented by a dotted line. (C) Diagram comparing sequence differences in the Vcn and MVcn tail domain. MVcn tail contains an insert of 68 amino acid between residue 915 and 916 (H1' in red, residues 916-983). (D) Structural schematic depicts sequence differences that lead to a helix replacement of H1 with H1' (red) in MVcn tail (Vh: Vcn head domain; Vt: Vcn tail domain; MVt: MVcn tail domain (PDB:3MYI); H: helix; NT: N-terminus; CT: C-terminus; and P: proline-rich region).

The role of vinculin-mediated actin-binding and actin-bundling

Similar to Vt, MVt directly binds F-actin (95, 98, 99). However, one interesting difference is in their ability to crosslink F-actin. Vt has been shown to bundle F-actin *in vitro*; however, unlike Vt, MVt does not bundle filamentous actin into higher order structures *in vitro* (90, 98-100). We and others have previously shown that binding of F-actin to Vt causes a conformational change in Vt that promotes dimerization and actin filament bundling (101, 102). However, the structure of the actin-induced Vt dimer is currently unknown. The susceptibility of H1 to proteolysis, combined with the lack of electron density observed for H1 in our cryo-EM reconstruction of the Vt-actin complex, suggests that H1 partitions away from the helix bundle upon engagement with filamentous actin to promote vinculin dimerization (99) (Fig. 4). Furthermore, the C-terminal tail of Vt plays a significant role in the formation of this actin-induced Vt dimer, as the deletion of the last five residues abrogates the ability of Vt to bundle actin (101). Expression of vinculinΔC5 mutant in vinculin-null MEFs lead to fewer and larger FAs and deficiency in cells to respond to external force (101). Similarly to Vt, H1' in metavinculin is not observable in the cryo-EM reconstruction of the metavinculin-actin complex (99), and the MVt binding site on F-actin is similar to that of Vt (99). The presence of H1 appears to interfere with the ability of metavinculin to bundle F-actin, as its deletion promotes actin filament bundling (95).

While vinculin and metavinculin show similar modes of binding to F-actin, metavinculin is unable to bundle actin filaments (90, 98-100). As metavinculin is co-expressed with vinculin in muscle tissues (42, 79, 84), it is likely that vinculin and metavinculin coordinately regulate actin filament rearrangement. Because of the studies that showed the reduction of metavinculin expression in tissues associated with less contractility and tension (83, 84), it has been

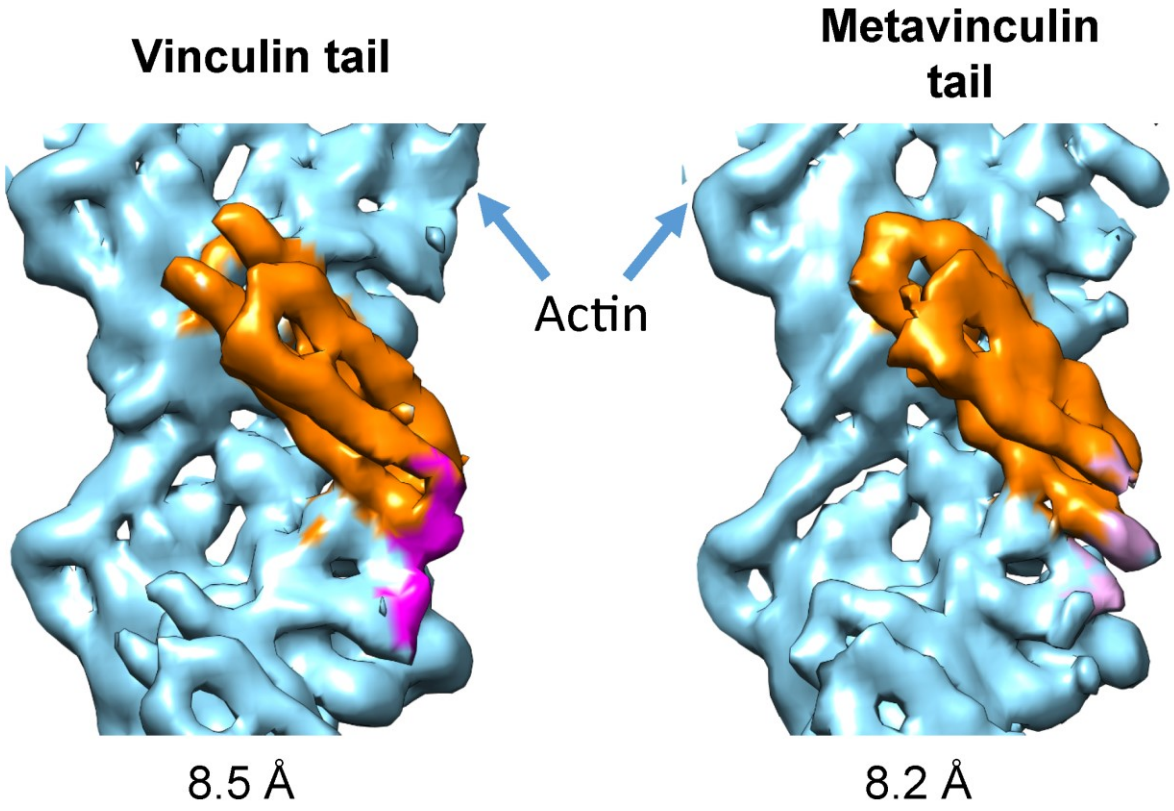

Figure 4. Cryo-EM reconstruction of Vt: F-actin and MVt:F-actin complex.

traditionally thought that metavinculin is more likely have a supporting role for vinculin in actin bundling. However, more recent studies seem to suggest that metavinculin may have a role in negatively regulating the actin bundling properties of vinculin physiologically. We and others have previously observed that the presence of metavinculin at sub-stoichiometric ratios impairs vinculin mediated F-actin bundling (99, 103), suggesting that MVt may negatively regulate Vt-mediated actin bundling. Furthermore, studies by Janssen *et al.* also observed actin filament fragments in the presence of MVt alone (98), and they attributed this observation to a potential ability of MVt to sever actin filaments. Additionally, studies by Durer *et al.* not only showed that MVt increases the proteolysis of F-actin by itself but also suggested that MVt may "tune" the flexibility and the architecture of vinculin-induced actin bundling (103). Durer *et al.* suggested this potential role of MVt as a negative-regulator of Vt-induced actin bundling as they found that MVt decreases the density and the thickness of actin filament bundles generated by Vt (103). However, unlike the studies by Janssen *et al.*, Durer *et al.* found negligible actin severing activity by MVt (103). Though further studies are necessary to understand the molecular basis for the ability of MVt to negatively regulate actin bundling by Vt, several observations associated with metavinculin-associated diseases seem to support this perspective. Metavinculin mutants associated with DCM and HCM are able to form higher order actin assemblies *in vitro* (90), suggesting that the disturbance of metavinculin's ability to disrupt vinculin-mediated actin bundling leads to cardiomyopathies. Similarly, Zemlijic-Harp *et al.* found decreased level of metavinculin expression in mice that's developed DCM (93). Further molecular studies of how disease-associated MVt mutants lead to higher-order actin bundling will be helpful in determining the cause of associated HCM and DCM.

In addition to the molecular characterization of actin bundling by metavinculin, there has been a significant lack of cellular characterization of metavinculin. Although some studies on metavinculin have been done at the tissue and organismal level, there has yet to be a study that's been done at the cellular level. Our lab has previously shown that the expression of actin bundling deficient mutant, vinculin ΔC5, in vinculin null MEFs led to changes in cellular properties, such as the increase in FA area, decrease in the average number of FA per cell, decrease in cell spreading, and the decrease in cell stiffening in response to applied force (101). It will be important to assess whether actin bundling differences observed between vinculin and metavinculin at the molecular level will lead to differences at the cellular level, and ultimately determine what those differences mean physiologically. Such studies complement work done at the tissue and organismal level.

CHAPTER 2 – The Strutural Basis of Actin Organization by Vinculin, Metavinculin, and Metavinculin Cardiomyopathy-associated Mutants

Introduction

Vinculin functions as an important scaffolding protein and can engage at least 19 direct binding partners at both cell-cell junctions and cell-matrix adhesions. Included in these direct binding partners are several actin-binding proteins (104). These interactions alter cytoskeletal organization, which in turn play a role in cell morphology, motility, and force transduction. However, for the purposes of this study, we focused on direct interactions between Vt and F-actin. Vinculin also strengthens the physical connection between membrane receptors and actin cytoskeleton (105), and this mechanical reinforcement is primarily through vinculin's interactions with talin (47, 105, 106). Talin is a critical adhesion protein that binds to integrin (12) within its N-terminus and also to actin through its C-terminus end (1). Like vinculin, talin is a scaffolding protein that exists in an autoinhibited state (107). Once tension is applied across talin molecule, talin unfurls, revealing 11 binding sites for vinculin (30) and actin (108), though the actin-binding affinity is relatively weak (108). It is thought that the recruitment of vinculin by talin stabilizes the actin linkage to integrins by keeping talin in an active, unfurled state and also additionally increasing the linkage to actin through vinculin's interactions with actin (109).

In addition to binding to filamentous actin, vinculin tail crosslinks actin filaments into parallel bundles *in vitro* (101, 102, 110). Both actin binding and bundling properties play an important role in vinculin function, as selectively disrupting them in the context of the full-length molecule leads to defects in cell spreading, focal adhesion formation and maturation, and

mechanotransduction (32, 101, 111, 112). While the vinculin tail domain in monomeric in solution, engagement to F-actin promotes a conformational change in Vt that facilitates Vt dimerization and actin bundling, as observed by cross-linking and electron tomography studies (101, 102, 110, 113). Unlike Vt, MVt cannot bundle actin filaments but can bind to actin failments (76, 82, 92, 100). The ability of vinculin, but not metavinculin, to reorganize actin filaments into bundles indicates that metavinculin and vinculin have distinct functions. Moreover, metavinculin and vinculin are co-expressed in muscles cells, suggesting a coordinate role in muscle cell regulation. Metavinculin contains a 68 amino acid insert in the tail domain, and part of this insert not only replaces the Vt H1 with MVt H1' but also replaces the N-terminus of the MVt (Fig. 3). Other than this difference in the helix bundle, the role of MVt insert is currently unknown. To better understand the unique functions of vinculin and metavinculin, we investigated how these two isoforms directly bind actin using cryo-electron microscopy (cryo-EM). We were able to obtain sub-nanometer-resolution cryo-EM reconstructions of Vt-actin and MVt-actin complex, providing models for both interfaces (99). We then validated the Vt-actin model through mutagenesis. Based on the limited proteolysis data by Durer *et al.* (103) and our experimental data, we proposed that F-actin engagement causes the Vt and MVt helical bundles to undergo a torqueing conformational change, resulting in explusion of Vt H1 and MVt H1' from the helical bundle. These reconstructions show that while Vt and MVt have similar actin-binding interfaces, both proteins undergo structural transitions that lead to differences in actin bundling. The presence of H1 appears to interfere with the ability of metavinculin to bundle F-actin, as its deletion promotes actin filament bundling (95). These observations provide us with a conceptual model in which Vt and MVt partially unfold upon actin-binding, and either the presence or absence of the MVt insert dictates whether dimerization and actin bundling occur.

The cryo-EM reconstruction of Vt-actin and MVt-actin complexes provided us with a valuable insight into how Vt or MVt undergoes a conformational change upon binding to actin. However, as metavinculin is co-expressed with vinculin in muscle tissues (42, 79, 84), it is likely that vinculin and metavinculin coordinately regulate actin filament rearrangement in contractile cells. In fact, we found that the presence of MVt can suppress the actin bundling properties mediated by Vt in our actin cosedimentation assays, providing us with a hypothesis that MVt may negatively regulate the actin bundling properties of Vt. To better understand the role of metavinculin in actin filament assembly, we conducted a series of actin co-sedimentation and negative stain EM experiments in the absence and presence of vinculin. Consistent with our previous findings (99), MVt is unable to induce actin bundling, and the presence of sub-stoichiometric amounts MVt relative to Vt inhibits the assembly of actin filaments into parallel bundles. Furthermore, we investigated whether cardiomyopathy (CM)-associated MVt mutants induce actin bundling either in the presence or absence of Vt. In contrast to wild type MVt, MVt CM mutants (which are all within the MVt insert) induce moderate actin assemblies but not defined parallel actin bundles induced by Vt. To better understand the molecular basis for the ability of MVt to negatively regulate Vt-mediated actin bundling, we performed DMD simulations. Actin binding to vinculin promotes release of H1 from the tail domain helix bundle, exposing an interface in vinculin that promotes dimerization. However, our computational analyses indicates that in the case of metavinculin, the insert forms a higher order structure with H1' that is released from the helix bundle upon actin binding, which occludes actin assembly into parallel F-actin bundles. Our MD simulations also indicate that cardiomyopathy mutations within the metavinulin tail domain, destabilize formation of this higher order structure. Consistent with these observations, the presence of MVt CM mutants failed to inhibit the

formation of Vt-mediated actin bundles. Instead, all three MVt CM mutants, enhanced the fraction of higher order actin assemblies.

Materials and Methods

Cloning and generation of expression constructs

Construct for chicken Vt residues 879-1066 was cloned into pQlinkH vector (Addgene, Cambridge, MA), and the C-terminally GFP-tagged construct VtΔC5-GFP (Vt residues 879-1061 with C-terminal GFP fusion linked by the sequence "GIGSGSNGSSGS") was generated using ligation-independent cloning in the H6-msfGFP vector (Addgene #29725). VtΔC5-GFP construct encodes an N-terminal TEV (tobacco etch virus) cleavable hexa-histidine tag, the linker, and a C-terminal EGFP tag. The N-terminally tagged construct was generated using sequence- and ligation-independent cloning, inserting the open reading frame in-frame after the GFP (GFP-E892-VtΔC5, Vt residues 892-1061 with an N-terminal GFP fusion and no linker sequence). The codon-optimized sequence of human MVt (residues 858-1134) for bacterial expression was synthesized (Geneart), and MVt and MVtΔC5 (residues 858-1129) were sub-cloned into the 2HR-T vector (#29718), which encodes an N-terminal TEV cleavable hexa-histidine tag. MVtp (residues 879-1134) was also generated in 2HR-T vector, and this construct was designed to lack the proline-rich linker region. Plasmids for MVt cardiomyopathy (CM) mutants, A934V, ΔL954, and R975W, were generated using QuikChange site-directed mutagenesis kit (Stratagene) and verified by DNA sequencing (Genewiz). All of the Vt and MVt vectors contain TEV cleagable hexa-histidine tag.

Protein expression and purification

Constructs were transformed into *Escherichia coli* strain BL21 (DE3) and grown at 37 ºC until reaching the optical density of 0.6-0.8 (600nm). Protein expression was then initiated by addition of IPTG (0.5 mM for Vt, 1mM for all MVt constructs). Cells were then grown at 18 ºC overnight and harvested by centrifugation at 4,500 rpm for 30 min. Cell pellets were resuspended in lysis

buffer [20mM Tris, 150 mM NaCl, 5mM imidazole, 2mM β-mercaptoethanol (pH 7.5) for Vt; 50 mM Tris, 200 mM NaCl, 10mM imidazole, 2mM β-mercaptoethanol (pH 8.0) for MVt]. Cells were then lysed by sonication, and the proteins (either Vt or MVt) that remained in the soluble fractions were separated by centrifugation at 15,000 rpm for 45 min. Proteins were purified by using Ni-NTA agarose beads (Qiagen) as they bound to the beads through His-tag. Wash buffer [20 mM Tris, 150 mM NaCl, 60 mM imidazole, 2mM β-mercaptoethanol (pH 7.5) for Vt; 50 mM Tris, 200 mM NaCl, 25 mM imidazole, 2mM β-mercaptoethanol (pH 8.0) for MVt] was run through the column to wash away any impurities bound to the column. Finally, the proteins were eluted using elution buffer [20 mM Tris, 150 mM NaCl, 500 mM imidazole, 2mM β-mercaptoethanol (pH 7.5) for Vt; 50 mM Tris, 150 mM NaCl, 250 mM imidazole, 2mM β-mercaptoethanol (pH 8.0) for MVt] from the column. His-tags from all proteins were removed by dialyzing the eluted volume into TEV cleavage buffer [20 mM Tris, 150 mM NaCl, 50 mM imidazole, 2mM β-mercaptoethanol (pH 7.5) for Vt; 50 mM Tris, 200 mM NaCl, 20 mM imidazole, 2mM β-mercaptoethanol (pH 8.0) for MVt] overnight at 4 ºC in presence of TEV protease. Vt and MVt proteins were then collected by running the dialyzed/TEV-cleaved volume over the Ni-NTA beads again. Size exclusion chromatography was used to purify these proteins further in gel filtration buffer [10 mM Tris, 200 mM KCl, 10 mM imidazole, 2.5 mM $MgCl_2$, 1 mM EGTA, and 2mM DTT (pH 7.5)]. Purifed proteins were concentrated between 200-500 μM by centrifugation and used for experiments.

Actin co-sedimentation assays

The actin binding and bundling properties of individual Vt and MVt WT and CM proteins as well as their mixtures were investigated using an adapted actin co-sedimentation assay previously reported (114). Monomeric actin (G-actin), purified

from rabbit muscle acetonepowder (Pel-Freez Biologicals, Rogers, AR), was stored at − 80 °C in storage buffer [50 mM imidazole, 100 mM NaCl, 10 mM $MgCl_2$, 10 mM EGTA, 0.5 mM DTT, 0.2 mM ATP (pH 7.0)]. Polymerization to filamentous actin (F-actin) was done by diluting and incubating G-actin at 100 μM concentration in actin polymerization buffer [10 mM Tris, 200 mM KCl, 10 mM imidazole, 2.5 mM $MgCl_2$, 1 mM EGTA, 2 mM DTT (pH 7.5)] at room temperature for 30 min. The actin concentrations reported in this work were based on G-actin concentration, since the heterogeneity of F-actin polymers made it difficult to quantify F-actin concentrations. Vt and MVt variants were also diluted by actin polymerization buffer to prepare 100 μM stocks. To assess actin binding, 100 μl samples were prepared containing 10 μM Vt/MVt variants and 10 or 20 μM actin. The samples were incubated at room temperature for 1 h and then centrifuged at 100,000 RCF for 30 min. To assess actin bundling, 100 μl samples were prepared containing 10–20 μM Vt/MVtvariants and 10 μM actin. The samples were incubated at room temperature for 1 h and then centrifuged at 12,000 RCF for 15 min. For both binding and bundling co-sedimentation, the supernatant and pellet were separated, resuspended to equal volumes, and analyzed by 15% SDS-PAGE. Actin binding properties were calculated by determining the fractions of Vt/MVtvariants present in pellets using the densities of the pellet and supernatant bands. Actin bundling properties were calculated by determining the fractions of actin present in pellets using the densities of the pellet and supernatant bands. Densitometry was performed using ImageJ (115). Statistical significances (*p* values) of the measurements were determined using the Microsoft Excel t-Test function.

Negative-stain transmission electron microscopy

An aliquot of actin (1 μM) without or with Vt or MVt (10 μM) was incubated in actin polymerization buffer [10 mM Tris, 200 mM KCl, 10 mM imidazole, 2.5 mM $MgCl_2$, 1 mM

EGTA, 2 mM DTT (pH 7.5)] for 15 min and absorbed directly onto glow-discharged carbon-coated 400 mesh copper grids for 3 min, and then stained with 2% (w/v) uranyl acetate in water. TEM images were obtained using a FEI Tecnai 12 electron microscope at 80 kV and captured on a Gatan First Light CCD camera using Gatan Digital Micrograph software (Gatan, Pleasanton, CA). F-actin and the indicated Vt ± MVt constructs were mixed in KMEI [50 mM KCl, 1 mM $MgCl_2$, 1 mM ethylene glycol bis(*b*-aminoethyl ether) *N*,*N*′-tetraacetic acid (EGTA), 10 mM imidazole, 1 mM dithiothreitol (DTT), pH 7.0)] and incubated at room temperature for 15 min. Sample (4 µl) was then applied to a glow-discharged continuous carbon grid (Ted Pella) and incubated for 60 s. After incubation, the grid was washed with three 100 µl drops of 1% uranyl acetate, then blotted to dryness. Images were acquired with the SerialEM package (116) on a Tecnai F20 operating at 120 kV with a Gatan Ultrascan 4000 CCD camera. Tiled images with 20% overlap were acquired at 7800 × magnification, 3 µm underfocus, and 4-fold camera binning, corresponding to a calibrated pixel size of 5.7 nm at the specimen level. Stitched images were assembled with the "blendmont" program from the IMOD software package (117). This work was done by Muzaddid Sarker, former lab member from Campbell lab, in collaboration with Lindsey M. Constantini fromJack Griffith's lab.

F-actin assembly quantification

Images were thresholded and binarized using ImageJ (115), then segmented into contiguous regions of pixels using the built-in "Analyze Particles" plugin, including regions 100–500,000 pixels in size and with a circularity of 0–0.3. This procedure does not always capture every region that an expert user would designate to contain F-actin in every image. However, we find its performance superior to both manual segmentation of the images, which requires user

decisions on region boundaries and the minimum size of regions, as well as a sliding-box quantification (a measure of local density), which is extremely sensitive to noise introduced by slight differences in thresholding (data not shown).

Size measurements of regions were pooled from all images for a given condition, then divided into 10,000 equally sized bins per data set and plotted via a normalized cumulative histogram. Data were binned and cumulative sums calculated with a python script (available at www.github.com/alushinlab/FactinAssemblyQuant) using the function "binned_statistic" implemented in SciPy (www.scipy.org). Plots were generated and statistical tests were conducted with GraphPad Prism. This work was done by Lin Mei and Santiago Espinosade los Reyes from Greg Alushin's lab.

Molecular dynamics simulation

Modeling was performed using a DMD package (118-120). The initial structure was obtained by extending missing N- and C-termini of MVt (PDB ID: 3JBK) (99) with PYMOL built-in tool to include residues 896–1134. The initial structure was relaxed at temperature $T = 0.5$ with high heat exchange coefficient $C_{ex} = 10$ for 10,000 steps. The temperature unit is kcal/(mol k_B).The relaxation was followed by replica exchange simulations with 10 replicas ($T = 0.330$, 0.360, 0.390, 0.420, 0.450, 0.480, 0.510, 0.540, 0.570, 0.600; $C_{ex} = 0.1$ for 2 million steps). Replicas were exchanged every 1000 steps. To preserve contacts between MVt and actin, we applied harmonic constraints to the N, CA, and C backbone atoms of selected residues (R1044, I1045, N1048, R1055, T1058, I1059, Q1062, I1065, Q1086, E1089, M1090, H1093, N1094, E1104, R1107, E1108, A1111, I1114). These constraints restrict atoms to move within 2A around initial positions. All atoms within actin were considered static and were not allowed to move. The 100

lowest-energy structures were selected and clustered based on pairwise root mean square distance between structures. Two clusters were identified.

Structures representing the centroids of the two clusters were subject to DMD simulations at two constant temperatures $T_1 = 0.5$ kcal/(mol k_B) and $T_2 = 0.55$ kcal/(mol k_B). For each temperature and for each structure, 5 independent simulations were run for 1 million steps with $C_{ex} = 0.1$. To preserve contacts between MVt and actin, we applied harmonic constraints to N, CA, and C backbone atoms of selected MVt residues (as described above). All atoms within actin were considered static. This work was done by Andrey Krokhotin, a former lab member from Nikolay Dokholyan's lab.

Results

Cryo-EM reconstruction of Vt-actin and MVt-actin complex

In collaboration with the Alushin lab, we were able to obtain cryo-EM reonstructions of of both Vt and MVt in complex with F-actin complex. To circumvent the heterogeneity associated with actin bundles formed by Vt, we used a C-terminal truncation mutant (from now on referred to as VtΔC5) that preserves actin binding but disrupts actin bundling (101). I expressed and purified the VtΔC5 and MVtΔC5 proteins used by the Alushin lab for reconstructing the cryo-EM structures of Vt-actin and MVt-actin complexes. Both Vt and MVt have relatively low affinity for F-actin (~0.5 μM) (103, 121), making it technically challenging to fully decorate actin filaments. However, Alushin lab adapted a multi-reference iterative helical real-space reconstruction (IHRSR) (122) scheme that they developed for the study of heterogeneous microtubule specimens (123). They collected and processed a dataset of undecorated F-actin filaments, then subjected either VtΔC5 or MVtΔC5 -bound dataset to a multi-reference IHRSR in EMAN2/SPARX (124, 125) using the sub-stoichiometrically bound and unbound models as references. This resulted in VtΔC5 and MVtΔC5-bound models, in which the segments that contributed to these models were selected for further processing using FREALIGN (126). This produced an 8.5 Å-resolution reconstruction for Vt-actin complex, and likewise produced an 8.2 Å-resolution reconstruction for MVt-actin complex, each showing clearly resolved secondary structures.

Vt undergoes a structural rearrangement upon actin binding by activating H1-mediated bundling via steric mechanism

In Vt-actin complex reconstruction, we observed density for only four out of the five helices within Vt (Fig. 5), possibly due to disengagement of one helix from the bundle upon actin binding. Rigid-body docking of the isolated Vt crystal structure (PDB: 1QKR) (127) quantitatively supported the interaction pose produced using a DMD model our lab previously generated (112), in which helices 4 and 5 constitute the primary actin binding interface. Furthermore, we have performed actin binding and bundling co-sedimentation assays with Vt M898A, a mutant within H1 that is buried in the pre-bound state, reasoning that it would sterically promote H1 release or mediate binding interactions upon being exposed. We found that Vt M898A did not affect actin binding but abrogated actin bundling, suggesting that H1 release upon actin binding is an important second step to in vinculin activation that mediates Vt-mediated actin bundling (Fig. 6). This model suggests that helix 1 disengages from the helical bundle upon actin binding, which is further supported by our mutagenesis studies and that this region is susceptible to proteolytic cleavage upon actin binding by Vt (103).

In addition to the helix 1 displacement, the rigid-body fit of helices 2-5 showed inconsistencies with the density map, including a clash between the N-terminal tip of helix 5 and the actin surface (Fig. 5), suggesting that structural rearrangements occur throughout Vt upon actin binding. To visualize this conformational transition, Alushin lab performed molecular dynamics flexible fitting (MDFF) (128) of Vt residues 917-1047 and actin to generate a pseudo-atomic model of the interface (Fig. 7). Superposition of the crystal structure of Vt (PDB: 1QKR) (127) with the MDFF-derived model reveals a substantial remodeling of the H1 docking site on the Vt helical bundle, primarily produced by a twisting rearrangement of helices 4 and 5 relative

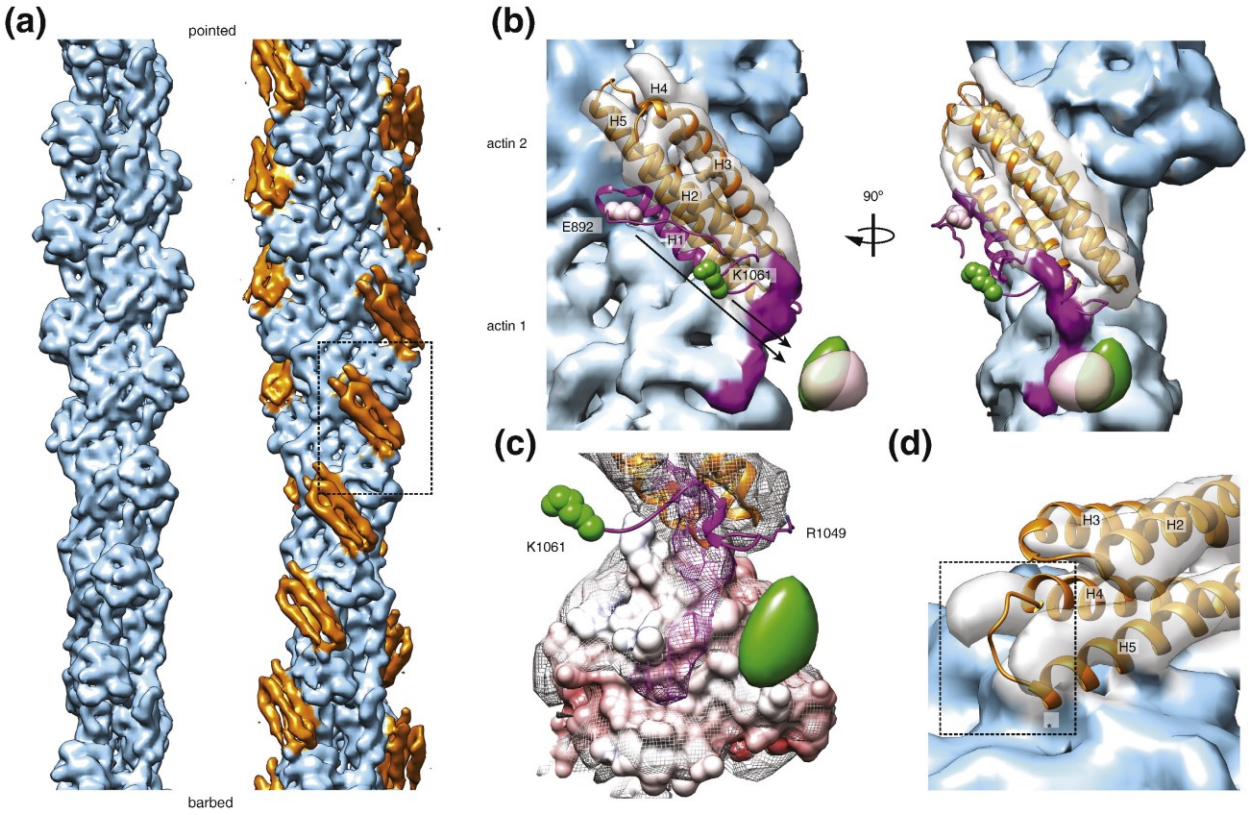

Figure 5. Sub-nanometer-resolution reconstruction of the Vt-actin interface.

(a) Reconstructions of actin alone (left) and actin decorated with VtΔC5 (right). Actin, light blue; Vt, orange. (b) Rigid-body docking of the Vt crystal structure. Helix 1 (H1), which was not visualized, is colored magenta. Cryo-EM densities attributed to actin and Vt by docking analysis are colored blue and transparent gray, respectively. Difference maps of GFP-E892-VtΔC5–VtΔC5 (pink) and VtΔC5-GFP–VtΔC5 (green) are displayed as isosurfaces contoured at 15 σ. The fusion sites for GFP constructs are labeled and displayed in space-filling representation in the same color as the corresponding difference maps. Density tentatively attributed to Vt rearrangements is magenta. (c) Colored as in (b), a view highlighting the density on the actin surface. Actin 1 is displayed as an electrostatic potential surface map, contoured at ± 10 k_BT/e (blue, positive; red, negative). (d) Colored as in (b), a view of the Vt H4–H5 helical hairpin,

which fits the density poorly. Asterisk highlights a clash with the actin surface.Generated by Alushin lab.

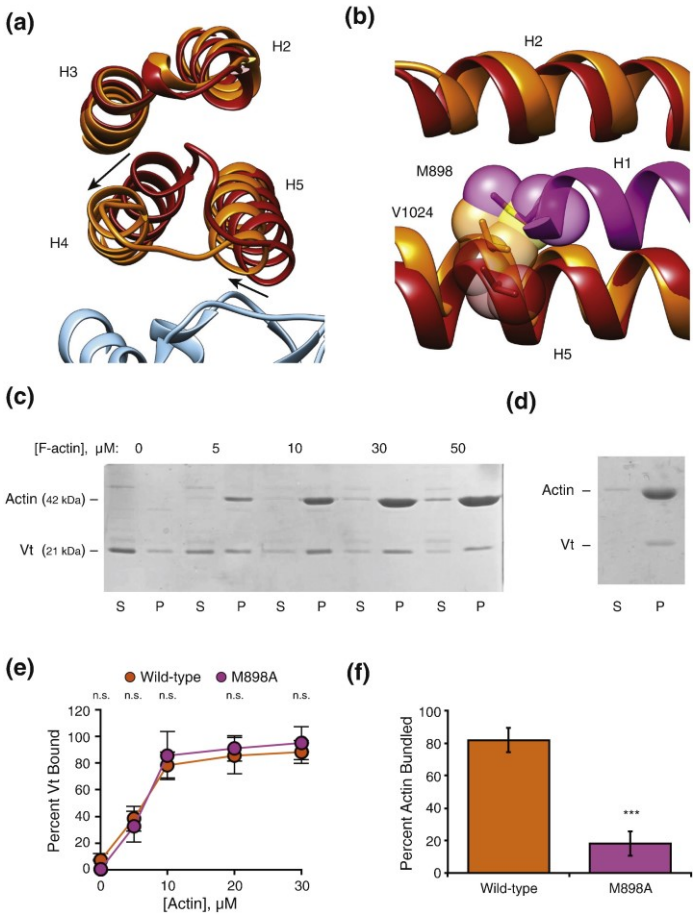

Figure 6. A steric mechanism promotes H1 release to bundle actin.

(a) Superposition of the MDFF Vt model (orange; view from pointed end) with helices 2–5 of the rigid-body docked crystal structure of Vt (PDB ID 1QKR, red). Rearrangement of helices H4 and H5 to relieve clashes with actin (blue). (b) clash of H1 (magenta) residue M898 with V1024 in the actin-bound state. (c) Representative SDS-PAGE of high-speed co-sedimentation assay demonstrates that Vt M898A retains F-actin binding. Vt M898A, 10 μM. S, supernatant, P, pellet. (d) Representative SDS-PAGE of low-speed co-sedimentation assay shows strongly impaired actin bundling of Vt M898A. Vt M898A, 10 μM; actin, 20 μM. S, supernatant, P, pellet. (e) Quantification of (c). Vt wild-type control. Error bars represent SD, $n \geq 3$. N.s., not

significant. (f) Quantification of (d). Wild-type. Actin, 20 μM; Vt, 10 μM. Error bars represent SD, $n \geq 10$. Triple asterisk, $p < 0.0001$ relative to wild-type control, *t*-test. Data generated by Peter Thompson, former Campbell lab member.

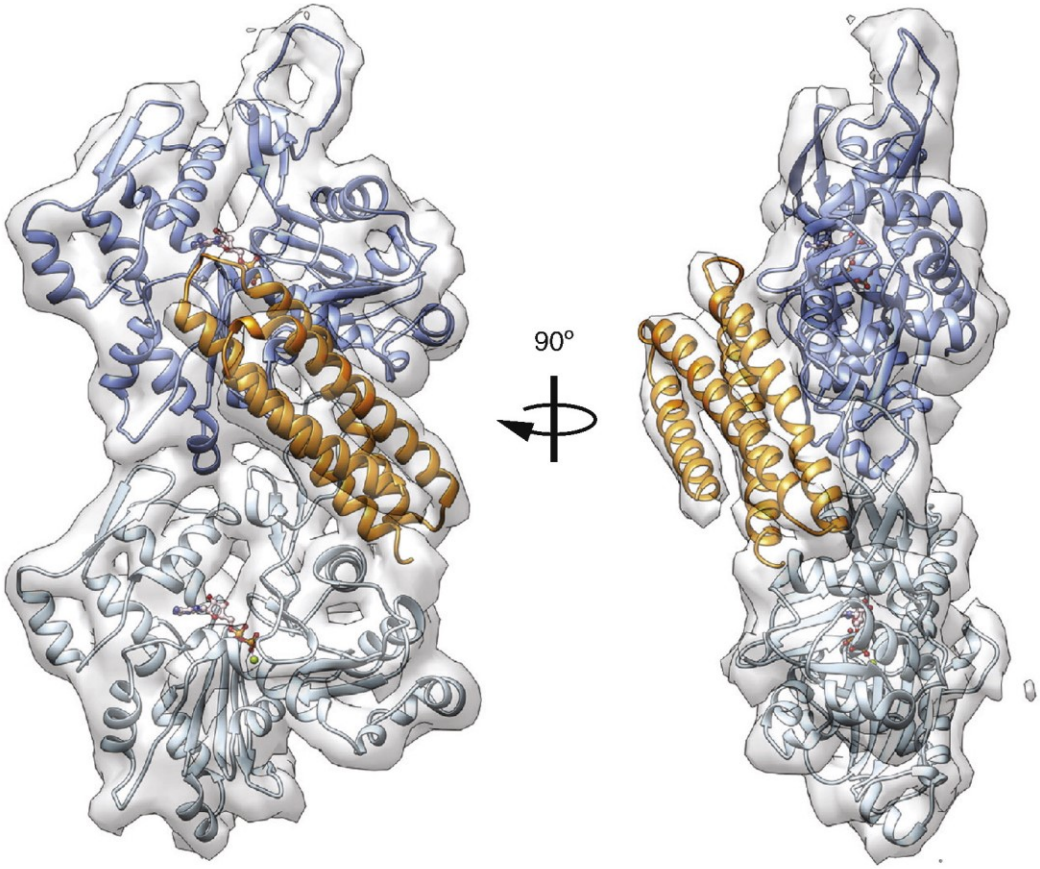

Figure 7. MDFF model of the Vt-actin surface.

The MDFF model (actin 1, light blue; actin 2, dark blue; Vt, orange; ADP, pink) is shown in the segmented density map (transparent gray). Data by Greg Alushin.

to the remainder of the bundle (Fig. 6) upon actin binding. We hypothesized that H1 displacement is necessary for this structural transition to occur as this would generate steric clashes between large inward-facing hydrophobic residues in H1 and the rearranged hydrophobic core of Vt. Thus, we propose a model in which the need to relieve multiple clashes allosterically couples actin binding to H1 release.

MVt undergoes a similar structural mechanism

We also obtained an 8.2 Å-resolution reconstruction for MVtΔC -actin complex (Fig. 4). At sub-nanometer resolution, this reconstruction is indistinguishable from the VtΔC5-bound reconstruction. In contrast to a previous negative-stain reconstruction where extra density was observed protruding from MVt when compared to Vt (98), rigid-body docking of the MVt crystal structure into our sub-nanometer-resolution density map showed that H1' is displaced from the helical bundle when MVt binds actin. This observation is in agreement with the similar proteolysis susceptibility reported for MVt H1' and Vt H1 upon actin binding (103).

MVt WT does not induce F-actin bundling

With this H1' displacement model, we next investigated the effects of MVt CM mutants. However, we first validated our WT Vt and MVt constructs to recapitulate previously reported binding and bundling activities (90, 98, 99, 103). I acquired actin co-sedimentation data with Dr. Muzaddid Sarker for these studies, while the negative-stain EM images were acquired by Dr. Muzaddid Sarker in collaboration with Griffith lab. We first confirmed that there were no significant differences between Vt and MVt in actin binding (Fig. 8), and also reproduced bundling differences between Vt and MVt proteins. We also determined whether the presence of the proline-rich link, that lies adjacent to the tail domain, contributes to higher order actin reorganization in the presence of Vt or MVt. We refer to proline-rich linker

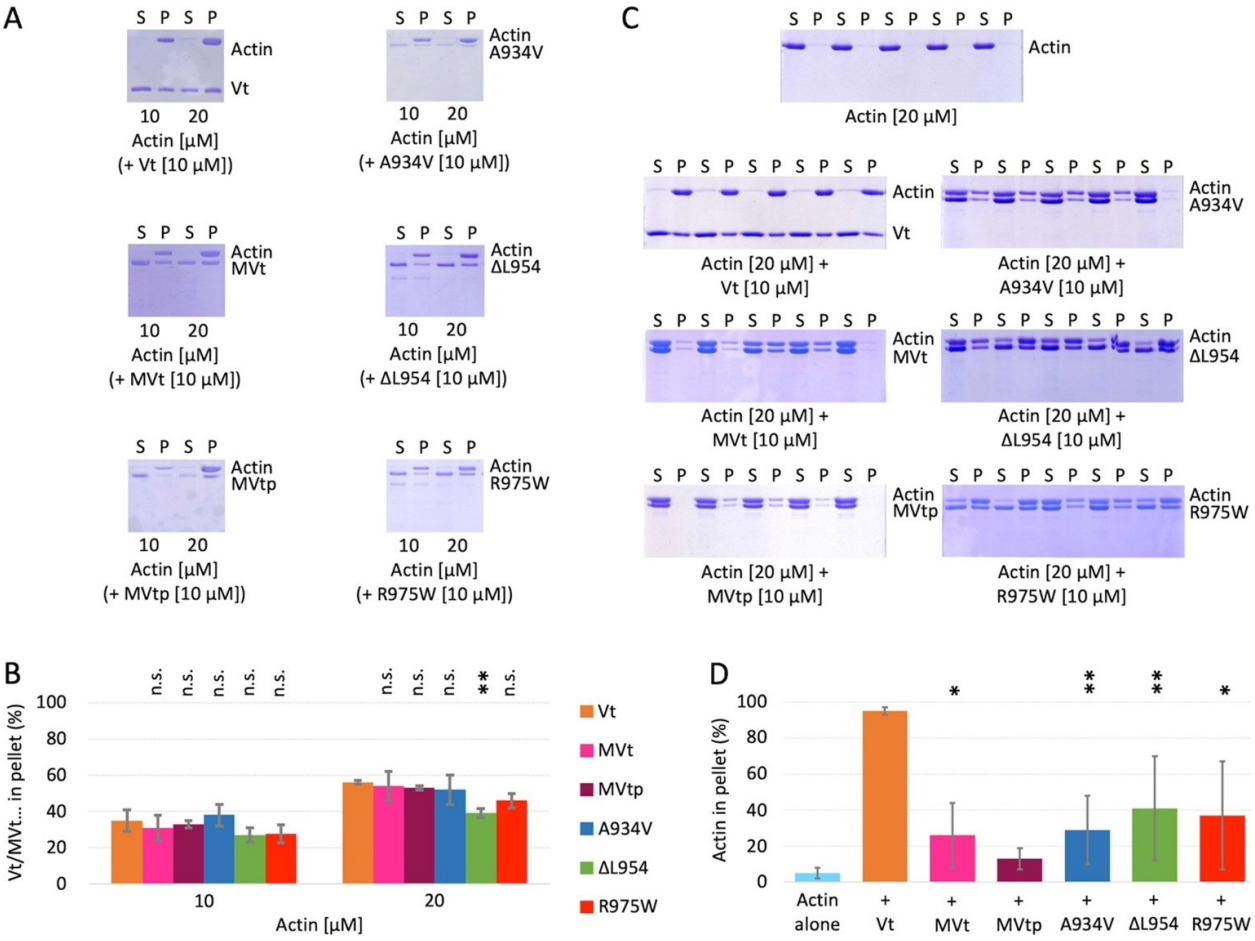

Figure 8. MVt WT and CM mutants exhibit similar actin binding but not crosslinking.

(A) Representative SDS-PAGE results from high speed F-actin co-sedimentation assays in the presence of Vt, MVt, or MVtp WT and CM proteins (S, supernatant; P, pellet). (B) Quantification of protein present in pellets representing individual sub-populations of Vt, MVt, or MVtp constructs bound to F-actin. Error bars represent standard deviation (SD) (n = 3). (C) Representative SDS-PAGE results obtained from low-speed F-actin co-sedimentation assays in the presence of Vt, MVt, or MVtp WT and CM proteins. (D) Quantification of actin fractions in pellets representing sub-populations of F-actin present in bundles or in higher-order assemblies induced by Vt, MVt, or MVtp constructs. Error bars represent SD. Statistical significances in (n.s.), *$p < 0.05$, **$p < 0.01$.

containing MVt as MVtp from here on out. While the actin-alone sample showed single, linear actin filaments, addition of Vt to F-actin induced crosslinking of filaments into parallel bundles as expected, resulting in the formation of thick fibers (Fig. 9). When MVt or MVtp was added to F-actin instead of Vt, F-actin bundling was dramatically reduced, with few observable thick fibers. This is consistent with previous reports by our group and others that MVt does not induce large linear actin bundles like Vt (90, 98, 99, 103), indicating that the MVt insert region prohibits actin-induced MVt dimerization. In addition, inclusion of the proline-rich linker (MVtp) has a minor, slightly decreased actin bundling effect *in vitro*.

MVt CM mutants form higher-order, mesh-like actin assemblies

We next employed F-actin co-sedimentation assays to examine F-actin binding and aggregation activities of MVtp CM mutants, including A934V, ΔL954, and R975W. First, we compared the F-actin binding of MVtp WT and CM mutants relative to Vt. Samples containing actin (10 or 20 μM) and either Vt or MVt variants (10 μM) were subjected to high-speed centrifugation to determine actin binding properties. Under these conditions, the supernatant (S) contains unbound Vt or MVt variant while the pellet (P) contains F-actin and bound protein. The percent of protein bound to F-actin were determined by SDS-PAGE (Fig. 8) and were quantified by ImageJ (115). All MVtp CM mutants, as well as the WT Vt, MVt, and MVtp, showed similar binding affinity to F-actin (Fig. 8). From these data, we demonstrate that MVt mutations do not impair F-actin binding, consistent with the distal location of the the mutations/deletions from the actin binding site.

After observing that MVtp CM mutants do not affect F-actin binding, we next performed low-speed centrifugation assays to assess whether F-actin cross-linking activities of MVtp CM

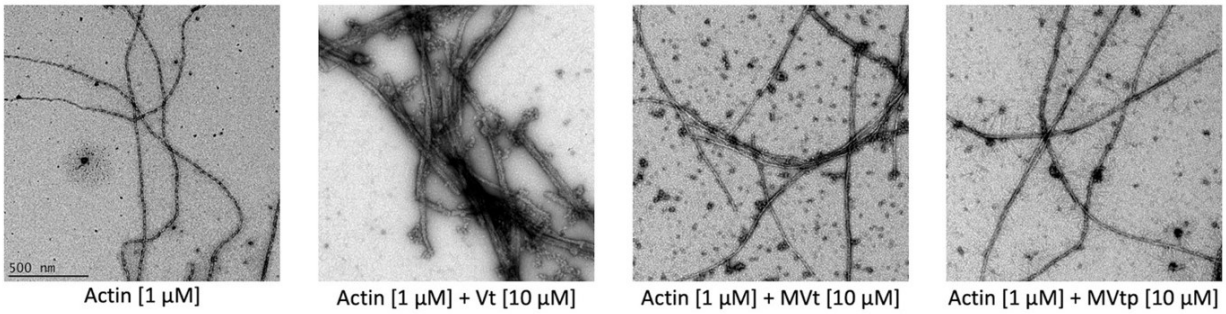

Figure 9. MVt exhibits reduced F-actin bundling (crosslinking) compared to Vt.

Negative-stain EM images of actin filaments. Micrographs are acquired at the same magnification (scale bar represents 500 nm, shown in the left panel). Crosslinking or bundling of actin filaments by Vt generates thick fibers. In contrast, MVt and MVtp do not promote actin filament bundling. Data by Muzaddid Sarker and Griffith lab.

mutants are altered compared to WT Vt, MVt, and MVtp. With the low-speed centrifugation assay, only large cross-linked F-actin and bound proteins are pelleted, while individual actin filaments remain in the supernatant. The fraction of actin present in the pellet was quantified to determine the amount of higher-order assemblies in these mixtures (Fig. 8). With F-actin alone, only ~5% was found in the pellet. However, when Vt was added, almost all of the F-actin (~95%) was found in the pellet (Fig. 8). The amount of actin found in the pellet dramatically reduced when MVt was added (~26%) and reduced even further when MVtp was added (~13%) (Fig. 8). Significantly, there was an increase in the amounts of pelleted actin when MVtp CM mutants were added. MVtp A934V increased the amount of pelleted actin to ~29%, ΔL954 to ~41%, and R975W to 37% (Fig. 8). Even though the low-centrifugation assay is typically used to assess F-actin bundling activity, pellets from this assay may contain both thick bundled actin fibers but also other large disordered actin structures. Because low-speed centrifugation assay is not sufficient to visualize the type of actin assemblies that pellet in the presence of MVt CM mutants, we additionally employed negative-stain EM in parallel. The negative-stain EM data were found to be consistent with the actin co-sedimentation data (Fig. 10). We observed a significant increase in assemblies in the presence of CM mutants MVtp A934V, MVt ΔL954, and MVt R975W, with R975W having the most dramatic effect, in accordance with the severity of disease caused by this mutation in patients. Examination of the images shows primarily an irregular, mesh-like organization of actin filaments, unlike the majority species present as linear bundles formed in the presence of Vt.

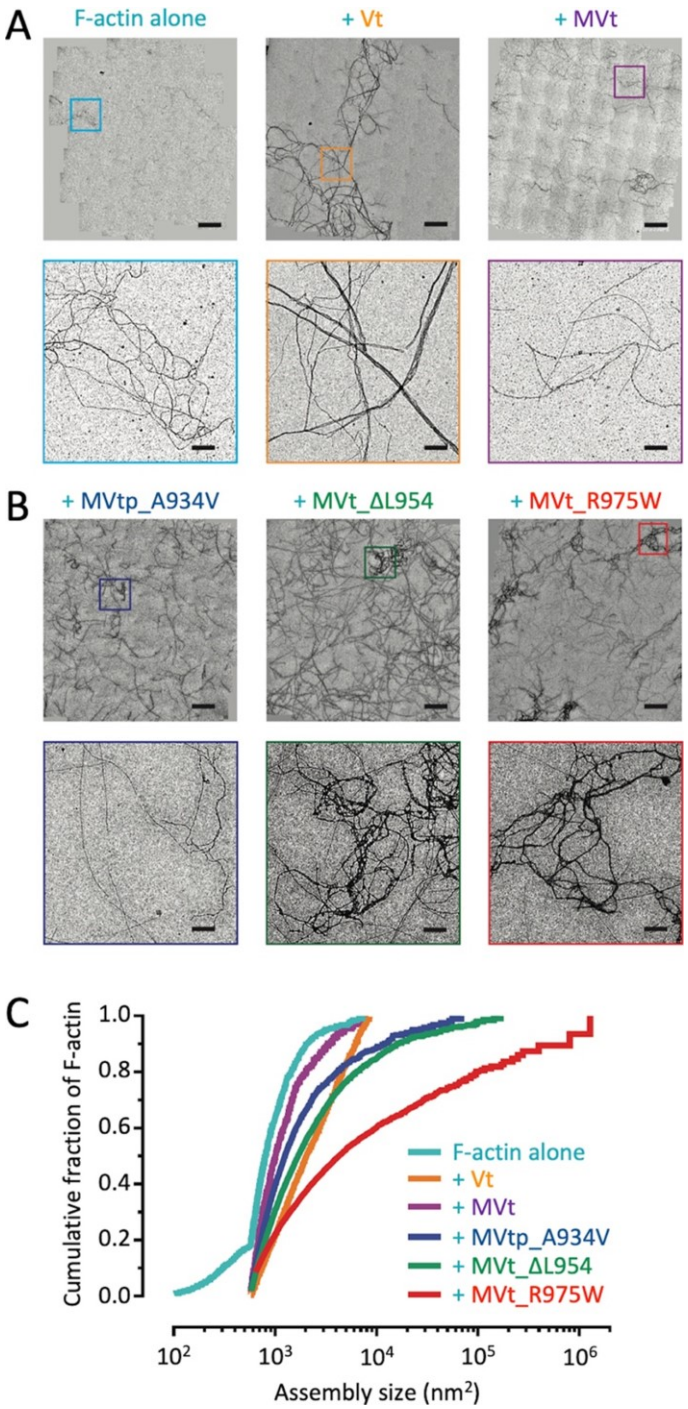

Figure 10. MVt CM mutants promote disordered, mesh-like F-actin assemblies.

(A) Stitched negative-stain EM images of F-actin alone and in the presence of WT Vt and MVt proteins (bars = 10 μm). Zoomed views of the boxed regions are shown in the bottom panel (bars = 1 μm). (B) Stitched negative-stain EM images of F-actin in the presence of MVt or MVtp proteins featuring CM mutations (bars represent 10 μm). Zoomed views of the boxed regions are

shown (bars = 1 μm). (C) Cumulative plots of F-actin assemblies from the indicated conditions. Pairwise comparisons show all distributions to be significantly different (KS test, $*p < 0.01$). $N \geq 10$ fields and $n \geq 764$ regions were quantified for each condition. F-actin, 0.5 μM; Vt/MVt/MVtp constructs, 2.0 μM.

MVt WT inhibits Vt-mediated actin bundling

As mentioned above, while Vt can bundle actin *in vitro*, MVt lacks the ability to bundle actin (90, 98, 99, 103). As metavinculin is co-expressed with vinculin at sub-stoichiometric levels under physiological settings, we next investigated higher order actin network organization in the presence of both WT Vt and MVt. Our observations that MVt H1′ and Vt H1 are released upon actin binding and that H1 mediates Vt's actin bundling activity suggest the following: MVt H1′, which differs in sequence from Vt H1, fails to promote MVt dimerization upon actin engagement. Interestingly, the H1 sequence is nevertheless present in our MVt construct, suggesting that the presence of H1′ inhibits the ability of released H1 to mediate MVt interactions. Here, we used MVtp for the purposes of our study. To determine the effect of MVtp on Vt-mediated actin bundling, we perfomed low-speed actin centrifugation assay and found that adding increasing amounts of MVt to constant amounts of Vt and actin decreased the amounts of Vt-mediated actin bundles (Fig. 11). This result suggests that MVtp can inhibit Vt-mediated actin bundling, consistent with the findings from Durer *et al.* (103).

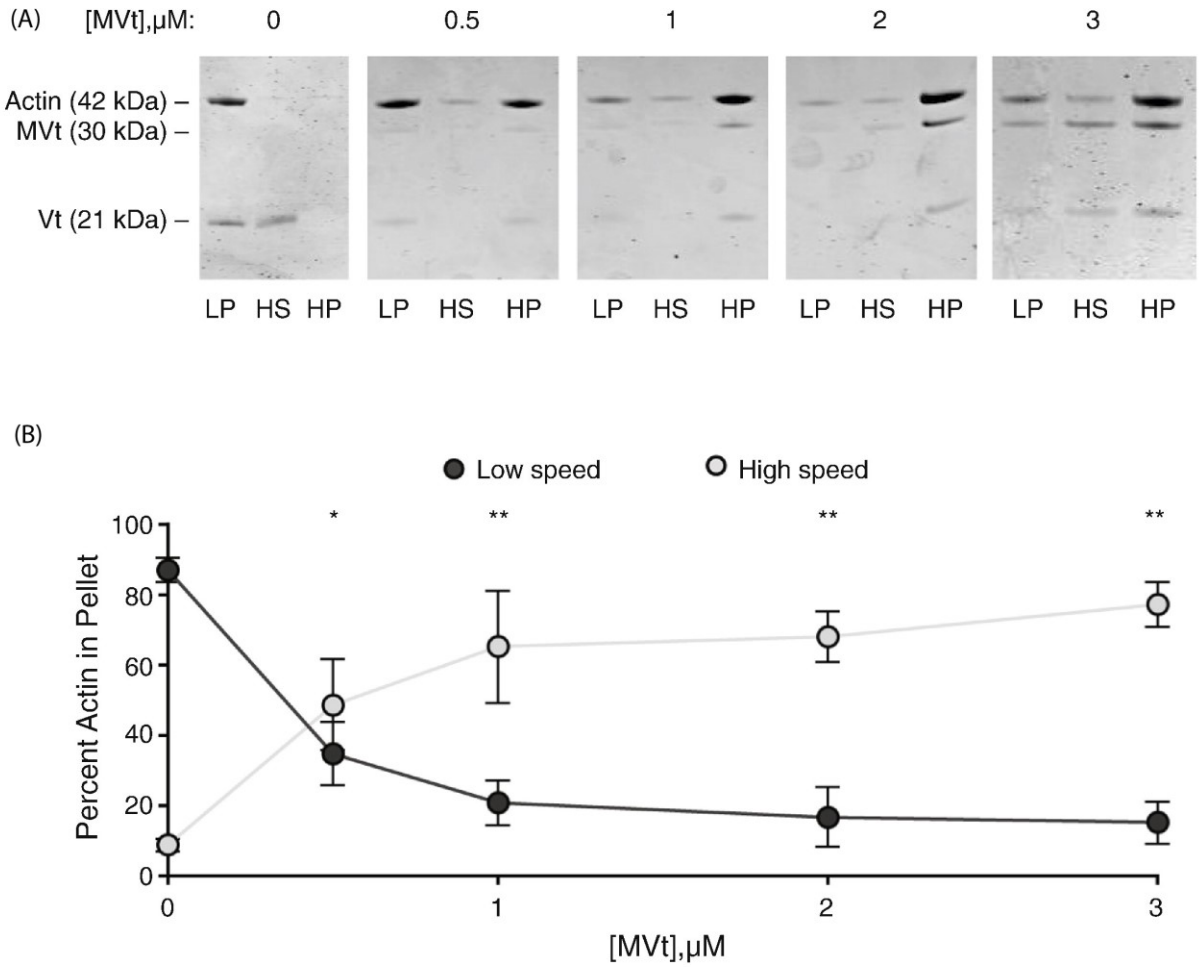

Figure 11. MVt WT inhibits Vt-mediated actin bundling.

(A). Representative SDS-PAGE analysis of differential centrifugation assays of 3.0 μM actin in the presence of 3.0 μM Vt and the indicated amounts of MVt. (B). Quantification of (A). Error bars represent SD, n=3. Single asterisk, $p < 0.05$; double asterisk, $p<0.01$, t-test *versus* Vt alone. All co-sedimentation assays were performed with full-length MVt and Vt constructs.

MVt CM mutants fail to inhibit Vt-mediated actin bundling

Given our finding that addition of WT MVtp at sub-stoichiometric levels relative to Vt inhibits Vt-mediated actin bundling, we next examined the effect of MVt or MVtp CM mutants on Vt-induced actin bundling. We employed low-speed actin pelleting assays to probe the effects of MVt or MVtp CM mutants in comparison to MVt WT, on Vt-induced F-actin assemblies. Three sets of actin co-sedimentation data were acquired, with 20 μM actin and Vt:MVtp at 5:5, 10:10, and 10:5 μM (Fig. 12). In the presence of WT MVt, we observed a proportionate reduction of Vt-induced F-actin assemblies as expected. We found ~47-52% F-actin in the pellet for Vt:MVt at 1:1 and ~74% F-actin in the pellet for Vt:MVt at 2:1, as opposed to 95% F-actin in the pellet for Vt alone. Interestingly, for all 3 MVt or MVtp CM mutatns, almost all of F-actin was found in the pellet fractions at both 1:1 and 1:2 ratios. We observed ~87-95% F-actin for A934V, ~81-90% for ΔL954, and ~84-89% for R975W. These results indicate that unlike WT MVt, MVt or MVtp CM mutants fail to negatively regulate higher-order actin assemblies in the presence of Vt.

In parallel with the actin co-sedimentation assays, negative-stain EM data additionally showed that higher-order assemblies are formed in the presence of both Vt and MVtp variants. Consistent with our actin co-sedimentation assays, we find that the presence of MVt WT inhibits the bundling activity of Vt at both 1:3 (MVt:Vt) and 1:1 (MVt: Vt) ratios while the presence of MVt or MVtp CM mutants dramatically increases the size of F-actin assemblies formed in the presence of Vt at both ratios (Fig. 13). The Vt and MVt or MVtp CM mutant negative-stain EM data complement the co-sedimentation data and indicate that larger actin assemblies are formed than in the presence of Vt alone.

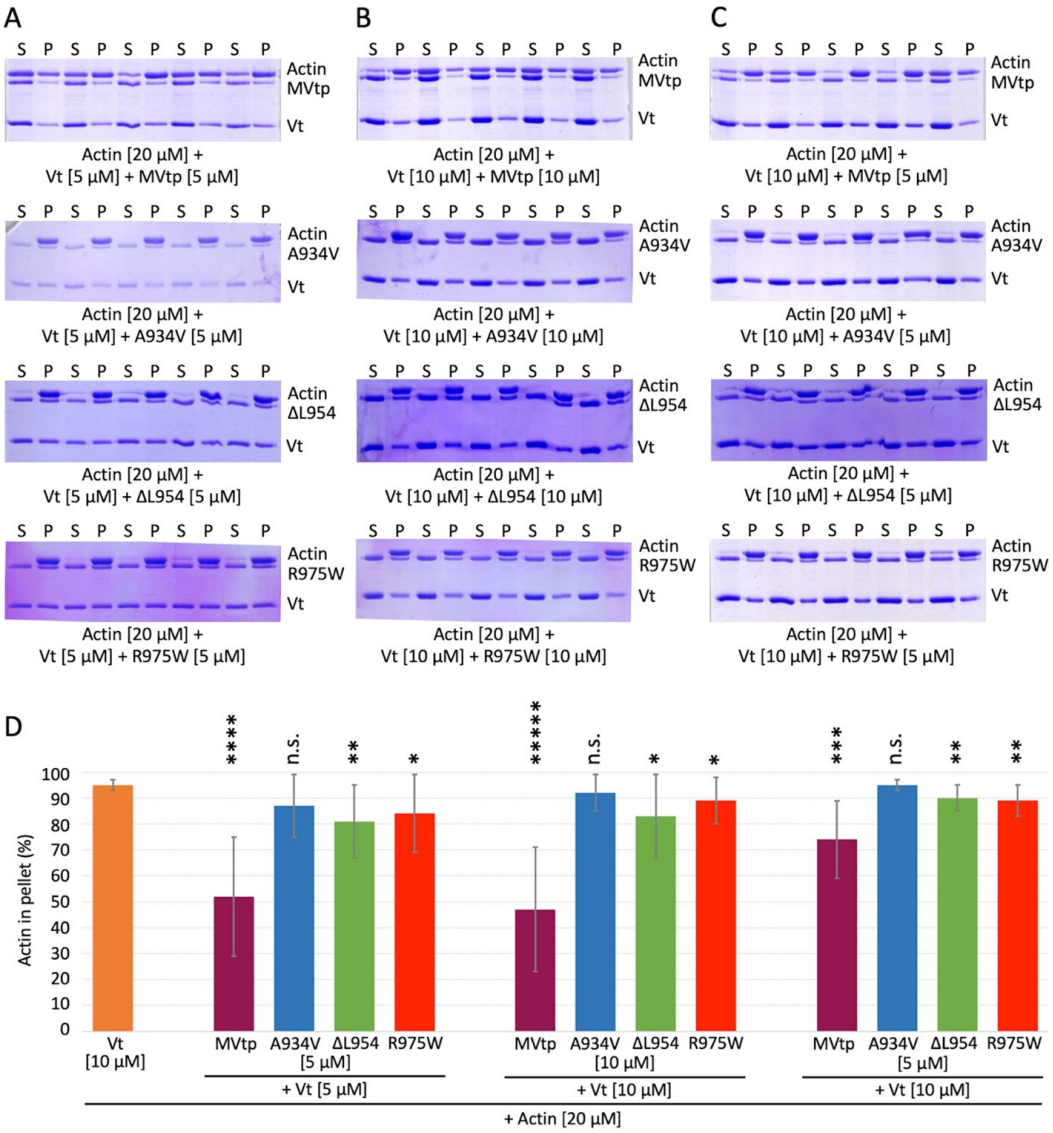

Figure 12. MVt CM mutants fail to inhibit Vt-induced F-actin bundling.

(A–C) Representative SDS-PAGE analysis of low-speed F-actin co-sedimentation assays incubated with Vt in the presence of MVtp WT protein (labeled as MVtp) or MVtp CM mutants at indicated concentrations (S, supernatant; P, pellet). (D) Quantification of the actin present in pellets representing higher-order F-actin assemblies that include F-actin bundles in case of Vt. Error bars represent standard deviation (SD) (n = 2, 5 replicates for each n). Statistical significances in panel D are indicated by the following: non-significant (n.s.), $*p < 0.05$, $**p < 0.01$, $***p < 0.001$, $****p < 0.0001$, $*****p < 0.00001$ with respect to Vt.

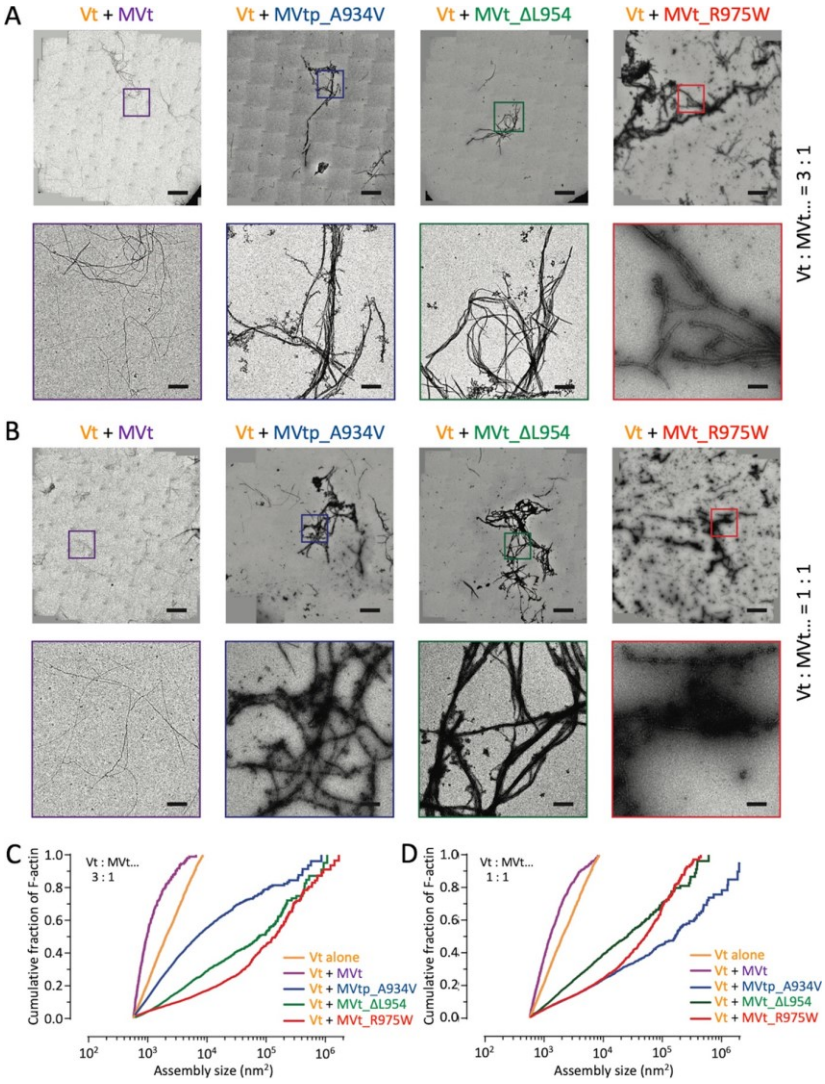

Figure 13. MVt CM mutants aggregate Vt-induced actin bundles.

(A) Stitched negative-stain EM images of F-actin in the presence of Vt + WT or CM mutant MVt(p) at Vt to MVt(p) ratio of 3:1 (bars=10 μm). Zoomed views shown in the bottom panel (bars=1 μm). F-actin 0.5 μM, Vt 3.75 μM, and MVt(p) 1.25 μM. (B) Stitched negative-stain EM images of F-actin in the presence of Vt + WT or CM mutant MVt(p) at Vt to MVt(p) ratio of 1:1 (bars=10 μm). Zoomed views shown in the bottom panel (bars=1 μm). F-actin 0.5 μM, Vt 2.5 μM, and MVt(p) 2.5 μM. (C) Cumulative plots of F-actin assemblies in the presence of Vt to MVt(p) at ratio of 3:1. (D) Cumulative plots of F-actin assemblies in the presence of Vt to MVt(p) at ratio of 1:1. (KS test, $p < 0.0001$) in panels C and D.

DMD suggests that MVt-specific insert region forms an additional sub-domain upon actin binding

To gain further structural insight into rearrangements associated with MVt-actin interaction, we worked in collaboration with the Dokholyan lab. Using a single MVt including residues 896-1134 bound to an actin homodimer (F-actin) as the starting point (PDB: 3JBK) (99), DMD simulations were performed using replica exchange for 2 million steps. One hundred minimal energy structures were selected and clustered. Through this method, two clusters were identified (Fig. 14), with different N- and C-termini conformations. While structures from the first cluster have tightly intertwined N- and C- termini (Fig. 14), structures from the second cluster show the C-terminus interacting with the surface of F-actin (Fig. 14). Both clusters form a new additional structural sub-domain protruding outwards from F-actin. The structures were subjected to DMD simulations and appeared to be stable throughout the simulations, further supporting the protruding MVt sub-domain formation upon actin engagement. Therefore, we hypothesize that this sub-domain mediates unique biological functions of MVt relative to Vt, such as the inability to produce F-actin bundles and the ability to suppress Vt- mediated F-actin bundling. As the MVt CM mutants fail to inhibit Vt-induced actin bundling, we hypothesize that the CM mutations within the insert impair formation of the protruding structure. Further supported by our simulations studies, we predict that the MVt CM mutations destabilize the folded sub-domain (Fig. 14) and consequently fail to antagonize Vt-induced actin bundling.

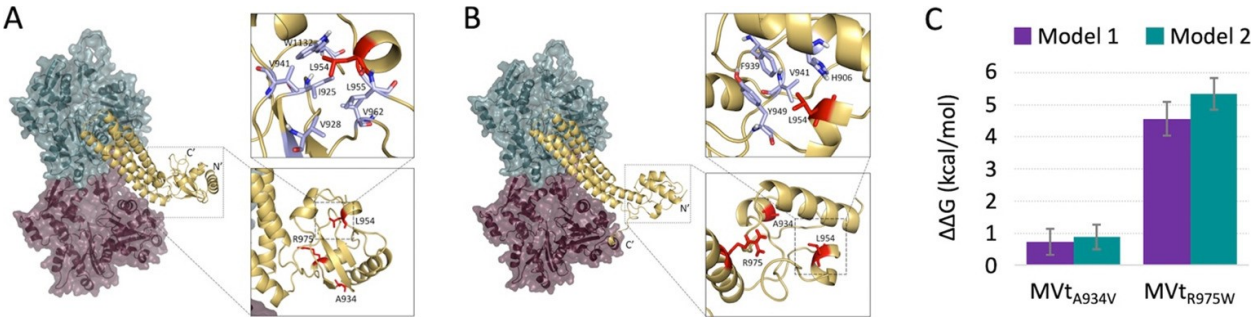

Figure 14. Actin binding to MVt may induce a formation of protruding structure.

Actin binding to MVt may induce a higher-order structural element that prevents F-actin bundling. DMD simulations identify two distinct MVt–actin clusters. In contrast to Vt, actin binding to MVt induces a protruding sub-domain. Representative MVt and F-actin models show that additional structure is formed between N-terminus, insert, and C-terminus in the first cluster (A) and between N-terminus and insert in the second cluster (B). MVt residues mutated in CMs (A934, L954, R975) are colored red. Point mutations A934V and R975W cause an increase in ΔΔG (D) and thus destabilize the folded sub-domain. These findings suggest that MVt CM mutants fail to antagonize Vt-induced actin bundling due to destabilization of the additional folded structure.

Discussion

Using cryo-EM, molecular modeling, and complimentary biochemical techniques, we have produced detailed models of the critical interactions between F-actin, vinculin, and metavinculin. First, our cryo-EM reconstructions of Vt-actin and MVt-actin show that both H1 and H1', respectively, are unfurled upon binding to F-actin. This finding adds an additional layer to the vinculin activation mechanism. After the interaction between Vh and Vt is disrupted, H1 must also be disengaged to license the Vt actin interaction. Although our data do not discriminate between H1 released followed by actin binding or *vice versa*, the steric incompatibility between the H1-docked state and the actin-bound state and NMR data suggesting that H1 undergoes conformational exchange in the isolated Vt (129) support the former model. Furthermore, vinculin sustains substantial tensile forces in adhesions *in vivo (77)*, and a previous study demonstrated that vinculin is, on average, oriented along the dorsal-ventral axis of an adherent cell with the Vh domain closer to the ventral surface (27). These data suggest that a vinculin molecule bound to both talin via Vh and actin by Vt will experience tensile forces in geometry that will favor the undocking of H1 from the Vt bundle. Based on this geometry, we hypothesize a mechanism where vinculin can reinforce adhesion in response to force. We speculate that if H1 is in equilibrium between the docked and undocked states, the presence of tension will favor H1 undocking and by extension, actin binding and bundling, further increasing the adhesion-cytoskeleton linkage (Fig. 15).

Next, we found that MVt suppressed actin bundling by Vt, suggesting that metavinculin may tune actin bundling by vinculin in highly contractile tissues. It is interesting to note that vinculin is ubiquitously expressed in all cell types but metavinculin, only other vinculin isoform, is expressed in smooth and cardiac muscle cells. Both of these cell types are highly contractile,

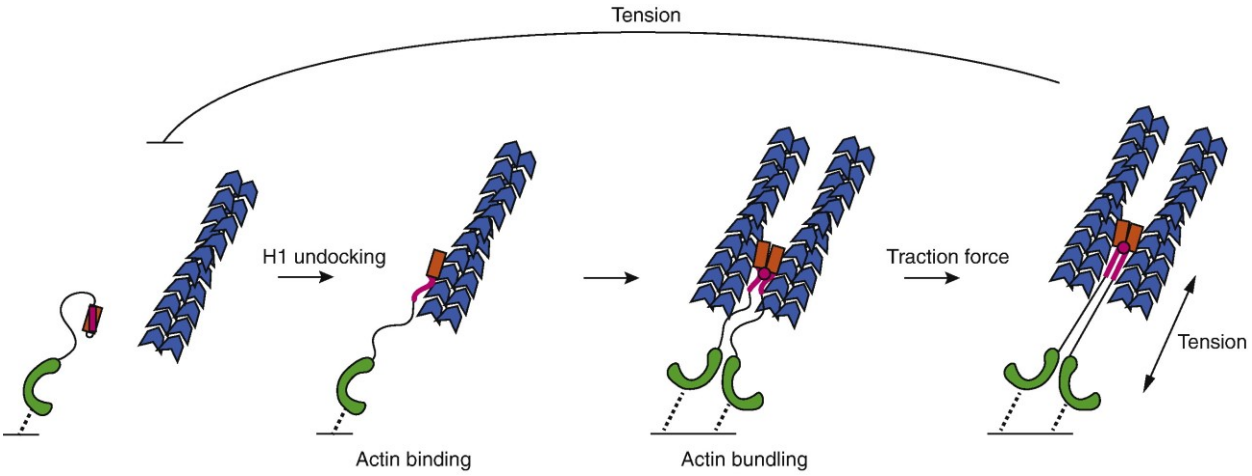

Figure 15. Model of vinculin activation and tension reinforcing actin engagement.

Upon entering an adhesion, the interaction between Vh (green) and Vt (orange) is broken by engaging multiple binding partners (not diagrammed). The linkage between Vh and the plasma membrane (black line) occurs through multiple layers of binding partners (e.g. talin, integrin, schematized as a broken line, not to scale). H1 (magenta) must undock from the Vt bundle for Vt to engage actin. After actin binding and H1 release, Vt is capable of bundling actin (note: the detailed structure of the actin-induced Vt dimer structure remains unknown; magenta circle indicates an interaction). In this configuration, tension across the vinculin molecule will prevent H1 from re-docking, reinforcing actin binding and bundling.

and metavinculin expression increases corresponding to the contractile load on the tissue (83, 84). Cardiomyocytes especially undergo rapid contraction and expansion as the heart beats. Based on these observations, we suggest that the presence of vinculin alone may cause the heart muscle to become stiff due to a large network of thick F-actin fibers, preventing the necessary contractile properties. Co-expression of metavinculin may be therefore necessary to regulate the vinculin-actin bundling so that cardiac cells remain flexible and functional. This hypothesis is further supported by our finding that MVt CM mutants are dysfunctional in suppressing the actin bundling by Vt.

We speculate that Vt H1 could mediate bundling contacts between Vt molecules after actin binding and further suggest that released H1' and the upstream disordered sequence in MVt are important for MVt's inhibitory activity by unknown mechanisms. As MVt CM-associated point mutants are located within the insert, either within H1' or very close to the N-terminus of H1', but distal from the direct actin binding regions of H2-H4, we hypothesize that these mutations would compromise MVt's regulation of Vt-mediated actin bundling without disrupting actin binding. Our results are in support of this model and accordingly, through actin co-sedimentation assays and negative-stain EM, we found that all of the MVt CM mutants have a defect in regulating Vt's actin bundling activity, in contrast to WT MVt, but are not impaired in actin binding. Mechanistically, we propose a steric occlusion model for metavinculin's ability to negatively regulate vinculin-induced actin bundling in sub-stoichiometric amounts, mediated by the formation of MVt sub-domain upon actin binding. Our simulation studies suggest that MVt insert coordinates the folding of a protruding globular sub-domain upon actin binding, as this induces a release of H1' and upstream sequences from the rest of the MVt helix bundle. While the detailed structure of the Vt-dimer that promotes 3D actin bundles is unknown and remains an

important subject for future studies, electron tomographic studies of Vt-induced 2D F-actin arrays on lipid monolayers suggested that filaments are very tightly apposed when cross-linked by Vt (110). We therefore propose that MVt sub-domain acts as a steric block that prevents another actin-bound Vt from coming in closer range, which would then prevent Vt-mediated actin bundling (Fig. 16).

Further in support of this model, our computational studies demonstrate that MVt CM mutants destabilize the MVt sub-domain formation, which would remove the steric block to actin-bound Vt and promote actin bundle formation (loss of function). However, it is important to note that the MVt sub-domain steric block model can only partially explain the effect MVt CM mutants have on actin network reorganization. Though not obvious through actin co-sedimentation assay, negative-stain EM results revealed that all MVt CM mutants had a gain-of-function effect where they induced an increase in the formation of higher-order F-actin assemblies (Fig. 10), with a disordered, mesh-like morphology. Also, our studies suggest that the MVt CM mutants additionally drive the coalescence of Vt-induced bundles into aberrantly large assemblies (Fig. 13). We hypothesize that MVt CM mutants stimulate aggregation of actin through the MVt insert region that would be exposed due to defects in sub-domain folding (Fig. 16).

While our biochemical and structural studies have focused on the three main components, Vt, MVt, and F-actin, vinculin is a scaffold protein that interacts with a number of ligands under physiological settings. Hence, the presence of metavinculin in conjunction with vinculin may not only affect their interactions with actin and each other, but also with other ligands. This is a complicated problem that will require additional studies, as these additional interactions could affect localization, formation of structural assemblies, and mechanotransduction properties.

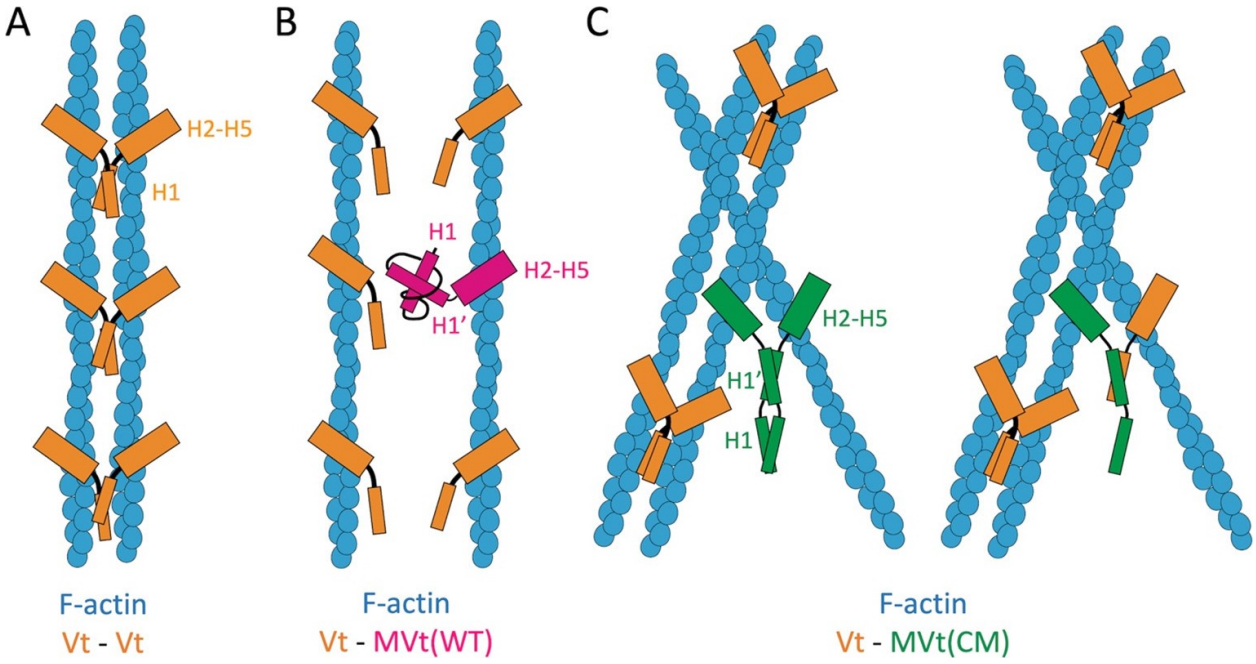

Figure 16. Model for how MVt WT and CM mutants affectVt-induced actin bundle.

Model for inhibition of Vt-induced F-actin bundle by MVt WT but failure of that by MVt CM mutants. (A) Release of H1 upon F-actin engagement enables Vt dimerization, thus resulting in parallel F-actin bundle formation. (B) An additional protruding structural sub-domain formed by the insert and displaced H1 at the N-terminus of MVt WT blocks homo- or hetero-dimer formation with Vt, thus preventing F-actin bundling. (C) The protruding sub-domain is destabilized by the CM related mutations in MVt CM , resulting in disordered F-actin assemblies due to alternative interactions with another subunit of MVt CM (left) or a subunit of Vt (right).

CHAPTER 3 – Vinculin and Metavinculin Exhibit Distinct Effects on Focal Adhesion Properties, Cell migration, and Mechanotransduction

Introduction

Vinculin (Vcn) is an essential, ubiquitously expressed cytoskeletal protein that localizes to focal adhesions (FAs) and adherens junctions (73, 130). It acts as a scaffold to link transmembrane proteins to actin filaments and plays a key role in cell adhesion, motility, and force transmission between cells and the cell-matrix interface. *Vcn* knockout mouse embryos do not survive past E10 and exhibit cardiac and neural tube developmental defects (43). Additionally, *Vcn* null murine embryonic fibroblasts (MEFs) exhibit a more rounded morphology, increased motility (43, 44) and resistance to apoptosis and anoikis (45). At the molecular level, Vcn is comprised of a large ~90 kD head domain, a flexible proline-rich linker, and a tail domain (46). As part of its scaffold function, Vcn engages a number of cytoskeletal and adhesion proteins as well as phosphatidylinositol 4,5-bisphosphate (PIP_2). The Vcn head interacts with talin at FAs, α-catenin at cell-cell junctions, and α-actinin at both cellular locations (47-49, 131). The proline-rich linker that connects Vcn head to Vcn tail can bind to a number of cytoskeletal proteins including VASP, vinexin, CAP/ponsin and the Arp2/3 complex (50-53). Vcn tail directly binds to filamentous actin (F-actin) (54), PIP_2 (55), paxillin (132, 133), and Raver1 (56). Autoinhibitory interactions between the Vcn head and tail promote a closed inactive state, which obscures ligand-binding sites available to other interacting proteins (46). Although mechanisms of activation are not fully understood, it is believed that engagement of talin or α-catenin to Vcn head in conjunction with binding of additional ligands such as actin (47, 72, 73), post-translational modifications (74), and/or

mechanical tension (75-78), promote Vcn activation and scaffolding function by exposing multiple ligand binding sites.

Metavinculin (MVcn) is a larger splice isoform of Vcn that is selectively expressed in smooth and cardiac muscle cells and at low levels in platelets (42, 79, 81). MVcn is expressed at sub-stoichiometric levels relative to Vcn (9-42%), and its expression correlates with the elevated contractile needs of these muscle cells (83, 84). Complete knockout or heterozygous inactivation of the *Vcn* gene is associated with dilated cardiomyopathy in mice (93, 94), while reduced MVcn expression is also associated with dilated cardiomyopathy (DCM) and disorganized intercalated disc structures in humans (89). Point mutations in MVcn have also been identified in patients with DCM and hypertrophic cardiomyopathy (HCM) (89-91). While A934V and ΔL954 MVcn mutations are associated with DCM (90), an R975W mutation has been identified in patients with both DCM and HCM (91). Both DCM and HCM are diseases of the myocardium that diminish blood flow within the heart due to reduced force transmission.

MVcn and Vcn structurally share the same head domains (95, 96); however, their tail domains differ. Vcn tail domain possesses an N-terminal strap followed by a 5-helix bundle and C-terminal hairpin (46), while the MVcn tail domain contains an additional exon that encodes a 68 amino acid insert (79). While MVcn tail has a 5-helix bundle fold similar to Vcn tail, the sequence that makes up the helix 1 (H1) and strap of Vcn tail is displaced in the MVcn tail by homologous sequences, which we term H1', contained within this insert (95) (Fig. 3). Similar to Vcn tail domain, MVcn tail directly binds F-actin (95, 98, 99) but unlike Vcn tail domain, MVcn tail does not bundle filamentous actin into higher order structures *in vitro* (90, 98-100). However, as MVcn and Vcn are co-expressed in muscle tissues (42, 79, 84), it is likely that they coordinately

regulate actin filament organization. In fact, we and others have previously observed that the presence of MVcn tail at sub-stoichiometric ratios impairs Vcn tail-mediated F-actin bundling (99, 103), suggesting that MVcn tail may negatively regulate Vcn tail-mediated actin bundling.

While these differences in the ability of MVcn tail and Vcn tail to independently and coordinately reorganize actin networks have been observed *in vitro*, the field currently lacks a comparison of MVcn and Vcn in a cellular context. To investigate whether these two isoforms regulate distinct cellular functions, we stably expressed either MVcn or Vcn in a *Vcn*-null MEF background and compared FA properties, cell migration, and cell reinforcement to external force. Though we initially sought to use smooth muscle or cardiac cells as a system of comparison, the difficulty in maintaining and controlling for MVcn expression in cell culture prevented us from using those cells. In smooth and cardiac muscle cells, MVcn loses expression in cell culture unless the contractile environment is mimicked properly (84). On the other hand, the *Vcn*-null MEF background allowed us to manipulate the expression levels of either Vcn or MVcn. We find that MVcn expression can fully rescue cell area and partially rescue FA number per cell. However, compared to Vcn-expressing cells, MVcn expression leads to larger individual FA area, faster cell migration, and decreased cell stiffening in response to external force. Our results suggest both overlapping and distinct cellular functions for MVcn and Vcn.

Materials and Methods

Cell Culture

WT MEFs and Vcn-null MEFs were a gift from Dr. Brent Hoffman (Duke University), originally from Drs. Ben Fabry and Wolfgang Goldmann of the Erlangen Biophysics Group at the University of Erlangen-Nuremberg in Germany (134). Human embryonic kidney (HEK) 293T cells were a gift from Dr. Channing Der at UNC. All cells were cultured in Dulbecco's modified Eagle's medium (DMEM; Invitrogen) supplemented with 10% fetal bovine serum (Sigma) and antibiotic-antimycotic solution (Sigma). They were grown in a 37°C incubator with 5% CO_2.

DNA Constructs and Generation of Stable Cell Lines

mEmerald-Vinculin-23 was a gift from Michael Davidson (Addgene plasmid #54302; http://n2t.net/addgene:54302; RRID: Addgene_54302). mRFP-C1 was a gift from Robert Campbell & Michael Davidson & Roger Tsien (135) (Addgene plasmid #54764; http://n2t.net/addgene:54764; RRID: Addgene_54764). Human MVcn gene, a generous gift from Dr. Tina Izard, was cloned into RFP-C1 between SalI and ApaI restriction sites. mEmerald-tagged full-length human Vcn construct (1-1066) and mRFP-tagged full-length human MVcn construct (1-1134) were then subcloned into the pBabe-puro vector. Both fusion proteins were inserted using the restriction enzyme sites NgoMIV and SnaBI. Using the pBabe retroviral system to generate stable cell lines, we first generated retroviruses by transfecting HEK 293T cells with either the pBabe-puro mEmerald-Vcn or mRFP-MVcn constructs and the retrovirus packaging vector pCL-10A. pBabe-puro and pCL-10A vectors were gifts from Dr. Channing Der (UNC-Chapel hill).

After 48 hours, the viruses were harvested and used to infect Vcn-null MEFs using 8 μg/mL polybrene. Vcn-null MEFs were infected for 24-48 hours and those expressing either mEmerald-Vcn or mRFP-MVcn proteins were selected with 7.5 μg/ml puromycin for a week. After the cells were kept under the selection pressure at 5 μg/ml puromycin for about 3 weeks, they were sorted for expression by flow cytometry. Expression levels of both mEmerald-Vcn and mRFP-MVcn were verified by Western blot analysis using anti-mouse vinculin antibody (Sigma), which recognizes both Vcn and MVcn, and HRP-conjugated anti-mouse IgG (Jackson). Actin bands were detected using a mouse anti-actin monoclonal antibody (Millipore).

Flow Cytometry

To select for established stable cells with consistent expression of mEmerald-Vcn or mRFP-MVcn, we sorted the established stable cells using a MoFlo XDP cell sorter from the UNC Flow Cytometry Core Facilty and chose cells with equivalent expression similar to physiological levels of Vcn. To ensure that any phenotypic differences between mEmerald-Vcn or mRFP-MVcn expressing cells were comparable, we tested the sorted cell populations for expression level via Western blot (Fig. 17A) and chose cells with equivalent expression of mEmerald-Vcn and mRFP-MVcn equal to endogenous levels of Vcn in WT MEFs as a guide. The resulting stable cell lines allowed for physiological levels of expression of either construct in the same Vcn-null MEF background.

Quantification of Focal Adhesion Area and Number per Cell

Prior to FA analysis, cells were serum-starved in DMEM media supplemented with 0.5% delipidiated bovine serum albumin (BSA) and antibiotic-antimycotic solution. Cells were then trypsinized, resuspended in this same media, and rotated at 37ºC for 2 hours before plating. Cells were seeded on glass coverslips coated with 50 µg/ml of FN and allowed to spread for 2 hours. Cells were then washed with phosphate-buffered saline (PBS), fixed in 3.7% formaldehyde for 15 min, and permeabilized in 0.2% TritonX-100 for 10 min in room temperature. Fixed cells were blocked with 5% BSA for 30 min at room temperature, and incubated with a mouse monoclonal anti-paxillin antibody (BD Transduction laboratory) for 1 hour. After washing with PBS, cells were stained with appropriate secondary antibody (either goat anti-mouse Alexa Fluor 488 (for mRFP-MVcn-expressing cells), or goat anti-mouse Alexa Fluor 568 (for mEmerald-Vcn-expressing cells) (Invitrogen) for an additional hour. Immunofluorescence images were then taken with a Zeiss Axiovert 200M microscope equipped with a Hamamatsu ORCA-ERAQ digital camera and 63x oil objective. A previously reported method (136) was adapted and used to identify and quantify the properties of paxillin-stained FA. This method applies a high pass filter to the images and a user-specified threshold to identify FA. Thresholded objects smaller than 10 pixels and larger than 200 pixels were excluded from analysis. FA number and size (area) was quantified for individual cells.

Real-time Cell Analysis (RTCA) and cell spreading

The RTCA xCELLigence system (Acea Biosciences) uses electrical impedance to monitor the status of cells grown on micro-electrode coated plates (137). With sparsely plated cells, changes in impedance reflect cell coverage of the substrate, i.e. cell attachment and spreading, reported as cell index (CI). Prior to seeding, cells were serum-starved in DMEM media supplemented with 0.5% delipidated BSA and antibiotic-antimycotic solution. Cells were then trypsinized, resuspended in this same media, and rotated at 37ºC for 2 hours before being plated on 50 µg/ml FN-coated E-plate 16 wells. Cell Index was recorded at an interval of 15 sec for the first 4 hours, and subsequently at an interval of 3 min for the next 6 hours. Experiments were repeated 4 independent times with at least triplicates per sample. The slope of the RTCA trace was quantified from a trend line determined in Excel from data points between 0-2 hours post cell seeding.

To complement the RTCA data, cell area was also quantified by immunofluorescence. For the purposes of imaging, after plating for 2 hr, cells were fixed and incubated with either Alexa Fluor 488-phalloidin (for mRFP-MVcn cells) or Alexa Fluor 568- phalloidin (for mEmerald-Vcn cells) (Invitrogen) for 1 hour. Cell area was quantified using ImageJ (115). Resulting data were represented as mean ± S.E.M.

Random Cell Migration Assay

Glass-bottomed culture dishes (MatTek Corp) were coated with 10 µg/ml FN at 37°C for 1 h. Cells were plated overnight before imaging. Cells were imaged at 37°C with 5% CO_2 with a 10× objective on an Olympus VivaView FL microscope (Hooker Imaging Core at UNC) for 11 hours

with 15 min intervals. Single cell tracking was manually performed in ImageJ (115) using the "Manual Tracking" plugin, in which cells are tracked based on the approximate centroid location over time. Only single cells were tracked and data was discarded if the cell experienced cell division, cell death, a collision event (with another cell or debris), or if it migrated out of the field of view. To obtain velocity and persistence values, raw tracking data were analyzed with the "Chemotaxis Tool" plugin (Ibidi) in ImageJ (115).

Focal Adhesion Assembly and Disassembly

TIRF images were collected on an Olympus IX81-ZDC2 inverted microscope equipped with a UAPON 100x/1.49NA DIC TIRF objective (Olympus), an automated XYZ stage (Prior) and an Andor iXon EM-CCD. Images were procured using the Metamorph acquisition software with 110 nm laser penetration depth. Time-lapse imaging was performed with a stage top incubator that maintained humidity, 37°C and 5% CO_2 (Tokai Hit). Images were acquired every 15 sec for 30 minutes. Acquired images were further processed in ImageJ (115) to subtract background noise and to correct for photobleaching. A previously reported method (136) was used to identify and quantify the assembly and disassembly rates of the tracked focal adhesions within a single cell. This method applies a high pass filter to the images and a user-specified threshold to identify FA. Thresholded objects smaller than 10 pixels were excluded from analysis. All adhesions within a single cell were analyzed.

Force Microscopy

Three-dimensional force microscopy (3DFM) (138), a magnetic tweezer system, was used to apply consistent pulses of local 60-100 piconewton force to FN-coated magnetic beads, which were

allowed to adhere to cells. Tosyl-activated magnetic dynabeads (2.8 um, Thermofisher) were washed with PBS and incubated overnight with FN at 37ºC. After three washes with PBS, the beads were pipetted up and down vigorously to break up the aggregates and incubated with the cells for 20 minutes. Cells with 1 bead per cell were chosen for analysis. Constant force was applied for 5 sec intervals followed by 10 sec relaxation; this pattern was repeated for a total of 5 pulses. Upon the application of force, bead displacements were recorded with high-speed video camera (Jai Pulnix, San Jose, CA). Beads were tracked using Video Spot Tracker software (139). The 3DFM system was calibrated prior to experiments using a fluid of known viscosity. We used 2.5 M sucrose as a fluid of known viscosity, which has a viscosity of 140 mPA-sec. Beads showing less than 10 nm of displacement (detection threshold for the 3DFM) were discarded for analysis. Custom Matlab scripts were used to calculate creep compliance, J_{max}, also known as the deformity, which is defined as the average time-dependent deformation normalized by constant stress applied. $J_{max} = \frac{r_{max}}{F \times 6\pi\alpha}$, where r_{max} is the bead displacement due to the magnetic force F and α is the radius of the bead. Bead displacements were normalized to the bead displacement for Pulse 1 for each cell type and experiment and reported as mean ± S.E.M.

Statistical Analyses

Unpaired 2-tailed t-test was used for comparisons between two means. One-way ANOVA followed by Tukey post hoc was performed for multiple comparisons. All data were presented as mean ± S.E.M. unless otherwise noted. Statistical significance was set at *P<0.05; **P<0.01; ***P<0.001; P>0.05, not significant (n.s.).

Quantification of FA number per cell and FA area.

One-way ANOVA followed by Tukey post hoc for FA number per cell was used to analyze significance. Unpaired 2-tailed student t-test was used for FA area analysis as one-way ANOVA with Tukey post hoc could not be performed because the number of groups is greater than 100.

Real-time Cell Analysis (RTCA) and cell spreading.

Cell Index of all cell types were analyzed using one-way ANOVA followed by Tukey post hoc at 2 hours after seeding the cells.

Results

MVcn-expressing cells have fewer but larger FAs compared to Vcn-expressing cells

To establish a systematic comparison between Vcn and MVcn, we stably expressed either mEmerald-Vcn or mRFP-MVcn in Vcn-null mouse embryonic fibroblasts (MEFs). Because fibroblasts do not express endogenous MVcn, Vcn-null MEFs lack both endogenous Vcn and MVcn, providing a cell line that enables comparison of phenotypes associated with exogenously expressed Vcn or MVcn. To ensure similar expression levels of Vcn and MVcn, we used flow cytometry to select cells with Vcn or MVcn expression at levels equivalent to endogenous Vcn expressed in wildtype MEFs (Fig. 17A and Fig. 18). We first confirmed that exogenously expressed Vcn and MVcn are both recruited to FA in the stable re-expressing cell lines (Fig. 17B). FA structures were identified by paxillin staining (Fig. 17B).

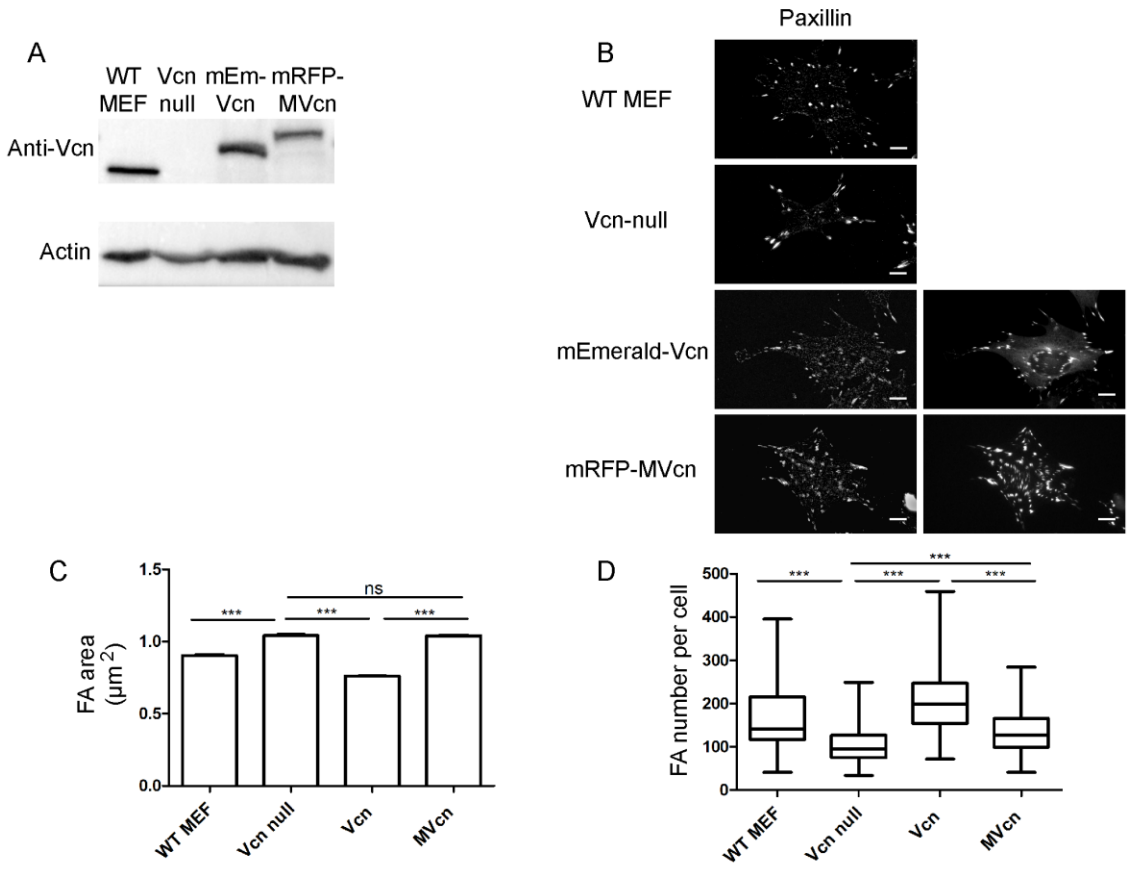

Figure 17. MVcn-expressing cells have larger but fewer FAs compared to Vcn-expressing cells.

(A) Western blot shows the expression level of either Vcn or MVcn in Vcn null MEF background. Both expression levels are equivalent to endogenous Vcn expression in WT MEFs. (B) Fluorescent images of WT MEF, *Vcn*-null parent MEF cell line, exogenous Vcn-expressing, and MVcn-expressing *Vcn*-null MEFs stained for paxillin and showing expression of either fluorescently-tagged Vcn or MVcn. Scale bar = 10 μm. FA number (C) and overall FA area per cell (D) were quantified. Graphs represent data pooled from 4 independent experiments ($n \geq 100$ cells; ***, $p<0.001$).

S1 Figure. mEmerald-Vcn and mRFP-MVcn cells were sorted for expression level using Flow activated cell sorting (FACS).

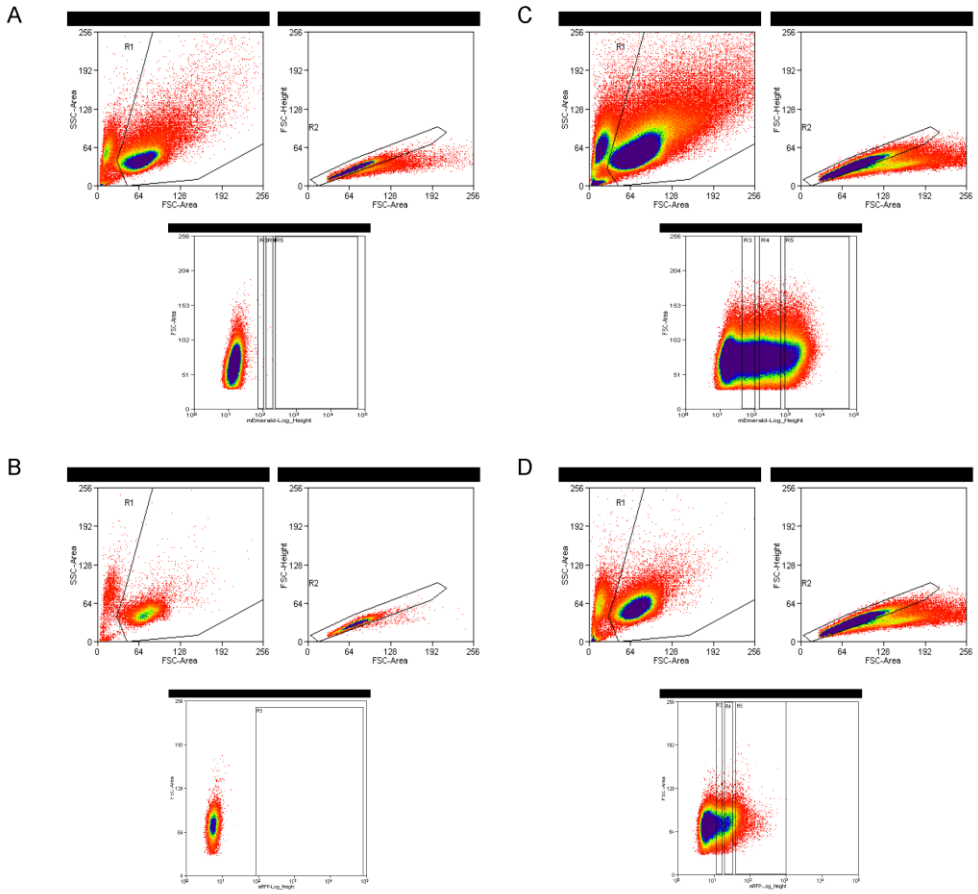

Figure 18. mEmerald-Vcn and mRFP-MVcn cells were sorted for expression using flow activated cell sorting (FACS).

For all panels, the top left figure represents population gated for cells of interest, top right figure represents population gated for doublet discrimination, and the bottom figure represents populations sorted based on the fluorescence intensity. Sort data for (A) Vcn-null MEF as non-fluorescent control for mEmerald-tag. (B) Vcn-null MEF as non-fluorescent control for mRFP-tag. (C) mEmerald-Vcn cell population. (D) mRFP-MVcn cell population. Population of high-expressing mRFP fluorescence from gate R5 used for experiments for (C) and (D).

As FAs are macromolecular structures that regulate cell adhesion, motility, and force response and transmission, we characterized FA properties of cells expressing either MVcn or Vcn, and compared them to the Vcn-null parent cell line. We employed immunofluorescence to quantify the mean FA area and the number of FA per cell using paxillin staining as a marker for FAs. The FAs of MVcn-expressing cells had larger areas but were fewer in number than the FAs of Vcn-expressing cells (Fig. 17C-D). The mean FA area in MVcn-expressing cells was ~37% larger relative to that of Vcn-expressing cells (Fig. 17C; Table 1). However, MVcn-expressing cells had 37% fewer FA per cell compared to Vcn-expressing cells (Fig. 17D; Table 1). Overall, the FA properties of MVcn-expressing cells were more similar to the Vcn-null parent cells: FA size was not significantly different between MVcn-expressing cells and Vcn-null cells, although MVcn-expressing cells had slightly increased number of FAs per cell (30% increase) (Fig. 17C-D; Table 1). Intriguingly, we have previously shown that a carboxyl-terminal deletion variant of Vcn that is defective in actin bundling shows similar FA properties to MVcn-expressing cells (101). Furthermore, our observations that Vcn-expressing cells form smaller but more FAs per cell is consistent with previous findings that Vcn promotes FA formation (32).

Table 1. Quantificatied values of experimental results.

Experiment	Vcn null	Vcn	MVcn
FA area (μm^2)	1.041±0.007	0.760±0.004	1.039±0.006
FA number per cell	103±3	212±6	134±4
Cell area (μm^2)	818±27	1457±38	1481±41
Cell spreading rate (RTCA slope)	0.04	0.12	0.13
Cell Index (CI) at 2 hours	1.04±0.01	1.13±0.01	1.15±0.01
Velocity (μm/min)	0.84±0.03	0.29±0.01	0.52±0.02
Persistence	0.39±0.02	0.55±0.02	0.66±0.01
FA assembly rate (min^{-1})	N/A	0.139±0.004	0.110±0.004
FA disassembly rate (min^{-1})	N/A	0.125±0.003	0.093±0.003

MVcn fully rescues cell area to the same extent as Vcn in Vcn-null MEFs

Given the differences in FA number and FA area observed between Vcn- and MVcn-expressing cells, we next investigated differences in cellular phenotype. *Vcn* deletion has previously been shown to significantly decrease cell size (44, 112), thus we examined whether re-expression of Vcn or MVcn could rescue cell area. *Vcn*-null, Vcn-expressing, and MVcn-expressing cells were stained with phalloidin to mark cell area (Fig. 19A). Both Vcn- and MVcn-expressing cells had comparable cell areas that were significantly increased over *Vcn*-null cell area by 78% and 81%, respectively (Fig. 19B; Table 1). Moreover, Vcn- and MVcn-expressing cells did not show significant differences in cell aspect ratios (Fig. 20). Upon finding that both Vcn and MVcn can rescue cell area in *Vcn*-null MEFs, we next quantified cell spreading on fibronectin (FN) using a real-time cell analyzer (RTCA) xCELLigence system. Compared to *Vcn*-null, cells expressing Vcn or MVcn had 10% higher Cell Index (CI), which represents electrical impedance, indicating increased cell area (Fig. 19C-D). Additionally, the slopes of these traces provide real-time information on cell spreading rate. Based on this, Vcn-null cells have a slower spreading rate compared to both Vcn- and MVcn-expressing cells (~66%; Table 1). Thus, both Vcn and MVcn can fully rescue the decreased cell area of *Vcn*-null MEFs and show comparable cell spreading rates to Vcn-expressing cells.

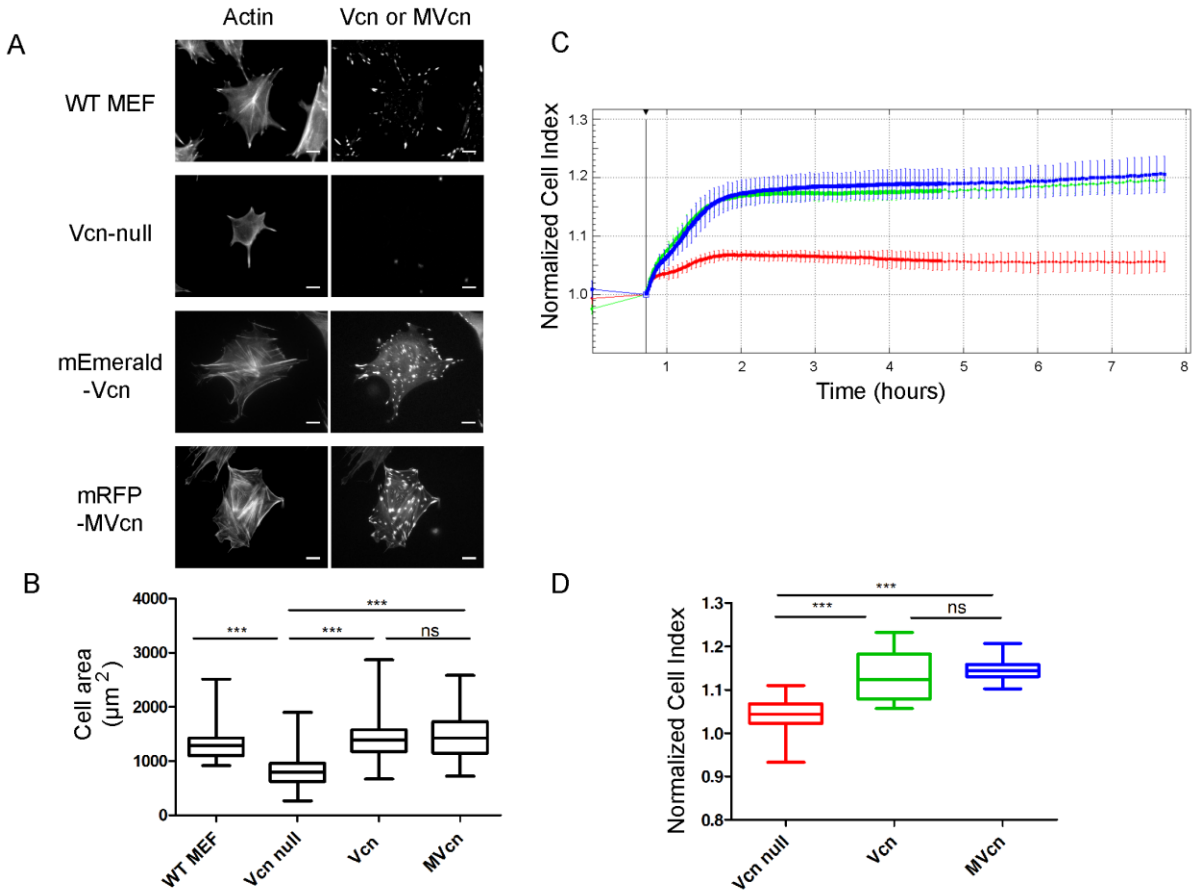

Figure 19. MVcn rescues decreased cell area in *Vcn*-null MEFs.

(A) Stable fluorescently-tagged Vcn or MVcn expression in *Vcn*-null MEFs, co-stained with phalloidin, to allow cell area quantification. WT MEFs and *Vcn*-null MEFs stained with phalloidin and Vcn antibody are shown for comparison. (B) Cell area quantification. ($n \geq 150$ cells per cell type, data pooled from 3 independent experiments; ***, $p<0.001$). (C) Representative real-time impedance traces from the RTCA xCELLigence system, measuring impedance every 15 s for the first 4 hours, and then every 3 min for the next 6 hours. Cell Index (CI) represents electrical impedance. First 8 hours are shown. CI is higher in cells expressing Vcn and MVcn compared to Vcn-null MEFs, indicating greater cell spreading. (D) Quantification of CI at 2 hours after seeding cells. Data pooled from 4 independent experiments ($n \geq 3500$ cells per cell type; ***, $p<0.001$).

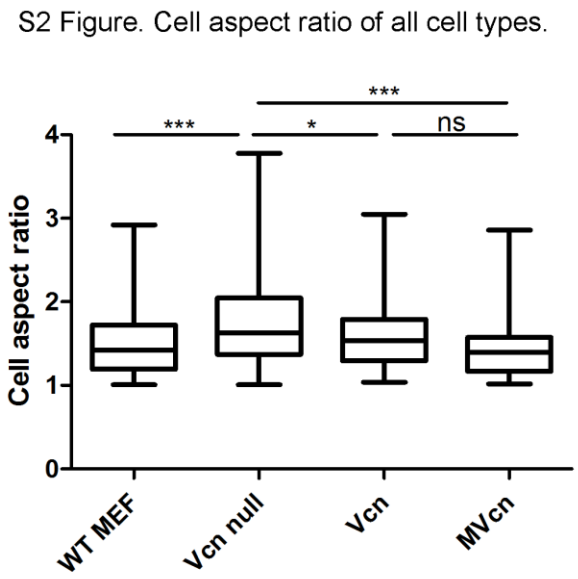

Figure 20. Cell aspect ratio for all cell types.

Data pooled from 3 independent experiments ($n \geq 90$ cells); ***, $p<0.001$).

MVcn-expressing cells have faster migration velocity and higher persistence than Vcn-expressing cells

Vcn plays a key role in regulating cell motility as deletion of Vcn increases cell motility and random migration in 2D environments (43, 44, 134). We assessed whether MVcn could restore a normal cell migration phenotype in the *Vcn*-null cell background. For *Vcn*-null, Vcn-, and MVcn-expressing cells, we monitored individual cell migration tracks every 15 minutes, manually tracking single cells and calculating both velocity and persistence via ImageJ (115). Cell migration tracks show distinct migration paths for each cell type, with MVcn-expressing cells displaying longer migration tracks compared to the cells re-expressing Vcn (Fig. 21).

Cell migration velocity and cell persistence of the three cell types were also quantified. MVcn-expressing cells migrated faster than Vcn-expressing cells by ~78%, while *Vcn*-null cells migrated faster than either Vcn- or MVcn-expressing cells by ~184% and ~60%, respectively (Fig. 21B; Table 1). Finally, we found that Vcn-expressing cells were more persistent than *Vcn*-null cells (~40%; Fig. 21C; Table 1), consistent with observations from other groups (43, 134, 140). Unexpectedly, MVcn-expressing cells were ~20% more persistent than Vcn-expressing cells and ~67% more persistent than *Vcn*-null cells (Fig. 21C; Table 1).

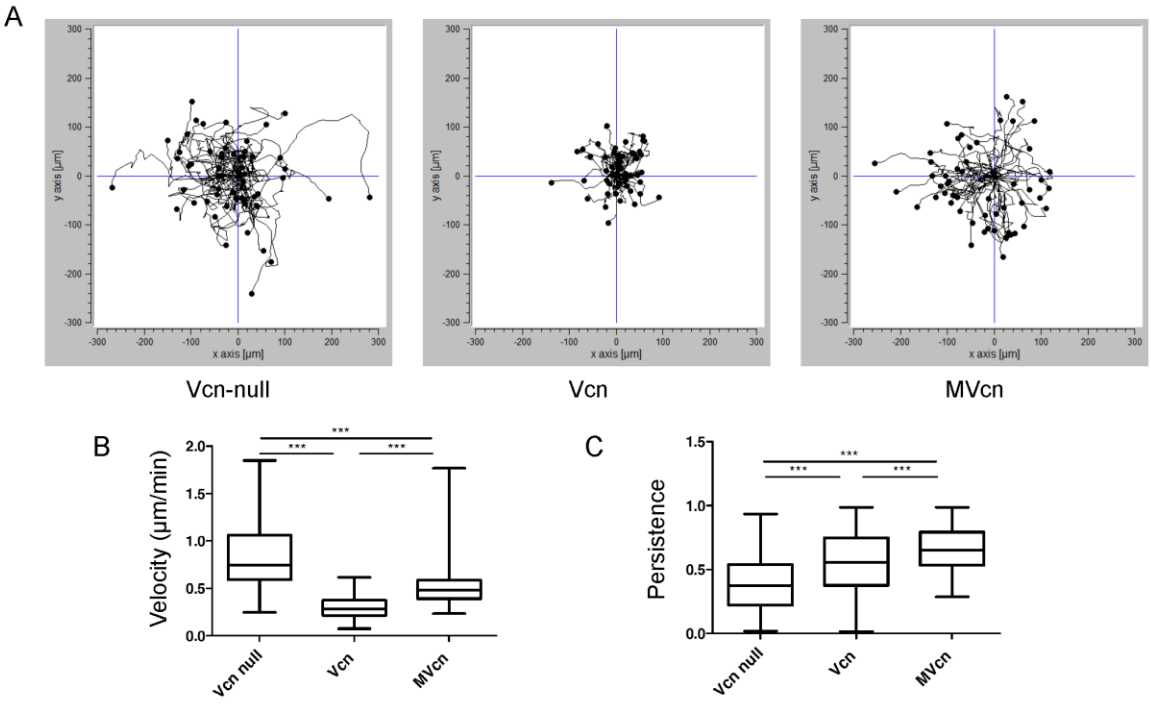

Figure 21. Random cell migration analysis shows enhanced migration velocity and higher persistence of migration for cells expressing MVcn compared to Vcn-expressing cells.

(A) Representative cell tracks plotted for n>50 cells. (B) Quantification of random migration velocity. (C) Quantification of directional persistence. Data pooled from 3 independent experiments (n ≥ 140 cells; ***, p<0.001).

Vcn has faster assembly and disassembly rates at FA than MVcn

Focal adhesion assembly rate and turnover are highly dynamic events underlying cell migration (130). Because the difference in average FA area and FA number per cell between Vcn- and MVcn-expressing cells suggested a potential difference in FA turnover, we examined FA dynamics of Vcn- or MVcn-expressing cells. Using total internal reflection fluorescence (TIRF) microscopy, we followed all of the adhesions within a single cell to quantify assembly and disassembly rates (Fig. 22; Table 1). Vcn-containing FAs assembled at a faster rate (~26%) compared to MVcn-containing FAs (Fig. 22B; Table 1). Likewise, Vcn-containing FAs showed a faster disassembly rate (~34%) compared to MVcn-containing FAs (Fig. 22C; Table 1). The plots of fluorescence intensity with respect to time are also shown (Fig. 23). To ensure that the difference in fluorophores between Vcn and MVcn was not a contributing factor in measurements of FA assembly and disassembly rates, we tagged both proteins with the same mEmerald fluorophore and found the results to be consistent (Fig. 24). These results indicate that Vcn-containing FAs undergo faster FA turnover compared to MVcn-containing FAs, consistent with the previous findings that Vcn promotes FA turnover (32).

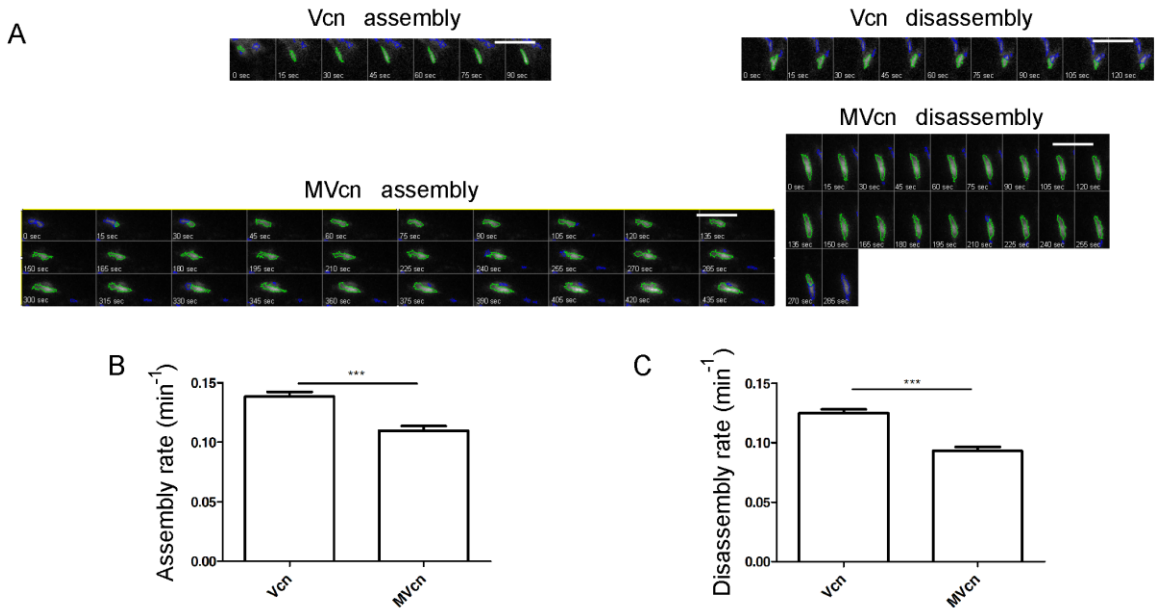

Figure 22. Focal adhesion assembly and disassembly rates are higher for Vcn-expressing cells compared to MVcn-expressing cells.

(A) Representative time-lapse image sequences of Vcn-null MEFs stably expressing either mEmerald-Vcn or mRFP-MVcn migrating on 10 μg/ml FN. Images (shown in grayscale) are taken every 15 sec. Green outlines (generated by focal adhesion analysis program) show individual FA. Scale bar = 10 μm. Graph of average rate constants of FA assembly (B) and disassembly (C) from FAs in each cell type. Data pooled from 3 independent experiments ($n \geq 13$ cells (and at least 400 adhesions); ***, $p<0.001$).

S3 Figure. Average and representative assembly and disassembly rates at FA.

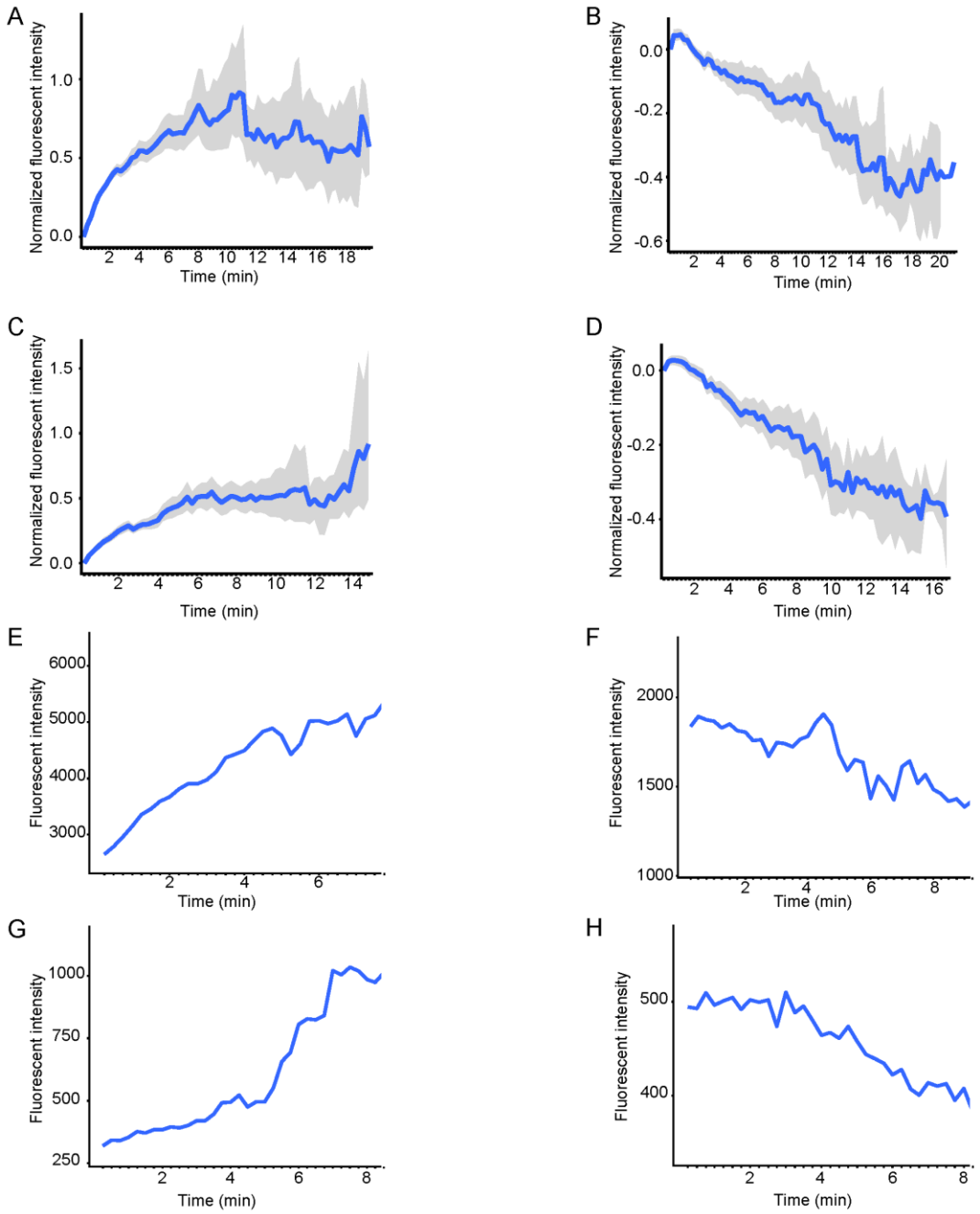

Figure 23. Average and representative assembly and disassembly curves at FA.

All panels show fluorescence intensity plotted with respect to time as FAs either assembled or disassembled. For (A)-(D), all shaded areas indicate S.E.M. (A) Average assembly plot of mEmerald-Vcn at FAs for all cells. (B) Average disassembly plot of mEmerald-Vcn at FAs for

all cells. (C) Average assembly plot of mRFP-MVcn at FAs for all cells. (D) Average disassembly plot of mRFP-MVcn at FAs for all cells. (E) Representative assembly plot of mEmerald-Vcn at FAs for a single cell. (F) Representative disassembly plot of mEmerald-Vcn at FAs for a single cell. (G) Representative assembly plot of mRFP-MVcn at FAs for a single cell. (H) Representative disassembly plot of mRFP-MVcn at FAs for a single cell. Data pooled from 3 independent experiments ($n \geq 13$ cells (or at least 500 adhesions); *$p<0.05$; ***, $p<0.001$; not significant (n.s.)).

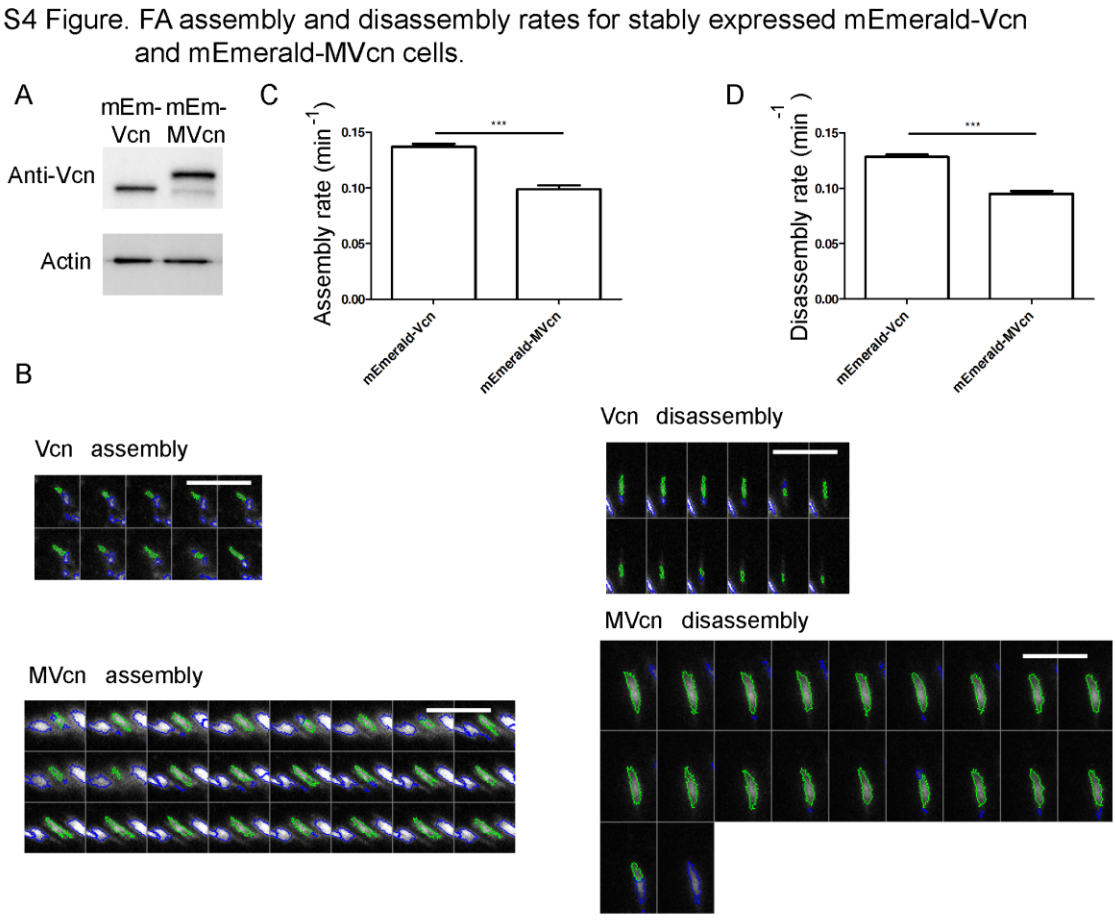

Figure 24. Focal adhesion assembly and disassembly rates display consistent results with the same tagged fluorophore.

(A) Western blot shows equivalent expression level of either mEmerald-Vcn or mEmerald-MVcn in Vcn-null MEF background. (B) Representative time-lapse image sequences of Vcn-null MEFs stably expressing either mEmerald-Vcn or mEmerald-MVcn migrating on 10 μg/ml FN. Images are taken every 15 sec and show individual FA. Scale bar = 10 μm. Graph showing average rate constants of FA assembly (C) and disassembly (D) in each cell type. Data pooled from 3 independent experiments ($n \geq 13$ cells (or at least 500 adhesions); ***, $p<0.001$).

MVcn-expressing cells lack a significant cell stiffening response to external force

Vcn is a mechanotransducing protein known to play an important role in force transmission by linking transmembrane receptors to the actin cytoskeleton (141-144), and knocking out Vcn leads to decreased traction force at FA (32). Previous work demonstrated that Vcn bears force between the head and tail domains, and that the Vcn tail domain associates with actin filaments in cells, which has been shown to play an important role in cell traction force (32, 77, 105). In addition, cells expressing Vcn were previously shown to respond to external force by displaying a cell stiffening response in 3D force microscopy (3DFM) while *Vcn*-null cells failed to show this response (77, 101, 145). Given these findings, we investigated whether MVcn was likewise involved in force transmission. To study how Vcn- and MVcn-expressing cells respond to external force, we used 3DFM (Fig. 25A) and assessed whether MVcn expression could restore the cell stiffening response in *Vcn*-null cells (77, 101, 145, 146). To test this, we applied uniform pulses of force to cells via attached FN-coated magnetic beads. Decreases in the relative bead displacements between the first and subsequent pulses were quantified to determine the cell stiffening response. Here, we ensured that the actual magnetic bead displacements were similar between individual cells (Fig. 26). Vcn-expressing cells revealed a stiffening response, which was absent in the *Vcn*-null cells, as expected based on previous findings (Fig. 25B) (101). Specifically, *Vcn*-null cells failed to show decreased bead displacement after the first pulse while Vcn-expressing cells showed a 30% decrease in bead displacement between the first and second pulse of force (Fig. 25B). In contrast, MVcn-expressing cells did not exhibit a significant bead displacement (8% decrease), indicating little or no stiffening response (Fig. 25B).

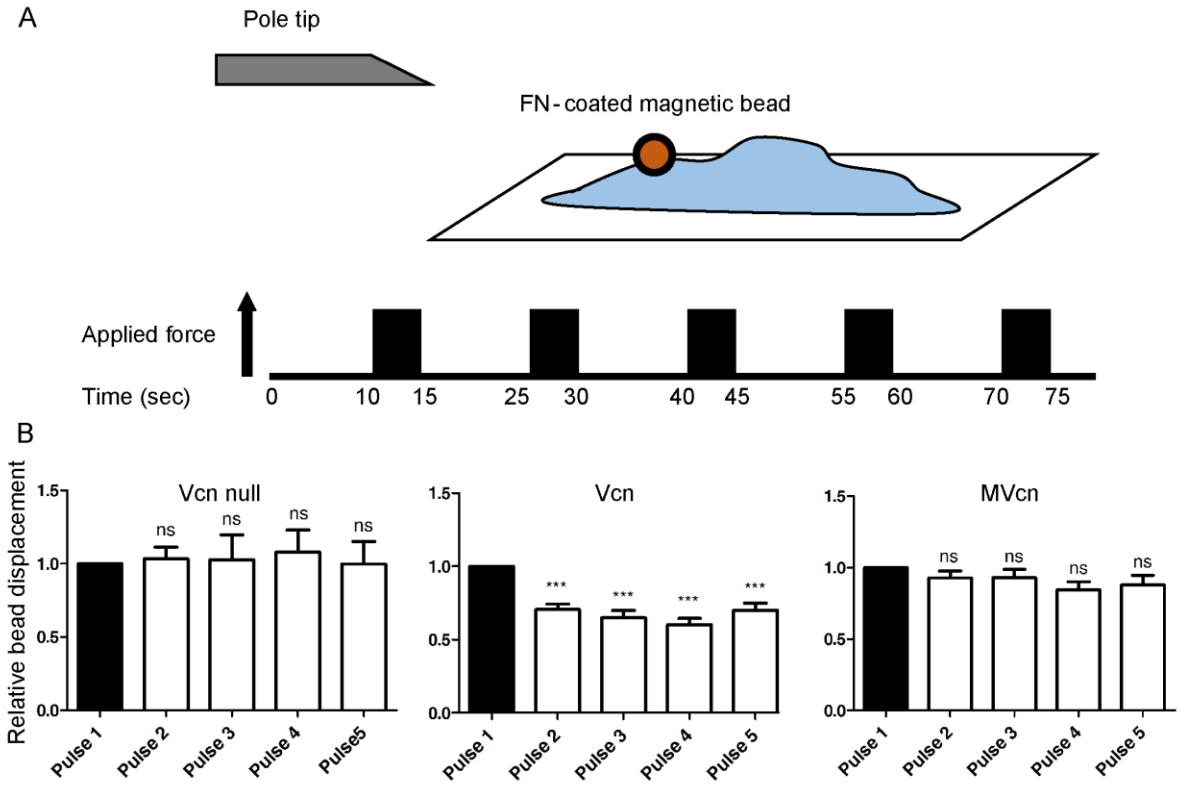

Figure 25. 3D-Force microscopy (3DFM) shows reduced ability of MVcn-expressing cells to rescue cell stiffening response compared to Vcn-expressing cells.

(A) 3D-force microscopy (3DFM) setup used to measure cell stiffening response. Constant force was applied for 5 sec intervals followed by 10 sec relaxation; this pattern was repeated for a total of 5 pulses. (B) Cell stiffening response is measured by quantifying the decrease in bead displacement after each subsequent pulse of magnetic force in *Vcn*-null, Vcn-, and MVcn-expressing cells. Cell stiffening response is lost in MVcn-expressing cells. Data pooled from 3 independent experiments (n ≥19 cells each cell type; ***, $p<0.001$).

S5 Figure. 3DFM experimental set-up and controls.

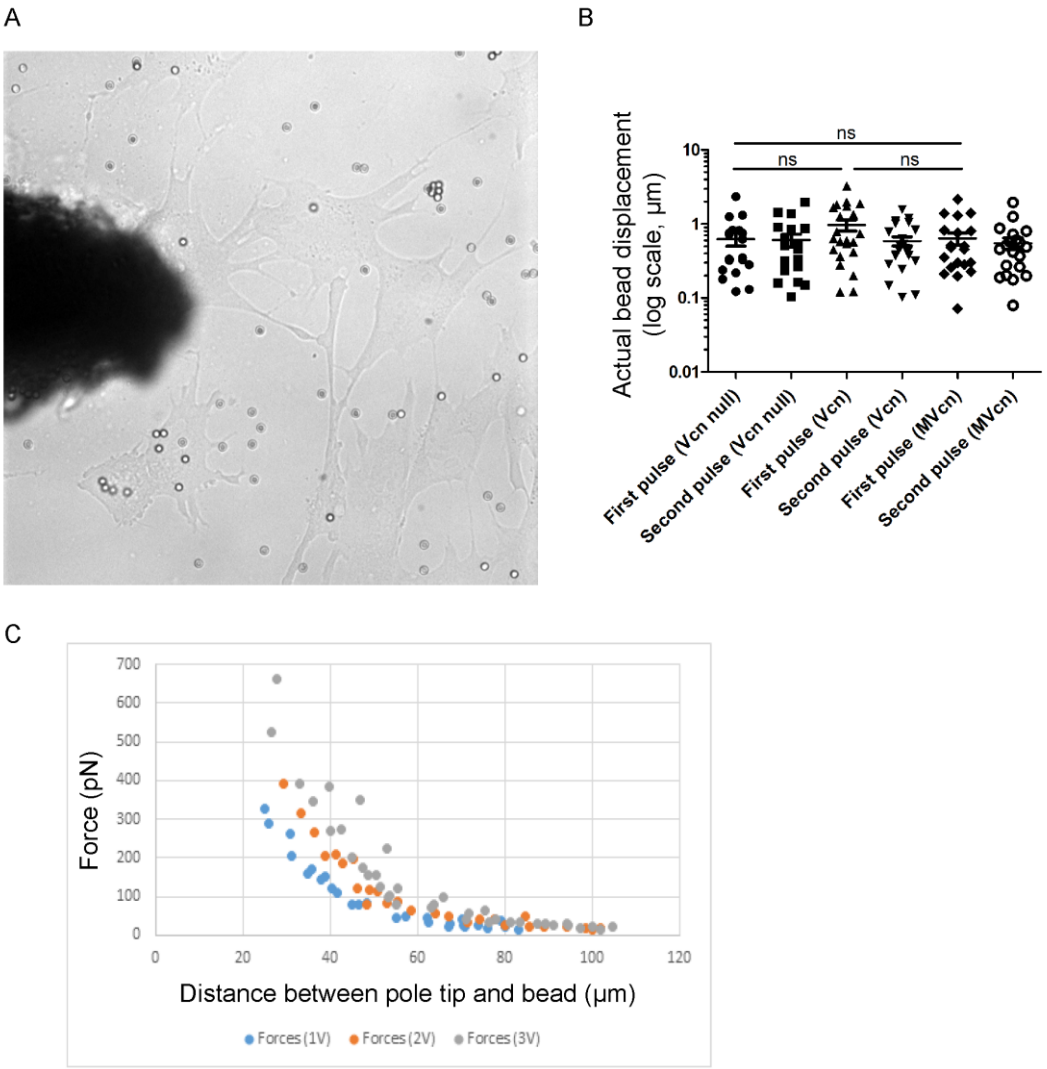

Figure 26. 3DFM experimental set-up and controls.

(A) Actual image of the experimental set-up. (B) Comparison of actual bead displacements between the first and second pulses for all cell types. Actual bead displacements between the first pulses of all cell types are similar. (C) Graph showing the relationship between the magnetic force experienced by the bead and the distance between the magnetic pole tip and the bead. Data pooled from 3 independent experiments (n ≥19 cells each cell type; not significant, n.s.).

Discussion

Vcn and its splice isoform, MVcn, have been studied at both the tissue level and the molecular level (42, 83, 84, 90, 93-95, 97, 99, 103). However, a direct comparison of their behavior in cells is lacking. MVcn is co-expressed with Vcn at sub-stoichiometric levels in smooth and cardiac muscles, where the expression level correlates with the contractile needs of the cell (42, 81, 84). The presence of MVcn in muscle cells is key, as mutations in the 68-residue insert lead to defects in the organization of intercalated discs and results in cardiomyopathy (90, 91). These observations have led to the idea that MVcn coordinates with Vcn to support force transmission in cells (84, 90, 91). Both Vcn and MVcn are localized to cell-cell and cell-matrix adhesion sites. How Vcn is recruited to cell-cell junctions is not completely understood, but the interaction between Vcn head domain and α-catenin is thought to play an important role. Vcn does not localize to cell-cell junctions in cells lacking α-catenin or in hearts lacking α-catenin (147, 148). Force is also thought to play an important role in the recruitment of Vcn to these cell-cell contacts as α-catenin undergoes a force-dependent conformational change that exposes Vcn binding sites (149, 150), and α-catenin is believed to play a role in Vcn activation at cell-cell junctions (151). Because the head domains of Vcn and MVcn are the same, it is likely that MVcn's ability to interact with α-catenin is not altered. However, the difference in the cell's ability to respond to force between cells may arise from potentially different ligand interactions of Vcn and MVcn, as the actin-regulating proteins (such as VASP) that bind to the proline-rich linker region in Vcn may not bind to MVcn due to the extra 68-residue insert near that region.

At the molecular level, MVcn has been proposed to fine tune force transmission by negatively regulating Vcn-mediated actin bundling (103). We and others have shown that *in vitro*, Vcn tail-mediated actin bundling is decreased as the MVcn tail concentration is increased (99,

103). These findings suggest that MVcn may play a role in limiting, rather than strengthening, force transmission via Vcn tail-mediated actin bundling (99, 103). MVcn tail has similar actin filament binding properties as Vcn tail, but does not dimerize and so does not bundle actin filaments (90, 95, 97-100, 103). These observations raise the following question. Is it possible that tail domain of MVcn competes with the Vcn tail domain in binding to actin filaments, providing a possible mechanism for modifying force transmission? However, before attempting to understand the role of MVcn in the context of Vcn, it is necessary to clarify the role of MVcn in cells. To start, due to the lack of information regarding how Vcn and MVcn compare at the cellular level, we investigated whether stable expression of either Vcn or MVcn in a *Vcn*-null MEF background affects various cellular properties, including cell mechanotransduction. We find that both Vcn and MVcn are localized to the FA. As Vcn-talin interaction has been shown to be critical for the localization of Vcn to FA, this result is not surprising given that both proteins share the same head domain, which interacts with talin (47, 79, 82, 105). Our findings indicate that some functions are shared between Vcn and MVcn at the cellular level, such as the ability of MVcn to partially rescue the number of FA per cell (Fig. 17D) and fully rescue the cell spreading phenotype of Vcn-null cells (Fig. 19). However, several distinct phenotypes including FA size, cell migration, FA dynamics, and cell reinforcement are observed (Fig. 17D, 4, 5, and 6). These results suggest that similar phenotypes may be modulated by the shared head domain of the two proteins, while the distinct phenotypes may reflect their different tail domains.

We and others have previously shown that while Vcn tail can organize actin filaments into parallel bundles, MVcn tail organizes actin filaments into a mesh-like network instead of bundles (90, 95, 98, 99). The presence of the insert, including H1', inhibits the ability of MVcn tail to bundle F-actin, as deletion of H1' promotes actin filament bundling (95). This difference in actin

filament cross-linking between the two proteins likely plays a role in how cells regulate FAs and force transmission. Of note, we have previously shown that expressing an actin bundling-deficient Vcn mutant (VcnΔC5) in Vcn-null MEFs leads to defects in FA properties and decreased cell reinforcement in response to mechanical force (101). As MVcn-expressing cells show similar defects in FA properties and force response, the inability of MVcn to bundle actin filaments might explain some of the differences observed between MVcn- and Vcn-expressing cells.

MVcn expression alters FA properties

We found that FAs in MVcn-expressing cells have a larger area but are fewer in number per cell compared to Vcn-expressing cells (Fig. 17). Similarly, we previously showed that VcnΔC5 expression in Vcn-null MEFs also results in larger mean FA area as well as fewer FAs per cell (101). While a direct comparison cannot be made due to differences in both expression levels and cell type used for these studies, these FA trends strongly suggest the importance of actin bundling in FA regulation. Furthermore, MVcn-expressing cells are similar to Vcn-null cells in that they have larger FA size and fewer FA number per cell compared to Vcn-expressing cells. In fact, Vcn-null cells have the fewest FA number per cell out of all three cell types.

MVcn expression affects mechanical response to force

In contrast to Vcn, expression of MVcn does not rescue the cell stiffening response in *Vcn*-null MEFs (Fig. 25). 3DFM revealed that while Vcn-expressing cells showed almost immediate and significant decrease in bead displacement after the first pulse of force, MVcn-expressing cells

did not show a significant decrease in bead displacement in response to successive pulses of tension (Fig. 25). Similar to MVcn, when VcnΔC5, an actin bundling deficient mutant, was expressed in Vcn-null MEFs, cells were similarly defective in their stiffening response, additionally supporting that Vcn tail-mediated actin bundling is important for cell reinforcement (101). It is possible that Vcn tail-mediated actin bundling is necessary for aligning actin in the regions of high tension. Recent studies using talin FRET sensors and cellular cryotomography demonstrated that regions of high talin tension had highly aligned linear actin filaments, while regions of low tension showed less well-aligned actin filaments in cells (152). However, the ability of MVcn-expressing cells to maintain stress fiber structure suggests that the presence of other actin-crosslinking proteins, such as α-actinin and myosin, may contribute to the formation and maintenance of stress fibers within these cells (153, 154).

MVcn expression alters cell migration and FA dynamics

Does the inability of MVcn to bundle actin filaments account for most of the differences observed between Vcn- and MVcn-expressing cells? Our data showing differences in migration phenotypes suggest that other factors may be involved. While Vcn-null and MVcn-expressing cells migrated faster than Vcn-expressing cells, consistent with a negative regulatory function of MVcn tail, the migratory paths associated with MVcn-expressing cells displayed increased persistence relative to both Vcn-null and Vcn-expressing cells (Fig. 19). MVcn in these cells also had slower assembly and disassembly rates in FAs compared to Vcn in Vcn-expressing cells (Fig. 22). It has previously been shown that Vcn can facilitate FA formation and turnover (32), consistent with our findings that Vcn-expressing cells had smaller but more FAs per cell and faster FA assembly and

disassembly rates, respectively. However, this is a curious result as increased FA turnover has been typically associated with faster cell migration, but the MVcn-expressing cells migrate faster than the Vcn-expressing cells. This could be partly due to differences in the ability of each isoform to engage particular binding partners. Moreover, the lack of Vcn-mediated actin bundling in MVcn-expressing cells may be compensated for by other actin-bundling proteins.

In conclusion, we find that MVcn can rescue some of Vcn's functions in *Vcn*-null cells. Targeting FAs, it rescues cell area. Moreover, while MVcn partially rescues FA number, it is unable to fully rescue FA area. It also fails to restore the cell stiffening response to mechanical force in *Vcn*-null cells. Some of these differences may be due to the ability of MVcn and Vcn to engage distinct binding partners at the proline-rich linker, such as Arp2/3 complex, vinexin, or VASP, as the presence of the MVcn insert at the tail domain may disrupt these interactions that occur with Vcn. Additionally, it is possible that the additional MVcn insert introduces new interactions with other unknown ligands. However, the properties of MVcn-expressing cells are strikingly similar to those of cells expressing a Vcn mutant construct that can bind but not bundle actin filaments (101). Consequently, we currently favor a model that attributes the different phenotype of the MVcn cells to be largely due to the inability of MVcn to bundle actin filaments. Future studies will continue to test this possibility

CHAPTER 4 – Conclusions and Future Directions

Overview

The overall goal of this dissertation was to determine the role of metavinculin in actin reorganization and force transmission. By using both *in vitro* biochemical and cell biology techniques, we have shed light on the mechanism of MVt-actin interaction and determined how the expression of metavinculin in MEFs leads to different phenotypes compared to vinculin expression. Our findings, reported in Chapter 2 and 3 of this dissertation, revealed that metavinculin's functions are distinct from those of vinculin at both the structural and cellular level. These results raise new questions that we are interested in pursuing. In this chapter, I will first summarize our findings and potential impact, and then discuss the ongoing studies and future directions. I hope that the work presented here will contribute to the field of mechanotransduction and set the stage for future studies elucidating the coordinated role of metavinculin and vinculin under physiological settings.

Review of Current Findings

We examine the role of metavinculin at both the molecular and cellular level in comparison to vinculin. First, we solved cryo-EM reconstructions of both MVt-actin and Vt-actin complexes, in collaboration with the Alushin lab at Rockefeller University. These reconstructions revealed, for the first time, how both Vt and MVt interact with F-actin. We showed that while both Vt and MVt bind to actin filament at the similar interface, H1 in Vt and H1'in MVt, disengage from the rest of the helix bundle upon binding to F-actin. In the case of

Vt, we hypothesize that helix partitioning exposes a new interface that facilitates Vt-dimerization and actin bundling. These findings not only provided valuable insight into the Vt-actin and MVt-actin binding interfaces but also important mechanistic insight regarding large scale conformational changes in Vt and MVt that occur upon actin binding. Our cryo-EM reconstructions, in combination with biochemical data, indicate that F-actin engagement with the Vt and Mt helical bundle causes a torqueing conformational change, prompting H1 and H1', respectively, to disengage from the rest of the helix bundle. We postulate that this conformational change exposes a cryptic dimerization site on Vt that allows for actin-bound Vt to dimerize, ultimately bundling actin filaments into parallel bundles observed *in vitro* (99). However, in the case of MVt, we believe that the presence of MVt insert interferes with the formation of this cryptic dimerization in MVt-actin complex by forming a protruding structure with H1, thereby disrupting the ability of MVt to bundle actin filaments *in vitro* (95). Overall, we hypothesize that Vt and MVt partially unfold upon actin-binding, but in the case of Vt, this rearrangement reveals a cryptic dimerization site that allows for Vt-mediated actin bundling, whereas in MVt, the partitioned H1 helix forms a globule domain that prevents MVt dimerization. Based on this conceptual model, we then studied how Vt-mediated actin bundles would be affected in the presence of WT MVt or CM-associated MVt mutants (A934V, ΔL954, and R975W). Through actin co-sedimentation assay and EM studies, we showed that the level of Vt-mediated actin bundles decreases in the presence of MVt WT. In contrast, MVt CM mutants did not inhibit Vt-mediated actin bundling, but rather, promoted higher actin assemblies. Hence, while MVt WT suppresses formation of Vt-mediated actin bundles, MVt CM mutants retain and/or enhance higher order actin structures (90, 99, 103, 155). This led us to hypothesize that MVt WT may negatively regulate the actin bundling properties of Vt, and that loss of negative

regulation by MVt CM mutants may contribute to HCM and DCM. At the molecular level, DMD simulations suggest that the extra residues on MVt may form a protruding structure that sterically prevents dimerization with another actin-bound Vt or MVt (155). Figure 16 highlight our model for how MVt WT or MVt CM mutants regulate actin bundling in the presence of Vt.

Next, we studied how vinculin and metavinculin functions differ at the cellular level. To establish a system of cellular comparison, we generated vinculin null MEFs that stably express either fluorescently-tagged vinculin or metavinculin. We controlled for the expression levels of both proteins in these cell lines by sorting the cells via flow cytometry. After ensuring that the expression levels between vinculin and metavinculin were comparable, we examined the focal adhesion properties, cell migration, and mechanotransduction of these cells. Though we initially sought to use smooth muscle or cardiac cells as a system of comparison, the difficulty in maintaining and controlling for metavinculin expression in cell culture prevented us from using those cells. In smooth and cardiac muscle cells, metavinculin loses expression in cell culture unless the contractile environment is mimicked properly (84). On the other hand, the *vinculin*-null MEF background allowed us to manipulate the expression levels of either vinculin or metavinculin. Results from our analyses indicate that metavinculin expression can fully rescue cell area and partially rescue FA number per cell. However, compared to vinculin-expressing cells, metavinculin expression led to larger individual FA area, faster cell migration, and decreased cell stiffening in response to external force. Our results suggest both overlapping and distinct cellular functions for metavinculin and vinculin.

Significance of this dissertation

This dissertation provides further insight into both molecular and cellular functions of metavinculin. First, the cryo-EM reconstructions of MVt-actin and Vt-actin complex provided an important insight into the critical interactions of both vinculin isoforms with filamentous actin. We found that helix Vt H1 or MVt H1' undocks upon actin binding and determined important mechanistic insight into conformational changes that control higher order actin assembly. We believe that this unfurling generates a docking site for vinculin tail dimerization required for vinculin's actin bundling activity. In the case of MVt, helix 1' unfurling due to actin binding facilitates formation of a protruding structure that sterically prevents the dimerization with another Vt, ultimately preventing MVt-mediated actin bundling. This structural model can also explain MVt's lack of actin bundling in the absence of Vt, and the suppression of Vt-mediated actin bundling in the presence of Vt. Extending this model into MVt CM mutants, this steric occlusion model can also explain the actin bundling we see in the presence and absence of Vt. We hypothesize that released H1' and the upstream sequence (including MVt H1) play an important role for the inhibitory functions of MVt in Vt-mediated actin bundling by forming a protruding structure. However, CM mutants are all located within the insert either directly in H1' or very close to H1' (N-terminal strap), and are distal from the direct actin-binding region in the rest of the MVt helix bundle. Therefore, we suggest that MVt CM mutants destabilize this insert-dependent globular structure and compromise MVt's regulatory function to inhibit Vt-mediated actin bundling without disrupting actin binding.

With this distinct structural difference between Vt and MVt *in vitro*, we wanted to determine whether this finding was significant in a cellular context. Hence, the second part of

this dissertation focused on developing a cellular system that can establish a systematic comparison between vinculin and metavinculin.

Comparison of vinculin and metavinculin in vinculin-null MEFs is an excellent starting point for determining the difference between cellular functions of the two isoforms. This is because vinculin and vinculin-null MEFs have been extensively characterized in MEFs, allowing us to make direct comparisons of complex properties at the level of FAs and whole cells. To reduce complexity associated with interpretation of adhesion and cellular phenotypes and as a first step toward evaluating function in muscle cells, we compared the behaviors of vinculin and metavinculin in cells that lack each component. In different cardiac and smooth muscles, the ratio of vinculin and metavinculin differs physiologically based on the contractility of the tissue, in which metavinculin is sub-stoichiometrically expressed at ~9-42% of vinculin expression and its expression level is higher in more contractile tissues. From this simpler system, we showed that metavinculin-expressing cells have different static and dynamic FA properties as well as different cell migration patterns. Moreover, they lack cell stiffening response to external force relative to vinculin-expressing cells. This is the first effort to elucidate the role of metavinculin in regulating cell function, and results suggest important potential implications in understanding vinculin-mediated mechanotransudction. Therefore, this study may stimulate further research and questions based on the novel cellular results of metavinculin functions.

Another interesting observation from these cellular studies with metavinculin-expressing cells is that metavinculin-expressing cells share much of the similar phenotypes as vinculin-null cells expressing vinculin ΔC5 mutant, which retains actin-binding but is deficient in actin-bundling. Metavinculin-expressing cells, much like cells expressing vinculin ΔC5 mutant, have larger and fewer average number of FAs per cell. Additionally, metavinculin-expressing cells

also do not stiffen in response to externally applied force, similar to cells expressing vinculin ΔC5 mutant. These observations point to similarities between the two cell types, suggesting that some of the cellular characterizations we see in metavinculin-expressing cells may be due to the lack of actin-bundling by metavinculin.

Ultimately, we would like to explore the possibility of metavinculin's function in negatively regulating vinculin-mediated actin bundling in cells, based on our *in vitro* actin co-sedimentation assay results where the presence of MVt suppressed the Vt-mediated actin bundles (99). Our long-term goal is to determine whether the two proteins interact competitively in cells. With only a difference of a single exon between the two proteins, we find that it is significant that this 68-residue difference leads to changes in multiple phenotypic properties. Our study serves as a key starting point for ultimately examining differing vinculin and metavinculin ratios in various muscles and how both proteins may interact with one another in cells.

Future directions

Though these findings provide an important starting point for distinguishing the functional differences between vinculin and metavinculin, much remains to be studied. Hene, in this section, I discuss several exciting components of this project that we hope to pursue in the future.

First, we would like to explore whether vinculin and metavinculin possess distinct binding partners. Based on our structural, computational, and biochemical studies on metavinculin, we hypothesize that the insert region present in metavinculin may potentially disrupt the interactions that vinculin typically makes with other molecules within the proline-rich linker, as the proline-rich linker is a disorganized region that immediately precedes the metavinculin insert. Actin-induced structural element lies proximal to the proline rich region, which contains multiple interaction sites, including vinexin, VASP, and Arp2/3. If metavinculin insert does form a protruding structure as the DMD modeling suggests (155), it is possible that the proline-rich region of metavinculin and vinculin differ in their ability to interact with ligands. On the other hand, the metavinculin protruding structure may also facilitate new interactions. We would like to clarify this question by first examining the known ligands that bind to vinculin proline-rich linker with metavinculin.

Second, with recent insights into metavinculin functions, it will be important to determine how the presence of both metavinculin and vinculin modulates cellular functions. Because metavinculin is always co-expressed with vinculin at sub-stoichiometric ratio dependent on the contractility level of the tissue (83, 84), it is more physiologically relevant to determine functions of metavinculin in the context of vinculin in cells. Additionally, based on MVt's suppression of Vt-mediated actin bundling in *in vitro* studies, we suspect that metavinculin plays an important

role in negatively regulating vinculin-driven actin bundling in cells. Therefore, we plan to examine the properties of cells that express both metavinculin and vinculin at different ratios. Stable cell lines have been established for vinculin-null MEFs that co-express fluorescently tagged vinculin and metavinculin, and these cells have been sorted based on the expression levels of each protein. In these cells, vinculin expression levels remain constant and are comparable to the vinculin expression in WT MEFs. However, it will be important to vary the co-expressing metavinculin expression in these cells to examine effects of different vinculin to metavinculin ratios on cells. To mimic the physiological expression of vinculin and metavinculin, expression of vinculin will be kept constant close to the WT vinculin expression level and the expression of metavinculin will be varied at sub-stoichiometric ratios relative to vinculin (~9-42%). We are curious to know whether metavinculin expression translates into cellular phenotypes that are indicative of metavinculin's function in inhibiting vinculin-mediated actin bundling. Specifically, we will examine FA properties, cell migration, cell spreading, and mechanotransduction of the co-expressing cells and compare them to the results of the cells that stably express either vinculin or metavinculin. It will be interesting observe whether the co-expressing cells behave more similarly to metavinculin-expressing cells as the ratio of metavinculin increases in these cells. If metavinculin's primary function is to negatively regulate vinculin-induced actin bundling, we expect that as the metavinculin expression increases, these cells will exhibit larger but fewer FAs per cell, faster and more persistent cell migration, and decrease in cell stiffening in response to external force.

Next, we would like to characterize the cellular functions of vinculin-null MEFs that express metavinculin CM-associated mutants either in the presence or absence of vinculin. Currently we have generated vinculin-null MEFs that stably express only metavinculin A934V,

ΔL954, or R975W to determine the effect of metavinculin mutant in these cells. Because we observed that MVt CM-associated mutants weakly induce the formation of disordered actin filament assemblies *in vitro*, we would like to examine whether this disordered actin assembly formation has any effect on cellular functions. We have additionally generated stable cells that co-express fluorescently tagged WT vinculin and one of the three metavinculin mutants (A934V, ΔL954, or R975W) to determine the effect that metavinculin CM-associated mutants have on cells in the presence of vinculin at sub-stoichiometric levels. Through *in vitro* studies, we have found that these mutants fail to inhibit Vt-mediated actin bundling and instead promote formation of large assemblies. Based on these *in vitro* results that affect actin bundling, we suspect that expressing metavinculin CM-associated mutants in cells that co-express vinculin may cause defects in FA properties, cell migration, and mechanotransduction properties.

Ultimately, we would like to extend to more physiologically relevent cellular studies. As metavinculin is specifically expressed in cardiac and smooth muscle cells, MEFs do not provide the most applicable information in terms of how metavinculin functions in the context of muscle cells. However, we believe that comparison of vinculin and metavinculin in MEFs is an excellent starting point at this point in the project. Vinculin functions in MEFs and vinculin-null MEFs have been well-characterized in the field, and this allows us to compare behaviors of vinculin and metavinculin in cells that lack each component in a simpler system. Furthermore, metavinculin and vinculin are scaffold proteins that interact with multiple ligands. While we are currently focused on actin, other ligands may play different roles as well. Other differences such as how their expression and splicing is controlled based on cell type, may be important to investigate. Moreover, cell adhesion, migration and mechanotransduction properties are complicated processes, and differnces here will require further study. In different cardiac and

smooth muscles, the ratio of vinculin to metavinculin differs physiologically based on the contractility of the tissue (83, 84). For example, high levels of metavinculin expression were found in smooth muscles of human uterus and aorta, while no metavinculin expression was observed in nonmuscle cells, such as liver, foreskin fibroblasts, and peritoneal macrophages (84). Additionally, culturing aortic medial cells leads to the loss of metavinculin expression, as this causes the cells to lose contractility (84). Therefore, we hope to address this complex but necessary problem in future studies by ultimately applying this system to smooth or cardiac muscle cells.

Speculations on metavinculin

In this last section, I would like to discuss aspects of metavinculin that I find curious but have not had a chance to pursue. The existence of metavinculin as a splice isoform of vinculin is fascinating, since metavinculin is an isoform that originates from the same gene as vinculin with the only difference from vinculin being the expression of the exon 19. The expression of metavinculin, in which the presence of exon 19 is the only difference relative to vinculin, in vinculin-null MEFs was sufficient to change cellular phenotypes compared to vinculin-expressing cells. That metavinculin is expressed from the same gene as vinculin and has only a single exon difference makes me speculate that metavinculin must possess a distinct, important function that vinculin lacks.

I will first briefly discuss the evolutionary perspective of cell adhesion in the context of vinculin and then go on to provide my perspective on how metavinculin may have evolved.

Cell-matrix adhesion and cell-cell interaction are important for mutlticellularity from an evolutionary perspective, as adhesion molecules anchor cells and tissues to secreted ECM and cell-cell adhesion molecules connect adjacent cells within tissues. Both focal adhesions (FAs) and adherns junctions (AJ) differ in protein composition, but both junctions contain vinculin. The similar architecture of both FAs and AJs throughout animals suggest that these structures evolved early. Some of the earliest cell adhesion experiment were done on sponges, and in 1907 Wilson famously demonstrated that cells from dissociated sponge tissues can re-aggregate and develop into a functional organism (156). Instead of FA and AJ adhesion molecules, sponges secrete proteoglycan complex called the aggregation factor (AF) that functions in both cell adhesion and self/non-self recognition (157-161). Core proteins of AF consist of calx-beta domains and sponge-specific “wreath” domain (162). Predominant adhesion mechanism in

sponges are considered to be the sulfated polysaccharide components of the AF that undergo calcium-dependent, hemophilic interactions (163). Although the differences between the AF model of sponges and FA or AJ adhesions in other animals contribute to the view that sponge tissues lack the organizational level found in epithelial cells, other comparative genomics studies demonstrate that sponges share homologs of core FA and AJ proteins, including those of vinculin (164). Miller *et al.* have recently found an orthalog to a vertebrate vinculin in the sponge *Oscarella pearsei* (*Op*) and examined the structure, biochemical properties, and tissue localization of this *Op* vinculin (164). Results from this study indicated that *Op* vinculin localize to both cell-cell and cell-ECM contacts and had similar biochemical and structural properties as vertebrate vinculin (164). They proposed that *Op* vinculin played a role in cell adhesion and tissue organization in the last common ancestor of sponges and other animals (164). These findings suggest that sponge tissues share similarities with epithelial tissue organization and that AJ- and FA-like structures extend to the earliest periods of animal evolution.

When I consider the evolutionary perspective of cell adhesion, I suspect that metavinculin must have diverged from vinculin after vinculin evolved as a component of the cell adhesion since vinculin sequence is conserved across most species. While vinculin itself is highly conserved among most species, greater sequence variation is observed in the metavinculin insert region among vertebrate species compared to the rest of the sequence (165, 166). Despite this sequence variation in the metavinculin insert region, it should be noted that the C-terminal region of the insert that contains MVt H1' helix is identical in higher vertebrate species. This sequence alignment in MVt H1' helix among species suggests that metavinculin helix H1' possesses a unique physiological function of the tail domain. Unfortunately, studies on the evolution of metavinculin is currently lacking, which limits my speculations. However,

considering that vinculin has orthologs in sponges, I surmise that metavinculin may be a separate isoform that was evolved in vertebrates as metavinculin has been found in most vertebrates, including but not limited to mice, cattle, rabbits, whales, bats, and birds. I have not yet been able to find any references on metavinculin sequence conservation in sponges, which suggests to me that metavinculin may have evolved in Metazoans (major division of the Animal Kingdom that comprises all animals other than Protozans and sponges). Examination of how metavinculin splicing occurs may provide more insight into the function of metavinculin and the evolutionary perspective of metavinculin in the future.

Another interesting aspect of vinculin and metavinculin is their roles in platelets. Both vinculin and metavinculin are found in megakaryocytes and platelets (81, 167, 168). Unlike most other cell types, platelets lack nuclei and are non-migratory. Instead, platelets roll, adhere, spread, and aggregate following a vascular injury as their main physiological role is to promote hemostasis by forming thrombi at sites of vessel injury.Vinculin is thought to play an important role in the structural reorganization of human platelet cytoskeleton upon platelet activation as it is incorporated into platelet cytoskeleton from cytosol upon thrombin-stimulated activation of the platelets (169). However, based on the more recent study using vinculin-deficient platelets, it seems that vinculin is not required for the traditional functions of αIIbβ3 or the platelet actin cytoskeleton, and vinculin may be more important for maintaining membrane cytoskeleton integrity in platelets under mechanical force (170). Because platelets do not engage in the same type of cell migration as the nucleated cells that migrate extensively during development (where migration is vinculin-dependent), perhaps the function of vinculin in actin cytoskeleton is different in platelets. Similarly, perhaps the function of metavinculin in platelets is different compared to those in smooth and cardiac cells as well. Rather than playing a role in force

response and actin contractility, perhaps the presence of metavinculin in platelets has a function in the maintenance and regulation of actin network organization at different stages of platelet activation.

Finally, though characterizations on MVcn-expressing cells were focused on cell-matrix adhesions, MVcn's roles may be more physiologically relevant for cell-cell adhesions. Not only that, but studies show that the balance of cell-cell and cell-matrix adhesions is critical for proper development (171). Studies have shown that there is considerable cross talk between cell-cell and cell-matrix adhesion sites with changes in adhesion and force transmission (172, 173). As vinculin and metavinculin (in muscle cells) localizes to both cell-cell and cell-matrix adhesion sites (sarcomeres and intercalated discs in muscle cells), it is likely that these proteins participate in this cross talk. One interesting point to note about the cross talk between cell-cell and cell-matrix adhesions is that adhesion/force transmission changes at one site does not always equate to changes at the other. For example, expanding the density of vascular endothelial cells plated on substratum increases cell-cell contacts but decreases cell-matrix adhesions (174). In cardiac or smooth muscle tissues, cell-cell contacts play a critical role in maintaining proper force transmission as uniform contractile response is necessary for their functions. As metavinculin expression led to fewer FAs per cell (fewer cell-matrix adhesions) compared to vinculin-expressing cells, perhaps one function of metavinculin in cardiac and smooth muscle cells is to limit FA formation to allow for stronger cell-cell adhesions. As decrease in metavinculin expression has been associated with disorganized intercalated discs and dilated cardiomyopathy (89), metavinculin's role at cell-cell junctions is critical. It would be interesting to explore more about metavinculin's function at not only cell-cell junctions but also in the cross talk between cell-cell and cell-matrix adhesions.

This dissertation serves as a first step in understanding how these proteins function individually in cells. With a difference of a single exon between the two proteins, we find that it is significant that this 68-residue difference leads to changes in multiple cellular phenotypes. I hope that this dissertation is able to contribute to the metavinculin field and expand on the limited knowledge of metavinculin function.

REFERENCES

1. Kanchanawong P, Shtengel G, Pasapera AM, Ramko EB, Davidson MW, Hess HF, et al. Nanoscale architecture of integrin-based cell adhesions. Nature. 2010;468(7323):580-4. PMCID: 3046339.

2. Abercrombie M, Heaysman JE, Pegrum SM. The locomotion of fibroblasts in culture. I. Movements of the leading edge. Exp Cell Res. 1970;59(3):393-8.

3. Izzard CS, Lochner LR. Cell-to-substrate contacts in living fibroblasts: an interference reflexion study with an evaluation of the technique. J Cell Sci. 1976;21(1):129-59.

4. Heath JP, Dunn GA. Cell to substratum contacts of chick fibroblasts and their relation to the microfilament system. A correlated interference-reflexion and high-voltage electron-microscope study. J Cell Sci. 1978;29:197-212.

5. Couchman JR, Rees DA. The behaviour of fibroblasts migrating from chick heart explants: changes in adhesion, locomotion and growth, and in the distribution of actomyosin and fibronectin. J Cell Sci. 1979;39:149-65.

6. Nobes CD, Hall A. Rho, rac, and cdc42 GTPases regulate the assembly of multimolecular focal complexes associated with actin stress fibers, lamellipodia, and filopodia. Cell. 1995;81(1):53-62.

7. Burridge K. Focal adhesions: a personal perspective on a half century of progress. Febs J. 2017;284(20):3355-61. PMCID: 5643231.

8. Geiger B. A 130K protein from chicken gizzard: its localization at the termini of microfilament bundles in cultured chicken cells. Cell. 1979;18(1):193-205.

9. Calderwood DA. Integrin activation. J Cell Sci. 2004;117(Pt 5):657-66.

10. Calderwood DA, Shattil SJ, Ginsberg MH. Integrins and actin filaments: reciprocal regulation of cell adhesion and signaling. J Biol Chem. 2000;275(30):22607-10.

11. Evans EA, Calderwood DA. Forces and bond dynamics in cell adhesion. Science. 2007;316(5828):1148-53.

12. Horwitz A, Duggan K, Buck C, Beckerle MC, Burridge K. Interaction of plasma membrane fibronectin receptor with talin--a transmembrane linkage. Nature. 1986;320(6062):531-3.

13. Otey CA, Pavalko FM, Burridge K. An interaction between alpha-actinin and the beta 1 integrin subunit in vitro. J Cell Biol. 1990;111(2):721-9. PMCID: 2116186.

14. Alon R, Dustin ML. Force as a facilitator of integrin conformational changes during leukocyte arrest on blood vessels and antigen-presenting cells. Immunity. 2007;26(1):17-27.

15. Harburger DS, Calderwood DA. Integrin signalling at a glance. J Cell Sci. 2009;122(Pt 2):159-63. PMCID: 2714413.

16. Sun Y, Chen CS, Fu J. Forcing stem cells to behave: a biophysical perspective of the cellular microenvironment. Annu Rev Biophys. 2012;41:519-42. PMCID: 4123632.

17. Mitra SK, Hanson DA, Schlaepfer DD. Focal adhesion kinase: in command and control of cell motility. Nat Rev Mol Cell Biol. 2005;6(1):56-68.

18. Mitra SK, Schlaepfer DD. Integrin-regulated FAK-Src signaling in normal and cancer cells. Curr Opin Cell Biol. 2006;18(5):516-23.

19. Huveneers S, Danen EH. Adhesion signaling - crosstalk between integrins, Src and Rho. J Cell Sci. 2009;122(Pt 8):1059-69.

20. Lessey EC, Guilluy C, Burridge K. From mechanical force to RhoA activation. Biochemistry. 2012;51(38):7420-32. PMCID: 3567302.

21. Ilic D, Furuta Y, Kanazawa S, Takeda N, Sobue K, Nakatsuji N, et al. Reduced cell motility and enhanced focal adhesion contact formation in cells from FAK-deficient mice. Nature. 1995;377(6549):539-44.

22. Owen JD, Ruest PJ, Fry DW, Hanks SK. Induced focal adhesion kinase (FAK) expression in FAK-null cells enhances cell spreading and migration requiring both auto- and activation loop phosphorylation sites and inhibits adhesion-dependent tyrosine phosphorylation of Pyk2. Mol Cell Biol. 1999;19(7):4806-18. PMCID: 84279.

23. Sieg DJ, Hauck CR, Ilic D, Klingbeil CK, Schaefer E, Damsky CH, et al. FAK integrates growth-factor and integrin signals to promote cell migration. Nat Cell Biol. 2000;2(5):249-56.

24. Sieg DJ, Hauck CR, Schlaepfer DD. Required role of focal adhesion kinase (FAK) for integrin-stimulated cell migration. J Cell Sci. 1999;112 (Pt 16):2677-91.

25. Richardson A, Malik RK, Hildebrand JD, Parsons JT. Inhibition of cell spreading by expression of the C-terminal domain of focal adhesion kinase (FAK) is rescued by coexpression of Src or catalytically inactive FAK: a role for paxillin tyrosine phosphorylation. Mol Cell Biol. 1997;17(12):6906-14. PMCID: 232547.

26. Taylor JM, Mack CP, Nolan K, Regan CP, Owens GK, Parsons JT. Selective expression of an endogenous inhibitor of FAK regulates proliferation and migration of vascular smooth muscle cells. Mol Cell Biol. 2001;21(5):1565-72. PMCID: 86702.

27. Case LB, Baird MA, Shtengel G, Campbell SL, Hess HF, Davidson MW, et al. Molecular mechanism of vinculin activation and nanoscale spatial organization in focal adhesions. Nat Cell Biol. 2015;17(7):880-92. PMCID: 4490039.

28. Gilmore AP, Burridge K. Regulation of vinculin binding to talin and actin by phosphatidyl-inositol-4-5-bisphosphate. Nature. 1996;381(6582):531-5.

29. Steimle PA, Hoffert JD, Adey NB, Craig SW. Polyphosphoinositides inhibit the interaction of vinculin with actin filaments. J Biol Chem. 1999;274(26):18414-20.

30. del Rio A, Perez-Jimenez R, Liu R, Roca-Cusachs P, Fernandez JM, Sheetz MP. Stretching single talin rod molecules activates vinculin binding. Science. 2009;323(5914):638-41.

31. Huang DL, Bax NA, Buckley CD, Weis WI, Dunn AR. Vinculin forms a directionally asymmetric catch bond with F-actin. Science. 2017;357(6352):703-6. PMCID: 5821505.

32. Thievessen I, Thompson PM, Berlemont S, Plevock KM, Plotnikov SV, Zemljic-Harpf A, et al. Vinculin-actin interaction couples actin retrograde flow to focal adhesions, but is dispensable for focal adhesion growth. J Cell Biol. 2013;202(1):163-77. PMCID: 3704983.

33. Chan CE, Odde DJ. Traction dynamics of filopodia on compliant substrates. Science. 2008;322(5908):1687-91.

34. Elosegui-Artola A, Bazellieres E, Allen MD, Andreu I, Oria R, Sunyer R, et al. Rigidity sensing and adaptation through regulation of integrin types. Nat Mater. 2014;13(6):631-7. PMCID: 4031069.

35. Elosegui-Artola A, Oria R, Chen Y, Kosmalska A, Perez-Gonzalez C, Castro N, et al. Mechanical regulation of a molecular clutch defines force transmission and transduction in response to matrix rigidity. Nat Cell Biol. 2016;18(5):540-8.

36. Gardel ML, Sabass B, Ji L, Danuser G, Schwarz US, Waterman CM. Traction stress in focal adhesions correlates biphasically with actin retrograde flow speed. J Cell Biol. 2008;183(6):999-1005. PMCID: 2600750.

37. Yoshigi M, Hoffman LM, Jensen CC, Yost HJ, Beckerle MC. Mechanical force mobilizes zyxin from focal adhesions to actin filaments and regulates cytoskeletal reinforcement. J Cell Biol. 2005;171(2):209-15. PMCID: 2171187.

38. Oakes PW, Wagner E, Brand CA, Probst D, Linke M, Schwarz US, et al. Optogenetic control of RhoA reveals zyxin-mediated elasticity of stress fibres. Nat Commun. 2017;8:15817. PMCID: 5477492.

39. Lazarides E, Burridge K. Alpha-actinin: immunofluorescent localization of a muscle structural protein in nonmuscle cells. Cell. 1975;6(3):289-98.

40. Sjoblom B, Salmazo A, Djinovic-Carugo K. Alpha-actinin structure and regulation. Cell Mol Life Sci. 2008;65(17):2688-701.

41. Collins KL, Gates EM, Gilchrist CL, Hoffman BD. Chapter 1 - Bio-Instructive Cues in Scaffolds for Musculoskeletal Tissue Engineering and Regenerative Medicine. Justin L. Brown SGK, Brittany L. Banik, editor. Academic Press2017.

42. Feramisco JR, Smart JE, Burridge K, Helfman DM, Thomas GP. Co-existence of vinculin and a vinculin-like protein of higher molecular weight in smooth muscle. J Biol Chem. 1982;257(18):11024-31.

43. Xu W, Baribault H, Adamson ED. Vinculin knockout results in heart and brain defects during embryonic development. Development. 1998;125(2):327-37.

44. Coll JL, Ben-Ze'ev A, Ezzell RM, Rodriguez Fernandez JL, Baribault H, Oshima RG, et al. Targeted disruption of vinculin genes in F9 and embryonic stem cells changes cell morphology, adhesion, and locomotion. Proc Natl Acad Sci U S A. 1995;92(20):9161-5. PMCID: 40944.

45. Subauste MC, Pertz O, Adamson ED, Turner CE, Junger S, Hahn KM. Vinculin modulation of paxillin-FAK interactions regulates ERK to control survival and motility. J Cell Biol. 2004;165(3):371-81. PMCID: 2172187.

46. Bakolitsa C, Cohen DM, Bankston LA, Bobkov AA, Cadwell GW, Jennings L, et al. Structural basis for vinculin activation at sites of cell adhesion. Nature. 2004;430(6999):583-6.

47. Johnson RP, Craig SW. An intramolecular association between the head and tail domains of vinculin modulates talin binding. J Biol Chem. 1994;269(17):12611-9.

48. Kroemker M, Rudiger AH, Jockusch BM, Rudiger M. Intramolecular interactions in vinculin control alpha-actinin binding to the vinculin head. FEBS Lett. 1994;355(3):259-62.

49. Weiss EE, Kroemker M, Rudiger AH, Jockusch BM, Rudiger M. Vinculin is part of the cadherin-catenin junctional complex: complex formation between alpha-catenin and vinculin. J Cell Biol. 1998;141(3):755-64. PMCID: 2132754.

50. Brindle NP, Holt MR, Davies JE, Price CJ, Critchley DR. The focal-adhesion vasodilator-stimulated phosphoprotein (VASP) binds to the proline-rich domain in vinculin. Biochem J. 1996;318 (Pt 3):753-7. PMCID: 1217682.

51. DeMali KA, Barlow CA, Burridge K. Recruitment of the Arp2/3 complex to vinculin: coupling membrane protrusion to matrix adhesion. J Cell Biol. 2002;159(5):881-91. PMCID: 2173392.

52. Kioka N, Sakata S, Kawauchi T, Amachi T, Akiyama SK, Okazaki K, et al. Vinexin: a novel vinculin-binding protein with multiple SH3 domains enhances actin cytoskeletal organization. J Cell Biol. 1999;144(1):59-69. PMCID: 2148117.

53. Mandai K, Nakanishi H, Satoh A, Takahashi K, Satoh K, Nishioka H, et al. Ponsin/SH3P12: an l-afadin- and vinculin-binding protein localized at cell-cell and cell-matrix adherens junctions. J Cell Biol. 1999;144(5):1001-17. PMCID: 2148189.

54. Huttelmaier S, Bubeck P, Rudiger M, Jockusch BM. Characterization of two F-actin-binding and oligomerization sites in the cell-contact protein vinculin. Eur J Biochem. 1997;247(3):1136-42.

55. Johnson RP, Niggli V, Durrer P, Craig SW. A conserved motif in the tail domain of vinculin mediates association with and insertion into acidic phospholipid bilayers. Biochemistry. 1998;37(28):10211-22.

56. Lee JH, Rangarajan ES, Yogesha SD, Izard T. Raver1 interactions with vinculin and RNA suggest a feed-forward pathway in directing mRNA to focal adhesions. Structure. 2009;17(6):833-42. PMCID: 2811071.

57. Huttelmaier S, Illenberger S, Grosheva I, Rudiger M, Singer RH, Jockusch BM. Raver1, a dual compartment protein, is a ligand for PTB/hnRNPI and microfilament attachment proteins. J Cell Biol. 2001;155(5):775-86. PMCID: 2150882.

58. Lee JH, Rangarajan ES, Vonrhein C, Bricogne G, Izard T. The metavinculin tail domain directs constitutive interactions with raver1 and vinculin RNA. J Mol Biol. 2012;422(5):697-704. PMCID: 3835166.

59. Honda A, Nogami M, Yokozeki T, Yamazaki M, Nakamura H, Watanabe H, et al. Phosphatidylinositol 4-phosphate 5-kinase alpha is a downstream effector of the small G protein ARF6 in membrane ruffle formation. Cell. 1999;99(5):521-32.

60. Holz RW, Hlubek MD, Sorensen SD, Fisher SK, Balla T, Ozaki S, et al. A pleckstrin homology domain specific for phosphatidylinositol 4, 5-bisphosphate (PtdIns-4,5-P2) and fused to green fluorescent protein identifies plasma membrane PtdIns-4,5-P2 as being important in exocytosis. J Biol Chem. 2000;275(23):17878-85.

61. Botelho RJ, Teruel M, Dierckman R, Anderson R, Wells A, York JD, et al. Localized biphasic changes in phosphatidylinositol-4,5-bisphosphate at sites of phagocytosis. J Cell Biol. 2000;151(7):1353-68. PMCID: 2150667.

62. van den Bout I, Divecha N. PIP5K-driven PtdIns(4,5)P2 synthesis: regulation and cellular functions. J Cell Sci. 2009;122(Pt 21):3837-50.

63. Di Paolo G, Pellegrini L, Letinic K, Cestra G, Zoncu R, Voronov S, et al. Recruitment and regulation of phosphatidylinositol phosphate kinase type 1 gamma by the FERM domain of talin. Nature. 2002;420(6911):85-9.

64. Ling K, Doughman RL, Firestone AJ, Bunce MW, Anderson RA. Type I gamma phosphatidylinositol phosphate kinase targets and regulates focal adhesions. Nature. 2002;420(6911):89-93.

65. Li X, Zhou Q, Sunkara M, Kutys ML, Wu Z, Rychahou P, et al. Ubiquitylation of phosphatidylinositol 4-phosphate 5-kinase type I gamma by HECTD1 regulates focal adhesion dynamics and cell migration. J Cell Sci. 2013;126(Pt 12):2617-28. PMCID: 3687698.

66. Wu Z, Li X, Sunkara M, Spearman H, Morris AJ, Huang C. PIPKIgamma regulates focal adhesion dynamics and colon cancer cell invasion. PLoS One. 2011;6(9):e24775. PMCID: 3171478.

67. Sun Y, Ling K, Wagoner MP, Anderson RA. Type I gamma phosphatidylinositol phosphate kinase is required for EGF-stimulated directional cell migration. J Cell Biol. 2007;178(2):297-308. PMCID: 2064448.

68. Legate KR, Takahashi S, Bonakdar N, Fabry B, Boettiger D, Zent R, et al. Integrin adhesion and force coupling are independently regulated by localized PtdIns(4,5)2 synthesis. Embo J. 2011;30(22):4539-53. PMCID: 3243596.

69. Gromak N, Rideau A, Southby J, Scadden AD, Gooding C, Huttelmaier S, et al. The PTB interacting protein raver1 regulates alpha-tropomyosin alternative splicing. Embo J. 2003;22(23):6356-64. PMCID: 291850.

70. Spellman R, Rideau A, Matlin A, Gooding C, Robinson F, McGlincy N, et al. Regulation of alternative splicing by PTB and associated factors. Biochem Soc Trans. 2005;33(Pt 3):457-60.

71. Rideau AP, Gooding C, Simpson PJ, Monie TP, Lorenz M, Huttelmaier S, et al. A peptide motif in Raver1 mediates splicing repression by interaction with the PTB RRM2 domain. Nat Struct Mol Biol. 2006;13(9):839-48.

72. Winkler J, Lunsdorf H, Jockusch BM. The ultrastructure of chicken gizzard vinculin as visualized by high-resolution electron microscopy. J Struct Biol. 1996;116(2):270-7.

73. Ziegler WH, Liddington RC, Critchley DR. The structure and regulation of vinculin. Trends Cell Biol. 2006;16(9):453-60.

74. Golji J, Wendorff T, Mofrad MR. Phosphorylation primes vinculin for activation. Biophys J. 2012;102(9):2022-30. PMCID: 3341567.

75. Galbraith CG, Yamada KM, Sheetz MP. The relationship between force and focal complex development. J Cell Biol. 2002;159(4):695-705. PMCID: 2173098.

76. Giannone G, Jiang G, Sutton DH, Critchley DR, Sheetz MP. Talin1 is critical for force-dependent reinforcement of initial integrin-cytoskeleton bonds but not tyrosine kinase activation. J Cell Biol. 2003;163(2):409-19. PMCID: 2173516.

77. Grashoff C, Hoffman BD, Brenner MD, Zhou R, Parsons M, Yang MT, et al. Measuring mechanical tension across vinculin reveals regulation of focal adhesion dynamics. Nature. 2010;466(7303):263-6. PMCID: 2901888.

78. Riveline D, Zamir E, Balaban NQ, Schwarz US, Ishizaki T, Narumiya S, et al. Focal contacts as mechanosensors: externally applied local mechanical force induces growth of focal contacts by an mDia1-dependent and ROCK-independent mechanism. J Cell Biol. 2001;153(6):1175-86. PMCID: 2192034.

79. Byrne BJ, Kaczorowski YJ, Coutu MD, Craig SW. Chicken vinculin and meta-vinculin are derived from a single gene by alternative splicing of a 207-base pair exon unique to meta-vinculin. J Biol Chem. 1992;267(18):12845-50.

80. Burridge K, Feramisco JR. Microinjection and localization of a 130K protein in living fibroblasts: a relationship to actin and fibronectin. Cell. 1980;19(3):587-95.

81. Turner CE, Burridge K. Detection of metavinculin in human platelets using a modified talin overlay assay. Eur J Cell Biol. 1989;49(1):202-6.

82. Koteliansky VE, Ogryzko EP, Zhidkova NI, Weller PA, Critchley DR, Vancompernolle K, et al. An additional exon in the human vinculin gene specifically encodes meta-vinculin-specific difference peptide. Cross-species comparison reveals variable and conserved motifs in the meta-vinculin insert. Eur J Biochem. 1992;204(2):767-72.

83. Belkin AM, Ornatsky OI, Glukhova MA, Koteliansky VE. Immunolocalization of meta-vinculin in human smooth and cardiac muscles. J Cell Biol. 1988;107(2):545-53. PMCID: 2115213.

84. Belkin AM, Ornatsky OI, Kabakov AE, Glukhova MA, Koteliansky VE. Diversity of vinculin/meta-vinculin in human tissues and cultivated cells. Expression of muscle specific variants of vinculin in human aorta smooth muscle cells. J Biol Chem. 1988;263(14):6631-5.

85. Glukhova MA, Kabakov AE, Belkin AM, Frid MG, Ornatsky OI, Zhidkova NI, et al. Meta-vinculin distribution in adult human tissues and cultured cells. FEBS Lett. 1986;207(1):139-41.

86. Siliciano JD, Craig SW. Meta-vinculin--a vinculin-related protein with solubility properties of a membrane protein. Nature. 1982;300(5892):533-5.

87. Siliciano JD, Craig SW. Isolation of metavinculin from chicken smooth muscle. Methods Enzymol. 1986;134:78-85.

88. Siliciano JD, Craig SW. Properties of smooth muscle meta-vinculin. J Cell Biol. 1987;104(3):473-82. PMCID: 2114539.

89. Maeda M, Holder E, Lowes B, Valent S, Bies RD. Dilated cardiomyopathy associated with deficiency of the cytoskeletal protein metavinculin. Circulation. 1997;95(1):17-20.

90. Olson TM, Illenberger S, Kishimoto NY, Huttelmaier S, Keating MT, Jockusch BM. Metavinculin mutations alter actin interaction in dilated cardiomyopathy. Circulation. 2002;105(4):431-7.

91. Vasile VC, Will ML, Ommen SR, Edwards WD, Olson TM, Ackerman MJ. Identification of a metavinculin missense mutation, R975W, associated with both hypertrophic and dilated cardiomyopathy. Mol Genet Metab. 2006;87(2):169-74.

92. Vasile VC, Edwards WD, Ommen SR, Ackerman MJ. Obstructive hypertrophic cardiomyopathy is associated with reduced expression of vinculin in the intercalated disc. Biochem Biophys Res Commun. 2006;349(2):709-15.

93. Zemljic-Harpf AE, Miller JC, Henderson SA, Wright AT, Manso AM, Elsherif L, et al. Cardiac-myocyte-specific excision of the vinculin gene disrupts cellular junctions, causing sudden death or dilated cardiomyopathy. Mol Cell Biol. 2007;27(21):7522-37. PMCID: 2169049.

94. Zemljic-Harpf AE, Ponrartana S, Avalos RT, Jordan MC, Roos KP, Dalton ND, et al. Heterozygous inactivation of the vinculin gene predisposes to stress-induced cardiomyopathy. Am J Pathol. 2004;165(3):1033-44. PMCID: 1618594.

95. Rangarajan ES, Lee JH, Yogesha SD, Izard T. A helix replacement mechanism directs metavinculin functions. PLoS One. 2010;5(5):e10679. PMCID: 2873289.

96. Borgon RA, Vonrhein C, Bricogne G, Bois PR, Izard T. Crystal structure of human vinculin. Structure. 2004;12(7):1189-97.

97. Witt S, Zieseniss A, Fock U, Jockusch BM, Illenberger S. Comparative biochemical analysis suggests that vinculin and metavinculin cooperate in muscular adhesion sites. J Biol Chem. 2004;279(30):31533-43.

98. Janssen ME, Liu H, Volkmann N, Hanein D. The C-terminal tail domain of metavinculin, vinculin's splice variant, severs actin filaments. J Cell Biol. 2012;197(5):585-93. PMCID: 3365496.

99. Kim LY, Thompson PM, Lee HT, Pershad M, Campbell SL, Alushin GM. The Structural Basis of Actin Organization by Vinculin and Metavinculin. J Mol Biol. 2016;428(1):10-25. PMCID: 4738167.

100. Rudiger M, Korneeva N, Schwienbacher C, Weiss EE, Jockusch BM. Differential actin organization by vinculin isoforms: implications for cell type-specific microfilament anchorage. FEBS Lett. 1998;431(1):49-54.

101. Shen K, Tolbert CE, Guilluy C, Swaminathan VS, Berginski ME, Burridge K, et al. The vinculin C-terminal hairpin mediates F-actin bundle formation, focal adhesion, and cell mechanical properties. J Biol Chem. 2011;286(52):45103-15. PMCID: 3247952.

102. Johnson RP, Craig SW. Actin activates a cryptic dimerization potential of the vinculin tail domain. J Biol Chem. 2000;275(1):95-105.

103. Oztug Durer ZA, McGillivary RM, Kang H, Elam WA, Vizcarra CL, Hanein D, et al. Metavinculin Tunes the Flexibility and the Architecture of Vinculin-Induced Bundles of Actin Filaments. J Mol Biol. 2015;427(17):2782-98. PMCID: 4540644.

104. Carisey A, Ballestrem C. Vinculin, an adapter protein in control of cell adhesion signalling. Eur J Cell Biol. 2011;90(2-3):157-63. PMCID: 3526775.

105. Humphries JD, Wang P, Streuli C, Geiger B, Humphries MJ, Ballestrem C. Vinculin controls focal adhesion formation by direct interactions with talin and actin. J Cell Biol. 2007;179(5):1043-57. PMCID: 2099183.

106. Burridge K, Mangeat P. An interaction between vinculin and talin. Nature. 1984;308(5961):744-6.

107. Goksoy E, Ma YQ, Wang X, Kong X, Perera D, Plow EF, et al. Structural basis for the autoinhibition of talin in regulating integrin activation. Mol Cell. 2008;31(1):124-33. PMCID: 2522368.

108. Hemmings L, Rees DJ, Ohanian V, Bolton SJ, Gilmore AP, Patel B, et al. Talin contains three actin-binding sites each of which is adjacent to a vinculin-binding site. J Cell Sci. 1996;109 (Pt 11):2715-26.

109. Yao M, Goult BT, Chen H, Cong P, Sheetz MP, Yan J. Mechanical activation of vinculin binding to talin locks talin in an unfolded conformation. Sci Rep. 2014;4:4610. PMCID: 3980218.

110. Janssen ME, Kim E, Liu H, Fujimoto LM, Bobkov A, Volkmann N, et al. Three-dimensional structure of vinculin bound to actin filaments. Mol Cell. 2006;21(2):271-81.

111. Jannie KM, Ellerbroek SM, Zhou DW, Chen S, Crompton DJ, Garcia AJ, et al. Vinculin-dependent actin bundling regulates cell migration and traction forces. Biochem J. 2015;465(3):383-93. PMCID: 4418518.

112. Thompson PM, Tolbert CE, Shen K, Kota P, Palmer SM, Plevock KM, et al. Identification of an actin binding surface on vinculin that mediates mechanical cell and focal adhesion properties. Structure. 2014;22(5):697-706. PMCID: 4039106.

113. Palmer SM, Schaller MD, Campbell SL. Vinculin tail conformation and self-association is independent of pH and H906 protonation. Biochemistry. 2008;47(47):12467-75.

114. Dixon RD, Arneman DK, Rachlin AS, Sundaresan NR, Costello MJ, Campbell SL, et al. Palladin is an actin cross-linking protein that uses immunoglobulin-like domains to bind filamentous actin. J Biol Chem. 2008;283(10):6222-31.

115. Schneider CA, Rasband WS, Eliceiri KW. NIH Image to ImageJ: 25 years of image analysis. Nat Methods. 2012;9(7):671-5. PMCID: 5554542.

116. Mastronarde DN. Automated electron microscope tomography using robust prediction of specimen movements. J Struct Biol. 2005;152(1):36-51.

117. Kremer JR, Mastronarde DN, McIntosh JR. Computer visualization of three-dimensional image data using IMOD. J Struct Biol. 1996;116(1):71-6.

118. Ding F, Tsao D, Nie H, Dokholyan NV. Ab initio folding of proteins with all-atom discrete molecular dynamics. Structure. 2008;16(7):1010-8. PMCID: 2533517.

119. Yin S, Ding F, Dokholyan NV. Eris: an automated estimator of protein stability. Nat Methods. 2007;4(6):466-7.

120. Proctor EA, Ding, F., & Dokholyan, N.V. Discrete Molecular Dynamics. Wiley IRC Mol Sci. 2011;1(1):80-92.

121. Johnson RP, Craig SW. F-actin binding site masked by the intramolecular association of vinculin head and tail domains. Nature. 1995;373(6511):261-4.

122. Egelman EH. The iterative helical real space reconstruction method: surmounting the problems posed by real polymers. J Struct Biol. 2007;157(1):83-94.

123. Alushin GM, Lander GC, Kellogg EH, Zhang R, Baker D, Nogales E. High-resolution microtubule structures reveal the structural transitions in alphabeta-tubulin upon GTP hydrolysis. Cell. 2014;157(5):1117-29. PMCID: 4054694.

124. Hohn M, Tang G, Goodyear G, Baldwin PR, Huang Z, Penczek PA, et al. SPARX, a new environment for Cryo-EM image processing. J Struct Biol. 2007;157(1):47-55.

125. Tang G, Peng L, Baldwin PR, Mann DS, Jiang W, Rees I, et al. EMAN2: an extensible image processing suite for electron microscopy. J Struct Biol. 2007;157(1):38-46.

126. Lyumkis D, Brilot AF, Theobald DL, Grigorieff N. Likelihood-based classification of cryo-EM images using FREALIGN. J Struct Biol. 2013;183(3):377-88. PMCID: 3824613.

127. Bakolitsa C, de Pereda JM, Bagshaw CR, Critchley DR, Liddington RC. Crystal structure of the vinculin tail suggests a pathway for activation. Cell. 1999;99(6):603-13.

128. Trabuco LG, Villa E, Mitra K, Frank J, Schulten K. Flexible fitting of atomic structures into electron microscopy maps using molecular dynamics. Structure. 2008;16(5):673-83. PMCID: 2430731.

129. Palmer SM, Campbell SL. Backbone 1H, 13C, and 15N NMR assignments of the tail domain of vinculin. Biomol NMR Assign. 2008;2(1):69-71.

130. Parsons JT, Horwitz AR, Schwartz MA. Cell adhesion: integrating cytoskeletal dynamics and cellular tension. Nat Rev Mol Cell Biol. 2010;11(9):633-43. PMCID: 2992881.

131. Mangeat P, Burridge K. Actin-membrane interaction in fibroblasts: what proteins are involved in this association? J Cell Biol. 1984;99(1 Pt 2):95s-103s. PMCID: 2275575.

132. Wood CK, Turner CE, Jackson P, Critchley DR. Characterisation of the paxillin-binding site and the C-terminal focal adhesion targeting sequence in vinculin. J Cell Sci. 1994;107 (Pt 2):709-17.

133. Turner CE, Glenney JR, Jr., Burridge K. Paxillin: a new vinculin-binding protein present in focal adhesions. J Cell Biol. 1990;111(3):1059-68. PMCID: 2116264.

134. Mierke CT, Kollmannsberger P, Zitterbart DP, Diez G, Koch TM, Marg S, et al. Vinculin facilitates cell invasion into three-dimensional collagen matrices. J Biol Chem. 2010;285(17):13121-30. PMCID: 2857131.

135. Campbell RE, Tour O, Palmer AE, Steinbach PA, Baird GS, Zacharias DA, et al. A monomeric red fluorescent protein. Proc Natl Acad Sci U S A. 2002;99(12):7877-82. PMCID: 122988.

136. Berginski ME GS. The Focal Adhesion Analysis Server: a web tool for analyzing focal adhesion dynamics F1000Research 2013;1(2):68.

137. Atienza JM, Yu N, Kirstein SL, Xi B, Wang X, Xu X, et al. Dynamic and label-free cell-based assays using the real-time cell electronic sensing system. Assay Drug Dev Technol. 2006;4(5):597-607.

138. Fisher JK, Cribb J, Desai KV, Vicci L, Wilde B, Keller K, et al. Thin-foil magnetic force system for high-numerical-aperture microscopy. Rev Sci Instrum. 2006;77(2):nihms8302. PMCID: 1513178.

139. Tim O'Brien E, Cribb J, Marshburn D, Taylor RM, 2nd, Superfine R. Chapter 16: Magnetic manipulation for force measurements in cell biology. Methods Cell Biol. 2008;89:433-50.

140. Goldmann WH, Schindl M, Cardozo TJ, Ezzell RM. Motility of vinculin-deficient F9 embryonic carcinoma cells analyzed by video, laser confocal, and reflection interference contrast microscopy. Exp Cell Res. 1995;221(2):311-9.

141. Cohen DM, Chen H, Johnson RP, Choudhury B, Craig SW. Two distinct head-tail interfaces cooperate to suppress activation of vinculin by talin. J Biol Chem. 2005;280(17):17109-17.

142. Izard T, Evans G, Borgon RA, Rush CL, Bricogne G, Bois PR. Vinculin activation by talin through helical bundle conversion. Nature. 2004;427(6970):171-5.

143. Golji J, Lam J, Mofrad MR. Vinculin activation is necessary for complete talin binding. Biophys J. 2011;100(2):332-40. PMCID: 3021670.

144. Auernheimer V, Lautscham LA, Leidenberger M, Friedrich O, Kappes B, Fabry B, et al. Vinculin phosphorylation at residues Y100 and Y1065 is required for cellular force transmission. J Cell Sci. 2015;128(18):3435-43. PMCID: 4582403.

145. Ji L, Lim J, Danuser G. Fluctuations of intracellular forces during cell protrusion. Nat Cell Biol. 2008;10(12):1393-400. PMCID: 2597050.

146. Guilluy C, Swaminathan V, Garcia-Mata R, O'Brien ET, Superfine R, Burridge K. The Rho GEFs LARG and GEF-H1 regulate the mechanical response to force on integrins. Nat Cell Biol. 2011;13(6):722-7. PMCID: 3107386.

147. Sheikh F, Chen Y, Liang X, Hirschy A, Stenbit AE, Gu Y, et al. alpha-E-catenin inactivation disrupts the cardiomyocyte adherens junction, resulting in cardiomyopathy and susceptibility to wall rupture. Circulation. 2006;114(10):1046-55.

148. Watabe-Uchida M, Uchida N, Imamura Y, Nagafuchi A, Fujimoto K, Uemura T, et al. alpha-Catenin-vinculin interaction functions to organize the apical junctional complex in epithelial cells. J Cell Biol. 1998;142(3):847-57. PMCID: 2148175.

149. Yonemura S, Wada Y, Watanabe T, Nagafuchi A, Shibata M. alpha-Catenin as a tension transducer that induces adherens junction development. Nat Cell Biol. 2010;12(6):533-42.

150. Yao M, Qiu W, Liu R, Efremov AK, Cong P, Seddiki R, et al. Force-dependent conformational switch of alpha-catenin controls vinculin binding. Nat Commun. 2014;5:4525.

151. Peng X, Maiers JL, Choudhury D, Craig SW, DeMali KA. alpha-Catenin uses a novel mechanism to activate vinculin. J Biol Chem. 2012;287(10):7728-37. PMCID: 3293531.

152. Kumar A, Anderson KL, Swift MF, Hanein D, Volkmann N, Schwartz MA. Local Tension on Talin in Focal Adhesions Correlates with F-Actin Alignment at the Nanometer Scale. Biophys J. 2018;115(8):1569-79.

153. Burridge K. Are stress fibres contractile? Nature. 1981;294(5843):691-2.

154. Choi CK, Vicente-Manzanares M, Zareno J, Whitmore LA, Mogilner A, Horwitz AR. Actin and alpha-actinin orchestrate the assembly and maturation of nascent adhesions in a myosin II motor-independent manner. Nat Cell Biol. 2008;10(9):1039-50. PMCID: 2827253.

155. Sarker M, Lee HT, Mei L, Krokhotin A, de Los Reyes SE, Yen L, et al. Cardiomyopathy Mutations in Metavinculin Disrupt Regulation of Vinculin-Induced F-Actin Assemblies. J Mol Biol. 2019;431(8):1604-18.

156. H.V. W. On some phenomena of coalescence and regeneration in sponges. Journal of Experimental Zoology. 1907;Part A: Ecological(*Wiley Online Library.*).

157. Humphreys T. Chemical Dissolution and in Vitro Reconstruction of Sponge Cell Adhesions. I. Isolation and Functional Demonstration of the Components Involved. Dev Biol. 1963;8:27-47.

158. Cauldwell CB, Henkart P, Humphreys T. Physical properties of sponge aggregation factor. A unique proteoglycan complex. Biochemistry. 1973;12(16):3051-5.

159. Haseley SR, Vermeer HJ, Kamerling JP, Vliegenthart JF. Carbohydrate self-recognition mediates marine sponge cellular adhesion. Proc Natl Acad Sci U S A. 2001;98(16):9419-24. PMCID: 55436.

160. Moscona AA. Cell aggregation: properties of specific cell-ligands and their role in the formation of multicellular systems. Dev Biol. 1968;18(3):250-77.

161. Henkart P, Humphreys S, Humphreys T. Characterization of sponge aggregation factor. Unique proteoglycan complex. Biochemistry. 1973;12(16):3045-50.

162. Grice LF, Gauthier MEA, Roper KE, Fernandez-Busquets X, Degnan SM, Degnan BM. Origin and Evolution of the Sponge Aggregation Factor Gene Family. Mol Biol Evol. 2017;34(5):1083-99. PMCID: 5400394.

163. Vilanova E, Santos GR, Aquino RS, Valle-Delgado JJ, Anselmetti D, Fernandez-Busquets X, et al. Carbohydrate-Carbohydrate Interactions Mediated by Sulfate Esters and Calcium Provide the Cell Adhesion Required for the Emergence of Early Metazoans. J Biol Chem. 2016;291(18):9425-37. PMCID: 4850283.

164. Miller PW, Pokutta S, Mitchell JM, Chodaparambil JV, Clarke DN, Nelson WJ, et al. Analysis of a vinculin homolog in a sponge (phylum Porifera) reveals that vertebrate-like cell adhesions emerged early in animal evolution. J Biol Chem. 2018;293(30):11674-86. PMCID: 6066325.

165. Thompson PM, Tolbert CE, Campbell SL. Vinculin and metavinculin: oligomerization and interactions with F-actin. FEBS Lett. 2013;587(8):1220-9.

166. Thoss F, Dietrich F, Punkt K, Illenberger S, Rottner K, Himmel M, et al. Metavinculin: New insights into functional properties of a muscle adhesion protein. Biochem Biophys Res Commun. 2013;430(1):7-13.

167. Koteliansky VE, Gneushev GN, Glukhova MA, Venyaminov SY, Muszbek L. Identification and isolation of vinculin from platelets. FEBS Lett. 1984;165(1):26-30.

168. Langer BG, Gonnella PA, Nachmias VT. alpha-Actinin and vinculin in normal and thrombasthenic platelets. Blood. 1984;63(3):606-14.

169. Asijee GM, Sturk A, Bruin T, Wilkinson JM, Ten Cate JW. Vinculin is a permanent component of the membrane skeleton and is incorporated into the (re)organising cytoskeleton upon platelet activation. Eur J Biochem. 1990;189(1):131-6.

170. Mitsios JV, Prevost N, Kasirer-Friede A, Gutierrez E, Groisman A, Abrams CS, et al. What is vinculin needed for in platelets? J Thromb Haemost. 2010;8(10):2294-304. PMCID: 2965783.

171. McCain ML, Lee H, Aratyn-Schaus Y, Kleber AG, Parker KK. Cooperative coupling of cell-matrix and cell-cell adhesions in cardiac muscle. Proc Natl Acad Sci U S A. 2012;109(25):9881-6. PMCID: 3382528.

172. DeMali KA, Sun X, Bui GA. Force transmission at cell-cell and cell-matrix adhesions. Biochemistry. 2014;53(49):7706-17.

173. Weber GF, Bjerke MA, DeSimone DW. Integrins and cadherins join forces to form adhesive networks. J Cell Sci. 2011;124(Pt 8):1183-93. PMCID: 3115772.

174. Nelson CM, Pirone DM, Tan JL, Chen CS. Vascular endothelial-cadherin regulates cytoskeletal tension, cell spreading, and focal adhesions by stimulating RhoA. Mol Biol Cell. 2004;15(6):2943-53. PMCID: 420116.